Report 4368

the

-Mg

oys

yle

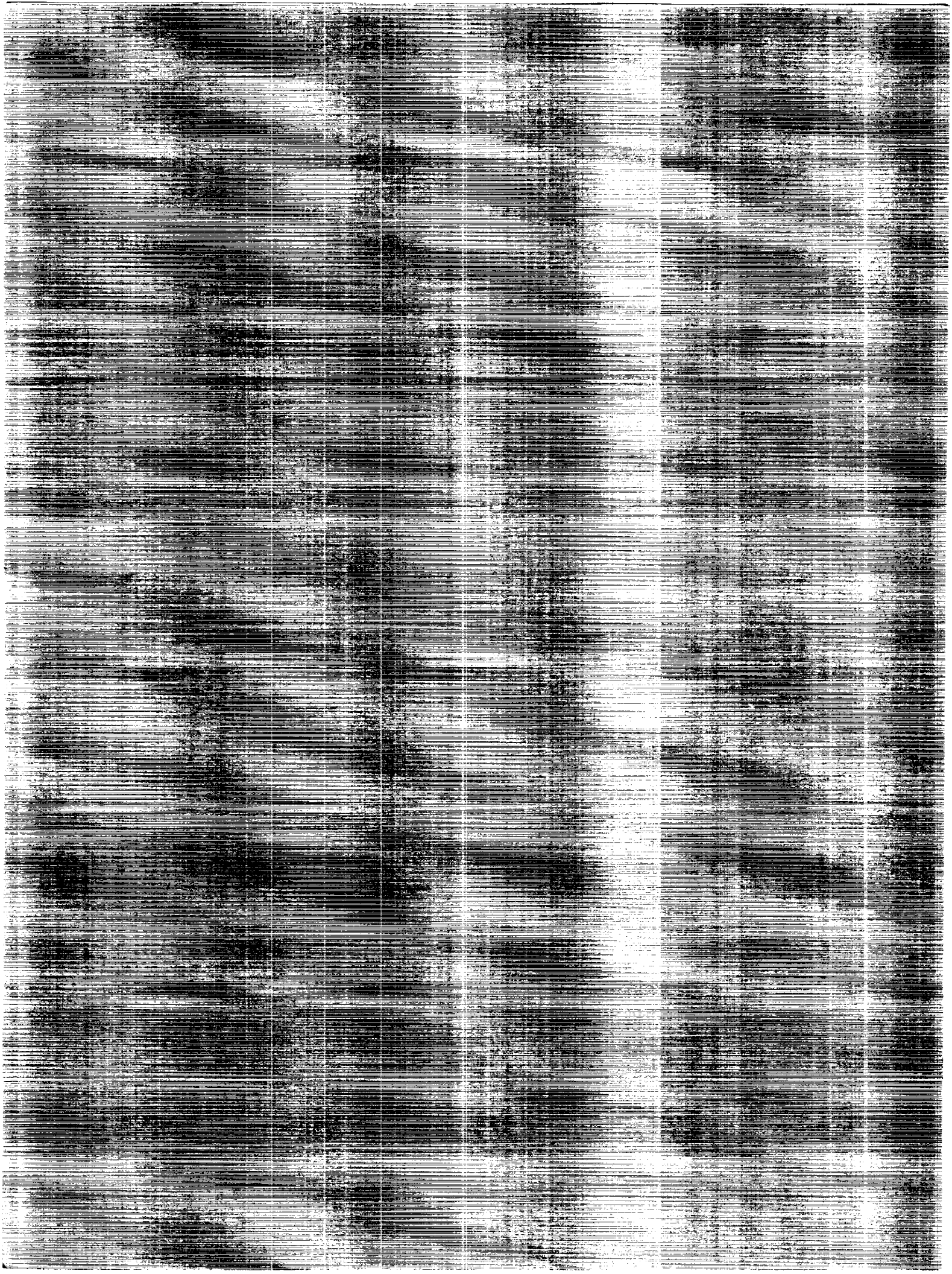

NASA Contractor Report 4368

Evaluation of the Microstructure of Al-Cu-Li-Ag-Mg Weldalite™ Alloys

J. R. Pickens, K. S. Kumar,
S. A. Brown, and F. W. Gayle
Martin Marietta Corporation
Martin Marietta Laboratories
Baltimore, Maryland

Prepared for
Langley Research Center
under Contract NAS1-18531

National Aeronautics and
Space Administration
Office of Management
Scientific and Technical
Information Division

1991

FOREWORD

This report documents our findings on the microstructural tasks of Contract NAS1-18531 during the period June 1989 to October 1990. The entirety of our microstructural understanding of ultra-high strength Weldalite™ alloys is highlighted in an Extended Executive Summary and discussed in detail in the five sections following the Executive Summary.

TABLE OF CONTENTS

Extended Executive Summary

OVERVIEW OF MICROSTRUCTURAL STUDIES

1.1 Weldalite™ 049

The microstructure of Al-Cu-Li-Ag-Mg-Zr alloy Weldalite™ 049 has been characterized from naturally aged conditions -- i.e., unstretched (T4) and stretched (T3) -- through artificially aged conditions, with emphasis on the underaged and peak-aged tempers. Weldalite™ 049 is capable of attaining ultra-high strength, i.e., ≥100 ksi tensile strength, in artificially aged tempers both with (T8), or without (T6) cold work to stimulate the nucleation of strengthening precipitates. The identification of strengthening phases along the T4→T6 and T3→T8 aging curves is an important first step in understanding the reasons for the unique properties of Weldalite™ 049. Note that insoluble, constituent particles exist in Weldalite™ 049 that are believed to be beneficial for weldability. These particles are most likely θ ($CuAl_2$) and T_B ($Al_{7.5}Cu_4Li$) and do not contribute significantly to strengthening.

1.2 Phase Identification in Weldalite™ 049 Without Prior Cold Work (T4→T6)

The Weldalite™ 049 used in these investigations had nominal compositions in the range Al-(4.5-6.3)Cu-1.3Li-0.4Ag-0.4Mg-0.14Zr (wt.%). Equivalent strengths can be attained in the technologically important tempers at any Cu level in this range. Excess Cu above about 4.5% partitions into the constituent particles, which do not contribute significantly to strength. In the early stages of this program, Cu levels in the higher part of the range were used to ensure excellent weldability. As weldability was demonstrated at Cu levels down to about 4% Cu in plant trials at Martin Marietta operating divisions, lower Cu-containing variants were introduced into this program. Increased ductility and fracture toughness accompany the decreased Cu level with the rest of the alloy composition unchanged.

In the T4 condition, δ' (Al_3Li) and Guinier Preston 1 (GP1) zones are the major strengthening phases present. In addition, $ZrAl_3$ dispersoids are present with a surrounding layer of δ' seen on some particles. The $ZrAl_3$ dispersoids (i.e. $L1_2$ variant) remain throughout artificial aging as is the case for other Zr-containing aluminum alloys. In the artificially aged conditions, no δ' envelopes surrounding the $ZrAl_3$ were observed. During the initial stages of artificial aging (i.e.,

15 minutes at 180°C) where reversion occurs, δ' and some GP zones dissolve. Consequently, strengthening in the non cold-worked reversion temper is provided largely by GP zones, some of which have coarsened during the reversion heat treatment. After about 2 h of aging at 180°C, numerous phases are present in this severely underaged temper. We observed GP zones, θ', ($CuAl_2$), S' (Al_2CuMg), T_1 (Al_2CuLi) and possibly a hitherto unreported phase, designated ν. As peak strength (T6 temper) is approached, the GP zones are not observed whereas θ', S', ν, and T_1 are present, with T_1 by far the most prevalent strengthening phase. The strengthening phases (i.e. not including the constituent phases) observed along the T4 ⟶ T6 aging curve are summarized in Table I. We observed that Weldalite™ 049 will naturally age from the non cold-worked reversion temper after an incubation period. Both GP1 and δ' are present in the reverted and naturally aged condition, but the distributions and morphologies of these phases are quite complex as described in detail in the subsequent sections that constitute the main body of this report.

Table I.

Strengthening Phases Present in Weldalite™ 049 from the Naturally Aged, Unstretched Condition (T4) to the Artificially Aged, Unstretched Condition (T6)

Aging Condition °C (h)	Description	Phases Identified
Naturally Aged 20 (>1000)	T4	GP1, δ'
180 (0.25)	Reversion	GP1
180 (2)	Underaged	GP1, θ', S', T_1, ν
180 (20)	T6	θ', S', ν, T_1 (predominant)

($ZrAl_3$ exists throughout)

1.3 Phase Identification in Weldalite™ 049 with Prior Cold Work (3% Stretch) T3→T8

During the first year of the program, we reported preliminary phase identifications in the T3 and T8 tempers. In the T3 condition, δ' was clearly observed with evidence of GP zones that were possibly modified by the presence of Li. In the T8 temper (24 h at 160°C after 3% stretch), T_1 was the predominant strengthening phase with minor amounts of θ' occasionally, but not always, observed. We recently augmented these characterizations along the T3 to the T8 aging curve for Weldalite™ 049 that contains 3% cold stretch, after quenching from the solution heat treatment temperature.

In the T3 temper, both δ' and GP zones are observed, as is the case for the unstretched T4 temper, but the GP zones are not as prominent as in the T4 condition. This is consistent with the higher strength measured in the T4 temper. During the initial stages of artificial aging at 160°C (i.e. for 15 minutes), reversion occurs in which a significant volume fraction of the GP zones dissolve, as does some δ'. Some evidence of θ' also exists in this reverted condition. If the artificial aging is performed for 15 minutes at 180°C, the alloy is slightly beyond the reversion well and some fine T_1 is present. After 2 h at 160°C, all four variants of T_1 are present as well as θ'. After 4 h at 160°C, a minor amount of S' is seen in addition to θ' and T_1. After 20 h at 160°C, which is slightly underaged, θ', S', and T_1 are present with the T_1 predominant. In the slightly overaged condition (102 h at 160°C), where strength is only about 3% lower than peak, T_1 is the only major strengthening phase observed. Once again, the $ZrAl_3$ dispersoid exists throughout this aging sequence with no δ' envelopes observed in artificially aged conditions. The strengthening phases identified along the T3→T8 aging curve are summarized in Table II.

Table II

Strengthening Phases Present in Weldalite™ 049 from the Stretched (3%) and Naturally Aged Condition (T3) to the Stretched and Artificially Aged (T8) Condition

Aging Condition °C (h)	Description	Phases Identified
Naturally Aged 20 (>1000)	T3	GP (less prominent than in T4), δ'
160 (0.25)	Reversion	GP, δ', θ'
180 (0.25)	Slightly beyond Reversion Well	GP, δ', θ', T_1
160 (2)	Underaged	θ', T_1
160 (4)	Underaged	θ', S', T_1
160 (20)	Slightly Underaged T8	θ', S', T_1 (predominant)
160 (102)	Slightly Overaged T8	T_1
	($ZrAl_3$ exists throughout)	

Thus, Weldalite™ 049 attains high strength in a variety of technologically useful tempers in which the strengthening phases can be dramatically different.

2. MICROSTRUCTURAL CHARACTERIZATION OF A WELDALITE™ VARIANT WITH INCREASED LITHIUM CONTENT (1.7 WT% LI)

Weldalite™ 049-type alloys display an interesting variation in strength as a function of the Li content where a significant maximum in yield and ultimate tensile strengths is observed for the nominal 049 composition, about 1.3 wt.% Li. For example, the yield strength

decreases from ~100 ksi at 1.3 wt.% to around 85 ksi at ~l.7 wt.% Li. It would be beneficial to use a Weldalite™ alloy variant containing 1.7 wt.% Li, as its density and modulus are improved over that of the 1.3 wt.% Li variant, if its strength could be increased. Consequently, we performed a detailed study of the microstructural evolution during aging of a Weldalite™ variant containing a nominal 1.7 wt.% Li to develop an understanding that might provide insights in developing heat treatments to increase strength, thereby enabling us to take advantage of its lower density and higher modulus. In addition, it is hoped that this study would elucidate the strengthening mechanisms in the standard 1.3 wt.% Li variant, Weldalite™ 049.

Using transmission electron microscopy (TEM) techniques, specifically selected area diffraction (SAD) and centered dark field (CDF) imaging, the phases present were identified in the naturally aged condition, as well as after artificial aging to various times along the aging curves. The effect of lithium content on the precipitation sequence was understood by comparing the higher Li-containing Weldalite™ variant Al-5.35Cu-1.64Li-0.40Ag-0.44Mg-0.16Zr (wt.%) with a Weldalite™ 049 heat containing the standard (1.3 wt% nominal) Li level. The effect of a prior stretching operation on the aging behavior in terms of the nature of precipitates present was appreciated by comparing a stretched and unstretched part of the same extrusion. Most artificial aging for the alloy in the unstretched condition was performed at 180°C, where peak strength could be attained in practical periods of time. Nevertheless, some investigations were performed at 160°C, which is the same aging temperature as that for the stretched material.

2.1 Hardness Measurements for Various Aging Conditions

The hardness of the 1.64 wt.% Li-containing alloy was measured in the naturally aged condition for the stretched and unstretched material. The unstretched material exhibits a stronger natural aging response compared to the stretched material (R_B 80 vs R_B 68 respectively after 600 h). In the early stages of artificial aging at 160°C for the stretched material and at 180°C for the unstretched material, reversion occurs with an appreciable decrease in hardness. This reversion is typically observed after approximately 15 minutes at temperature, with the depth of the "reversion trough" being considerably greater for the unstretched material which was aged at the higher temperature. Further artificial aging causes an increase in hardness with peak hardness in both cases being observed after 40-50 h.

2.2 Phase Identification of 1.7% Li Containing Weldalite™ Alloy Without Cold Work

In the naturally aged condition, a [100] zone axis diffraction pattern revealed the superlattice spots of δ' and the bidirectional <100> streaking characteristic of the GP zones. After 1/4 hour at 160°C, the GP zones were no longer present and no precipitates other than δ' were observed. The decrease in hardness during reversion is associated with the dissolution of GP zones and some of the δ' (note that the unstretched material is typically aged at 180°C). Exposure of the naturally aged material for 1/4 hour to 180°C results in a SAD pattern with weak δ' spots. If the reverted, unstretched material is allowed to naturally age for about 2-4 weeks, the δ' reprecipitates, providing a strong, natural aging response after the incubation period. This behavior may have technological significance in that it enables the material to be formed into shapes in the reverted condition, taking advantage of the lower-strength and high-ductility characteristic of this temper, and then subsequently being able to naturally age to higher strength levels.

Longer exposures of the unstretched material to 180°C (2 h, 6 h, 12 h) cause the precipitation of δ', T_1, and S', the last of these phases manifesting itself as streaks in the <110> directions, as well as in the <210> directions. The δ' phase precipitates on the θ' and Al_3Zr phases. This is in contrast to the 1.3 wt.% variant, Weldalite™ 049, in which δ' envelops around θ' and Al_3Zr are not observed in artificially aged conditions. All four variants of the T_1 phase are observed and, in general, the T_1 phase first comes out on the subgrain boundaries (2 h at 180°C), then in the interior of subgrains (6 h at 180°C) leaving a precipitate-free-zone which eventually fills out after 12 h at temperature.

After relatively long exposures (48 h and 100 h) to temperature, all four phases are still present (δ', θ', T_1 and S') although the δ' and θ' diffraction spots and streaks are significantly weaker.

2.3 Phase Identification of 1.7% Li Containing Weldalite™ Alloy with 3% Stretch

The naturally aged microstructure is similar to that observed for the unstretched material except that in the stretched material, the <100> streaks due to the G.P. zones are considerably weaker. This suggests that prior stretching discourages the formation of GP zones in this alloy, which is consistent with the lower natural aging response for the stretched material. A reversion treatment at 160°C for 1/4 hour results in the elimination of the GP zones and a significant weakening in the intensity of the δ' superlattice reflections. A similar reversion heat treatment at 180°C, eliminates δ' superlattice reflections altogether.

Longer exposures to 160°C, i.e., greater than about 6h, results in the precipitation of T_1, θ', and S'. Aging for extended time (240 h) at 160°C results in a microstructure consisting of δ', T_1, and S'. Thus, the overaged, stretched microstructure contains δ', but no θ', whereas in the overaged unstretched material, both δ' spots and θ' streaks are very weak. The phases present in this higher Li-containing Weldalite™ variant are summarized in the Table III.

Table III

Summary of Phases Present and Diffraction Information in Higher Li-Containing Weldalite™ Alloy

(Al-5.35Cu-1.64Li-0.40Ag-0.44Mg-0.16Zr, wt%)

Aging Time	Unstretched 180°C (aging temperature)	Stretched 3% 160°C (aging temperature)
0 (i.e. T4, T3)	δ', GP Zones	δ' + weak GP Zones
+ 1/4 h	weak δ'	weak δ'
+ 2 h	δ', θ', T_1, <110> streaks	δ', T_1?
+ 6 h	δ', θ', T_1, <110> streaks	δ', T_1, weak θ', weak <110>, S'
+ 10 h	-	δ', T_1, θ', <110>, S'
+ 12 h	δ', T_1, θ', <110> streaks, S'	-
+ 34 h	-	δ', T_1, θ', S'
+ 48 h	weak δ', T_1, θ', <110> streaks, S'	-
+ 100 h	weak δ', T_1, weak θ', <110> streaks, S'	-
+ 240 h	-	δ', T_1, S' [θ', not seen]

2.4 High Resolution Lattice Image Characterization of Plate-like precipitates on {111} Planes in Weldalite™ 049

The major strengthening precipitate in many Al-Cu-Li alloys in stretched and artificially-aged tempers (i.e. T8) is the T_1 phase which has the nominal stoichiometry Al_2CuLi. In earlier work in this program, Langan and Pickens[1] noted that T_1 is remarkably similar to the Ω phase, which is a potent strengthening phase in the Al-Cu-Ag-Mg system. Both phases are platelike, with {111} habit planes, have similar interatomic spacings, and look remarkably similar in transmission electron microscopy. In fact, Langan and Pickens[1] prepared a Weldalite™ 049 heat (Al-5.85Cu-1.25Li-0.38Ag-0.43Mg-0.13Zr) and a similar model Li-free alloy (Al-6.16Cu-0.41Ag-0.42Mg-0.14Zr; alloy 2 hereafter) to compare strengthening precipitation. This latter alloy is similar to an alloy developed by Polmear[2] in which the large strengthening contribution of Ω was noted. Langan and Pickens[1] concluded that Weldalite™ 049 T8 was primarily strengthened by the T_1 phase, but they could not rule out the existence of Ω. Consequently, they referred to the strengthening phase as T_1-like. We performed a high resolution lattice image investigation of the aforementioned platelike precipitates in the same two alloy heats used by Langan and Pickens[1].

The lattice image of the Ω in alloy 2 is clearly different from that of the "T_1-like" phase in the Weldalite™ 049. A sufficient number of platelets was imaged to conclude that Ω is not present in Weldalite™ 049 in the T8 temper examined.

---

1 T.J. Langan and J.R. Pickens, "Aluminum-Lithium Alloys", (Proceedings of the Fifth International Aluminum Lithium Conference), Williamsburg, VA, March, 1989, Materials and Component Engineering Publications, Ltd., pp 691-700.

2 I.J. Polmear, "Aluminum Alloys Their Physical and Mechanical Properties", Vol. I, E.A. Starke, Jr. and T.H. Sanders, Jr. Eds, Engineering Materials Advisory Services Ltd. Publishers, Warley UK, June 1986, pp. 661-674

92

N91-24405

I. NATURAL AGING AND REVERSION BEHAVIOR OF Al-Cu-Li-Ag-Mg ALLOY WELDALITE™ 049

Frank W. Gayle, Frank H. Heubaum, and Joseph R. Pickens

The lattice images of T_1-like platelets in Weldalite™ 049 were compared with those in the literature for T_1 in other Al-Cu-Li alloys. From the [110] direction, the structures appear identical. However, when viewed from the [112] direction, the structures are different. Dozens of platelets were imaged from the [112] direction and, in each case, the structure was different from that reported for T_1 in the literature. The modified structure apparently results from the presence of Ag+Mg, but the reasons for the slight structural change as well as the details of the T_1 structure in Weldalite™ 049 are unknown.

1. INTRODUCTION

Recently an aluminum-copper-lithium alloy capable of 700 MPa yield strength in either the T8 or T6 temper has been developed [1,2]. In addition to such high strength levels, the Weldalite™ 049 alloy exhibits excellent properties in material aged at room temperature, both with (T3 temper) and without (T4 temper) prior cold work, and a strong reversion behavior when these "naturally aged" samples are heated to 160-180°C for short periods of time. The reverted temper is characterized by a reduced yield strength and increased ductility, which may be technologically useful, for example, in cold-forming operations.

The present study was initiated to understand the natural aging and reversion behavior of Weldalite™ 049 in tempers without cold work. Of particular interest are: 1) the microstructural basis for the high strength in the T4 condition, 2) an explanation of the reversion phenomenon, and 3) the effect of re-aging at room temperature after a reversion treatment. Mechanical properties were measured and transmission electron microscopy (TEM) analysis performed at various stages of microstructural development during aging, reversion, and subsequent re-aging.

2. EXPERIMENTAL PROCEDURE

Samples of Weldalite™ 049, nominally Al-6Cu-1.3Li-0.4Ag-0.4Mg-0.14Zr (wt.%), were obtained as extruded bar (19 x 51 mm) or rolled sheet (5 mm). Unless indicated otherwise, material was solution-heat-treated (SHT) at 503°C for 1 hour, quenched in cold water, and allowed to naturally age at room temperature. The naturally aged temper (T4) was defined as >1000 hours post-SHT. Samples of T4 were reverted at 180°C for periods from 5 to 45 minutes and subsequently "re-aged" at room temperature. Aging and re-aging behavior were followed by hardness (Rockwell B) and electrical conductivity measurements.

TEM specimens were prepared in a twin-jet polisher, using 25% HNO_3 in methanol. Polishing was performed at -25°C at ~12 volts. After polishing, it was necessary to dip the specimen in 50 vol.% HNO_3 in H_2O to remove Ag which had redeposited during electropolishing. Specimens were examined at an accelerating voltage of 120 keV using a Phillips EM400T transmission electron microscope.

3. RESULTS

The alloy displayed a rapid and strong natural aging response without prior cold work, as shown in Fig.1. Shown for comparison is the commercial Li-free alloy 2519 (Al-5.7Cu-0.2Mg-0.25Mn-0.1Zr-0.1V) in the form of 22-mm plate. After reversion, Weldalite™ 049 naturally ages with an incubation period that varies with reversion time as shown in Fig. 2. Note that room temperature re-aging eventually brings the reverted alloy back to the original T4 hardness. Tensile properties of the T4, reverted, and re-aged conditions (Table 1) correlate well with the hardness behavior of Fig. 2.

The microstructure of the T4 condition exhibits a very well developed Guinier-Preston (GP) zone [3,4] structure (Fig.3a). The zones, lying on {100} planes, are dense yet fairly fine (~5 nm diameter). The selected area diffraction pattern (SADP) shows streaking associated with the GP zone platelets (Fig.3b). Additionally, superlattice reflections are present for Al_3Li (δ'). Dark field imaging

TABLE 1. Longitudinal tensile properties of naturally aged and reverted Weldalite™ 049. (25 mm gauge; $\dot{\varepsilon} = 3 \times 10^{-4}$ s^{-1})

Aging Condition	0.2% YS MPa (ksi)	UTS MPa (ksi)	Elong. %
T4 (1000 h)	420 (61)	580 (84)	15.5
Reverted (180°C/15 min)	280 (40.5)	480 (69)	25.5
Reverted + 10^4 h re-age	440 (64)	610 (88.5)	11.0

of δ' indicates that the phase is generally uniformly distributed throughout the matrix, except for a preferred nucleation on the Zr-rich dispersoid known as α' or β'. This preferred nucleation is common in aluminum-base alloys containing both Li and Zr [5-7]. Thus the strong natural aging response of Weldalite™ 049 results from both GP zones and δ'.

The alloy after a 45 minute reversion was also characterized by TEM. After 24 hours re-age (i.e., before substantial re-aging takes

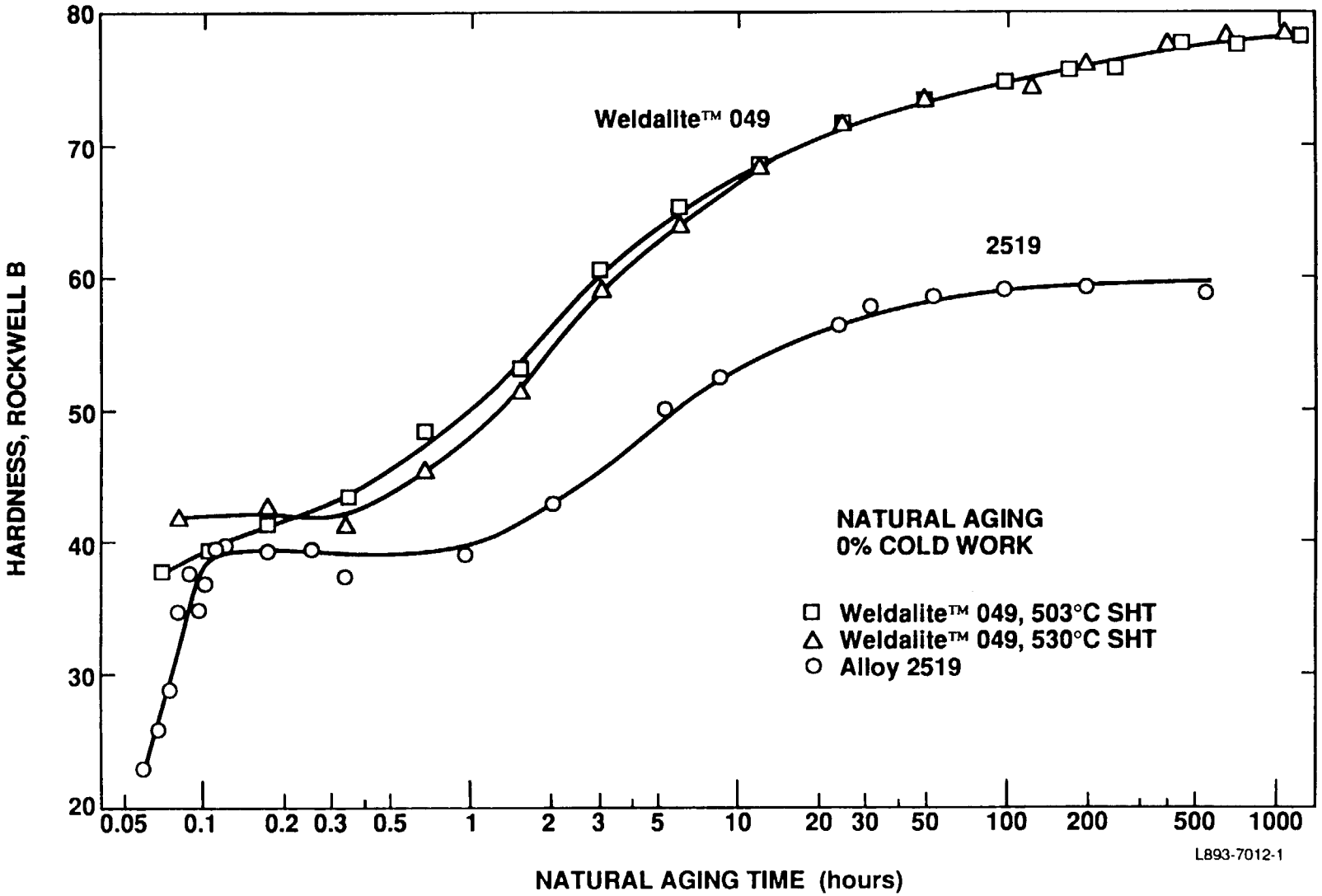

Figure 1 Natural aging curves for Weldalite™ 049 SHTed at 503°C and 530°C. Alloy 2519 is shown for comparison.

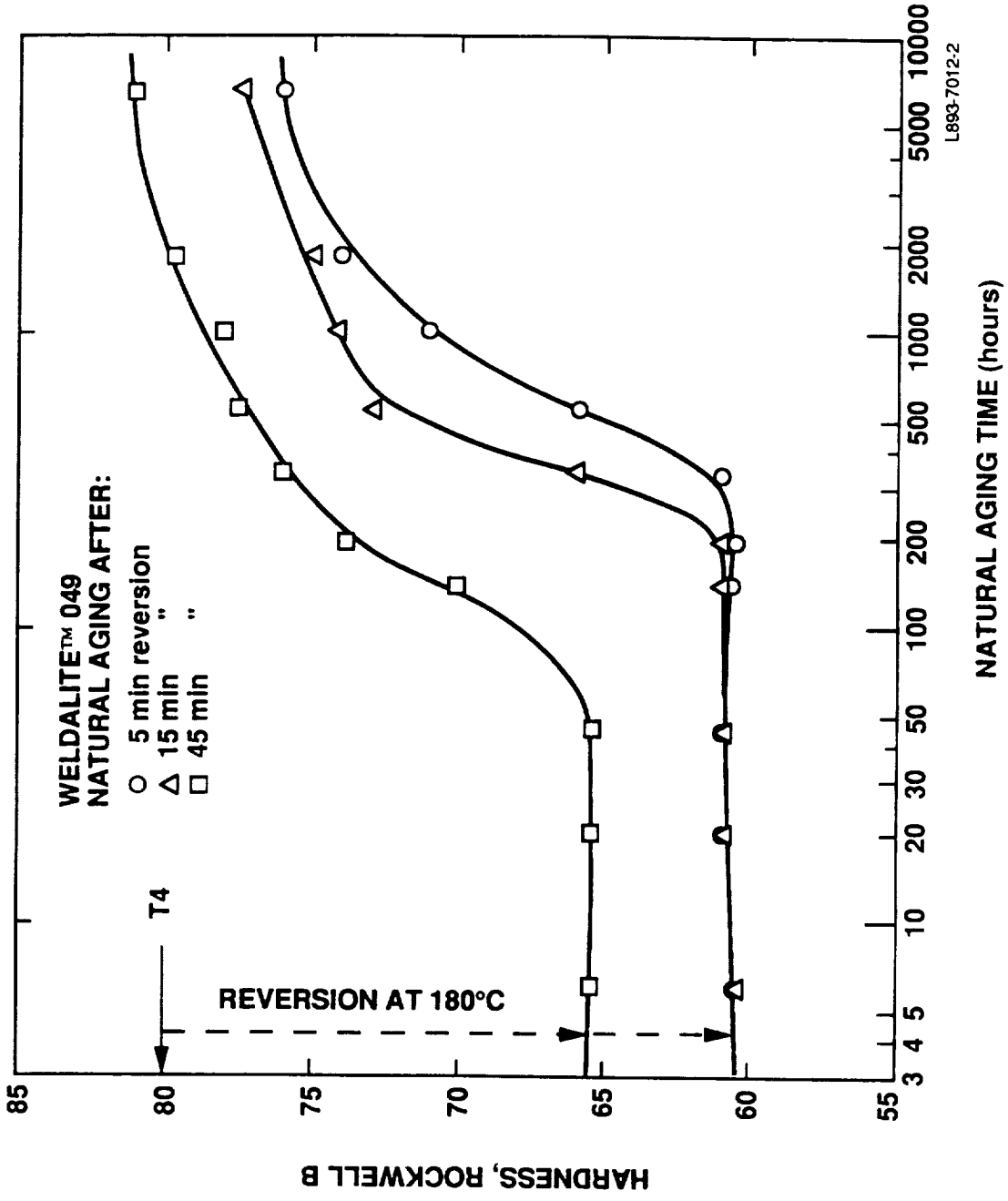

Figure 2 Natural aging response of Weldalite™ 049 after reversion at 180°C for 5, 15, and 45 minutes.

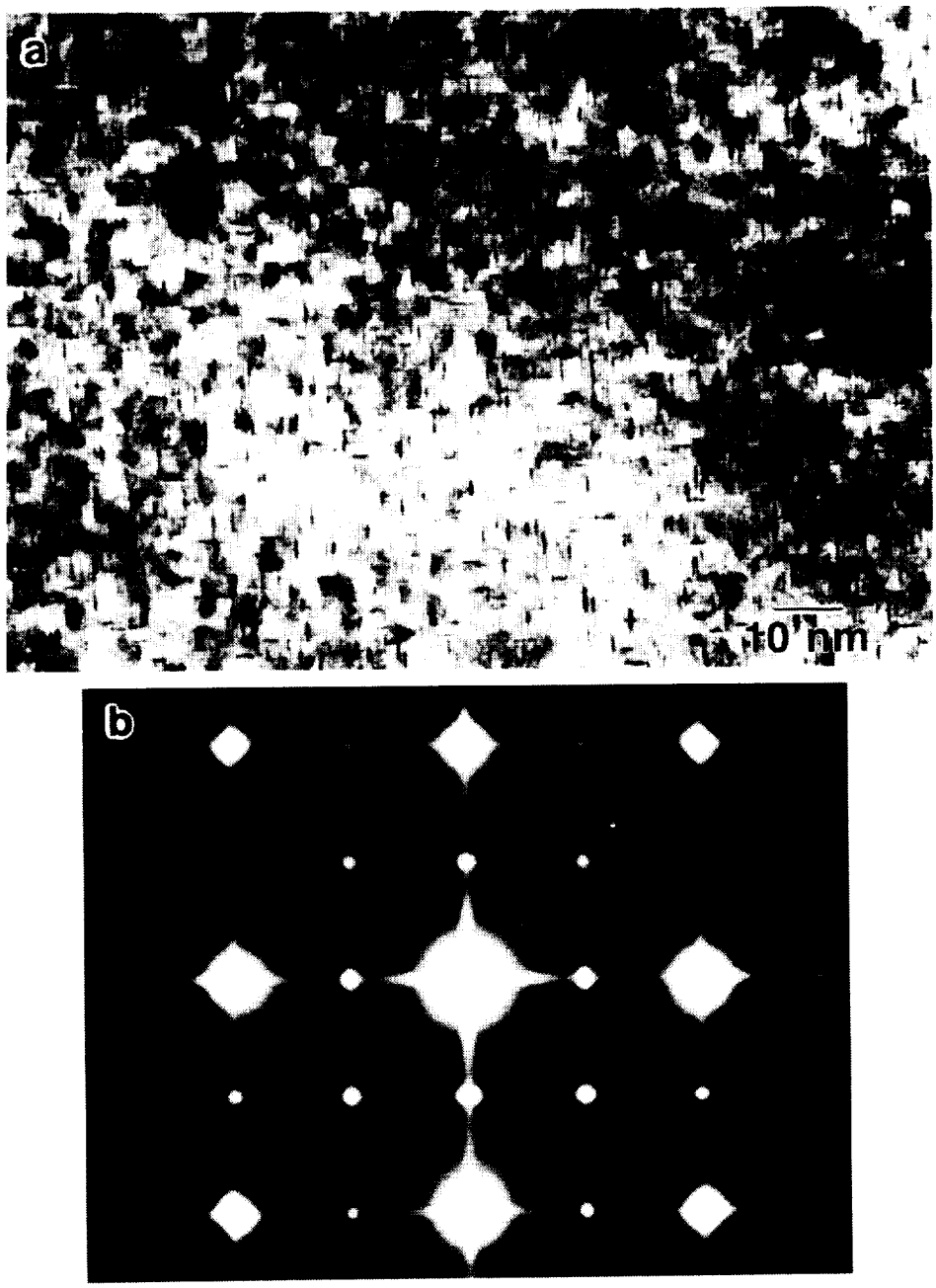

Figure 3 a) T4 microstructure consisting of fine but well-developed GP zones. The zones, lying on {100} matrix planes, are ~5 nm in diameter (TEM BF). b) B=001 selected area diffraction pattern which shows streaking associated with zones and superlattice reflections associated with δ'.

place), the structure reveals a coarser GP zone structure than for the T4 condition (Fig.4a). GP zones are now ~9-13 nm in diameter. The SADP contains continuous streaks without maxima, showing that the zones are still predominantly mono-layer GP1 zones. Multi-layered θ" (or GP2 zones), if present, would show streaks with intensity maxima developing at {100} locations [8]. The GP zones are homogeneously distributed, though the Zr-rich α' phase serves as a preferred nucleation site for the zones as well (arrow in Fig.4a). Additionally, the SADP gives little or no indication of superlattice reflections; thus the δ' has dissolved during reversion.

A 45 minute reversion sample was examined by TEM after 6400 hours of room temperature re-aging; at this point the material has regained its original T4 hardness. The structure contains a duplex GP zone population (Fig.5a), with larger zones (12-15 nm) resulting from growth of zones that were present after the reversion, and smaller zones (~2.5-5 nm) that nucleated during re-aging. Additionally, δ' revealed in a superlattice dark field image (Fig.5b) is present in at least three morphologies: 1) homogeneous, 1-2 nm spheres, 2) a coating on α' particles, and 3) a coating on the faces of the larger GP zones.

The SADP (Fig. 5c) is indicative of this complex structure. The continuous streaks are due to GP zones, and superlattice reflections from δ' are again present. Further, the superlattice reflections, both {100} and {110} type, are bi-directionally streaked due to the platelike morphology of δ' that occurs when coating the faces of GP zones.

4.0 DISCUSSION

The alloy under study has an extraordinary natural aging response with strengths similar to those of many aerospace alloys that are artificially aged to peak strength. The strength is due to a combination of fine GP zones and δ'.

The GP zone structure is developed far beyond that of other Al-Cu based alloys. For example, Wyss and Sanders [9] have studied alloys 2419 (Al-6Cu-0.3Mn) and 2519 (Al-6Cu-0.3Mn-0.2Mg) in the T4 temper and found little zone formation in the former and accelerated zone formation and concomitant strength enhancement in the latter. The Mg effect was suggested to be due to 1) enhanced diffusion associated with higher vacancy concentration when Mg is present, or 2) the

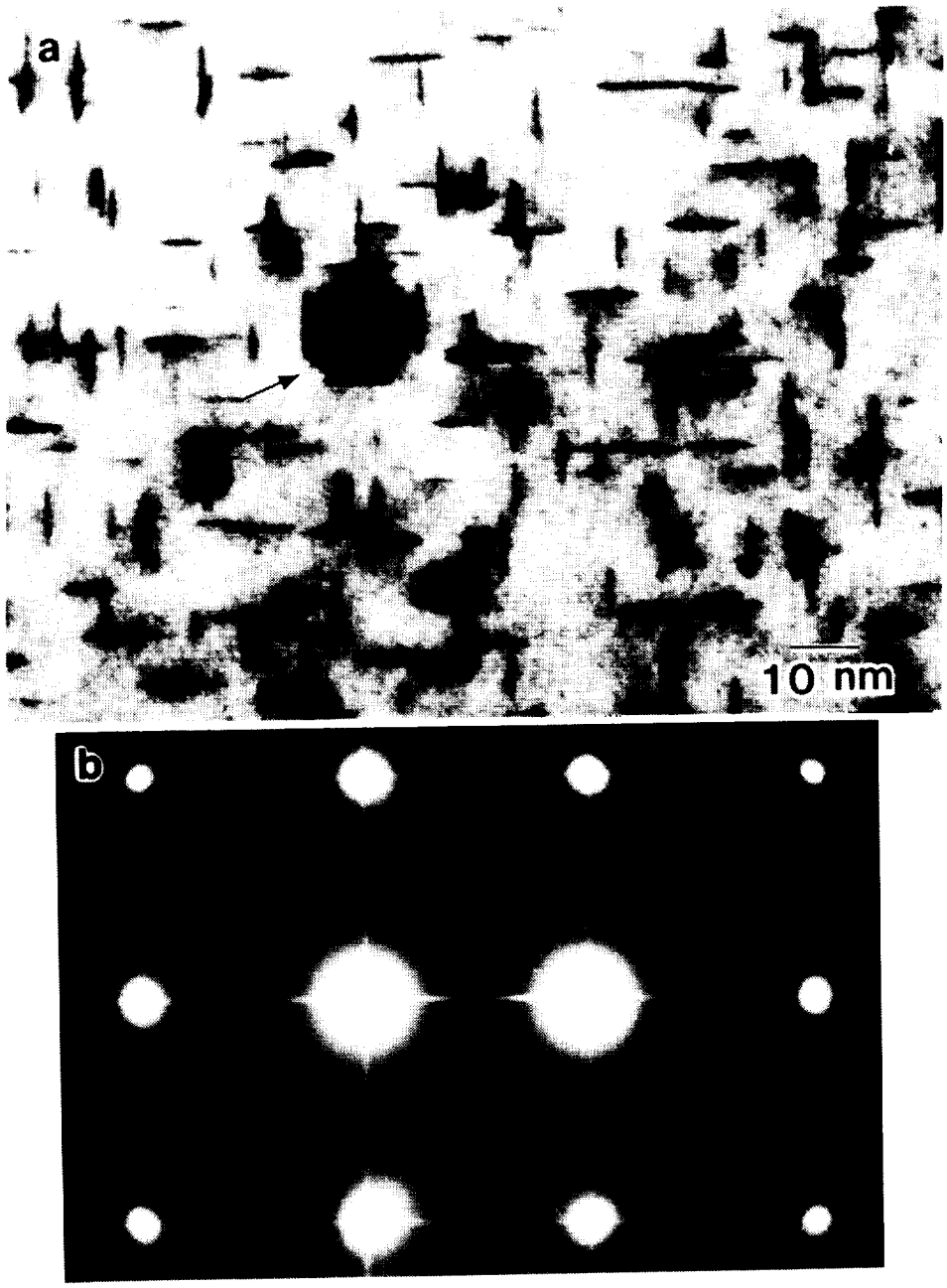

Figure 4 T4 temper, reverted 180°C/45 minutes and re-aged 24 h at room temperature (i.e., before significant re-aging has occurred). a) δ' has re-solutionized, leaving a coarser GP zone structure. Arrow indicates α' particle upon which GP zones heterogeneously nucleate. (TEM BF, B=001). b) Corresponding diffraction pattern containing continuous streaks and no δ' superlattice reflections.

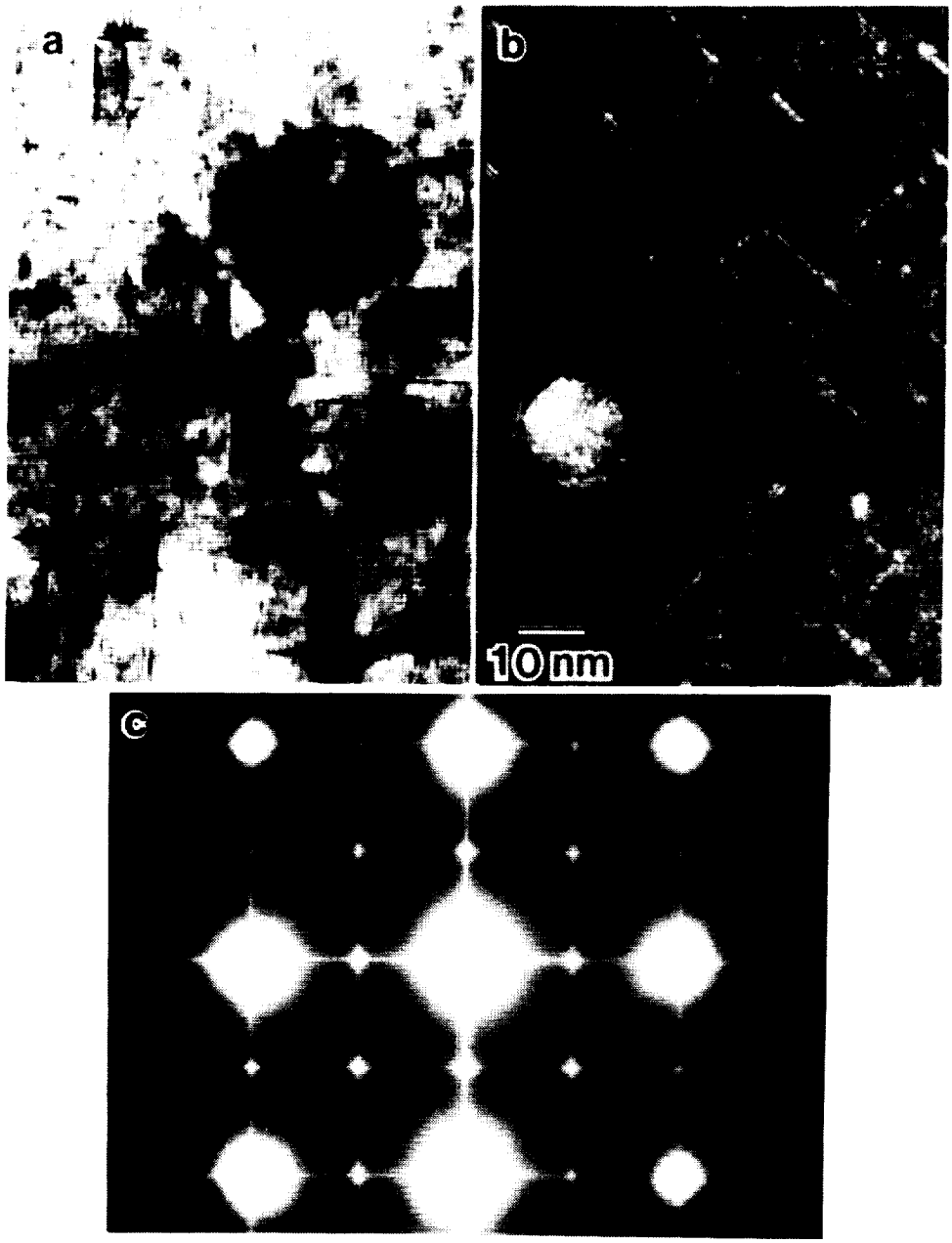

Figure 5 T4, reverted 180°C/45 min, re-aged 6400 h. at R.T. a) Two populations of GP zones, ~12-15 nm and 2.5-5 nm (BF TEM). b) g=110 dark field image showing δ' coating both sides of larger GP zones. δ' also appears as a coating on α' and as isolated 2nm spheres c) SADP shows streaking due to GP zones and superlattice spots due to δ'. Bi-directional streaking of the latter is due to plate-like nature of δ' on the faces of GP zones.

formation of Mg-vacancy complexes which serve as nucleation sites for GP zones.

In addition, Drits et al. [10] modified the Al-6.3Cu-0.3Mn Soviet alloy 1201 with minor Mg additions (0.05-0.12 wt.%) and observed dramatic increases in natural aging response. The standard 1201 alloy displayed a relatively small increase in yield strength of 19 MPa in 360 hours, whereas the alloy containing 0.12% Mg showed a rapid yield strength increase of 180 MPa in only 48 hours, and the strength was still increasing at 360 hours. The natural aging response increased monotonically with Mg content in the range studied. They explained the increase in strength by increased GP zone formation occurring at vacancy-impurity complexes, as previously proposed by Kelly and Nicholson [11]. Furthermore, Drits et al. imply that the high Mg-vacancy binding energy promotes the GP zone formation.

The present alloy exhibits far greater zone development than alloy 2519, based on both TEM images and streak development in SADPs. The Mg effect is likely similar to that observed in 2519 and Mg-bearing variants of alloy 1201. The contribution of Ag to this effect is being investigated in another study.

We propose a further effect to account for the rapid natural aging response -- a coupled growth of GP zones and δ'. The strain fields associated with each lead to a preferred juxtaposition of the two. In particular, δ,' which has a negative lattice misfit of ~0.08%, is favored in matrix compressive regions surrounding the perimeter of GP zones. Thus the energy barrier to nucleation associated with coherency strains (which are significant for coherent phases) would be reduced if the zones and δ' nucleated together or if either nucleated adjacent to the other. Preliminary dark field microscopy studies suggest the presence of such a relationship between δ' and zones of diameter <7 nm.

The reversion treatment lowers the yield strength by dissolving δ' and the fine GP zones. The coarser, lower density zone structure that remains is in a matrix with substantial Li and Cu supersaturation. With extended time at room temperature, fine GP zones and δ' re-precipitate, and original T4 strength returns, as shown in Table 1.

The microstructure after re-aging contains only two strengthening "phases", GP1 zones and δ', yet is quite complex. The GP zones, all on {100} planes, take three distributions with two major populations:

1) homogeneous zones, 12-15 nm } remaining after
2) zones nucleated on α', 12-15 nm } reversion
3) homogeneous zones, 2.5-5 nm, precipitated during re-aging.

The δ' phase, although present as a small volume fraction, also takes at least three distributions:

1) homogeneous, 1-2 nm spheres
2) heterogeneous envelopes on α'
3) face coatings on larger GP1 zones.

Additionally, there is preliminary evidence suggesting that δ' takes a fourth morphology, surrounding the perimeter of the small GP zones.

The long delay before significant re-aging occurs after reversion is surprising, considering the rapid aging response following SHT. Factors contributing to the long incubation are likely the annealing out of excess vacancies during the original aging and reversion treatments, and the solute depletion associated with the coarse GP zones after reversion. However, an understanding of the trends of incubation time with reversion duration time requires further investigation.

The observations in the present study of GP zone nucleation on α', and δ' nucleation on the faces of large GP1 zones adds to the already large number of configurations in which coherent phases can exist in Al-Li-Cu-Mg-Zr systems and subsystems. In each of these cases, one coherent phase serves as a heterogeneous nucleation site for another coherent phase (See Table 2). This behavior suggests new opportunities for strengthening and alloy design in Al-Li alloys.

TABLE 2. Coherent interfaces serving as nucleation sites for second coherent phases in Al-Li-Cu-Mg-Zr subsystems.

Nucleating Phase Desig.	Formula	Second Phase	Notes	Reference
α' or β'	$Al_3(Zr,Li)$	δ'	- - -	5-7
α' or β'	$Al_3(Zr,Li)$	GP1	P	- -
α' or β'	$Al_3(Zr,Li)$	θ'	- - -	12
α' or β'	$Al_3(Zr,Li)$	T_1	- - -	13
δ'	Al_3Li	T_1	A	14
θ'	Al_2Cu	δ'	- - -	12,15
GP1	(Cu)	δ'	P,B	- -
GP1 or θ'	- -	δ'	- - -	16

Notes: P - Present work

A - The nucleation of T_1 is proposed to occur within δ'.

B - Although GP1 zones are not considered to be a thermodynamically distinct phase, they effectively provide a coherent interface with the matrix.

5. SUMMARY

The Al-Cu-Li-Ag-Mg alloy known as Weldalite™ 049 exhibits remarkable strength following natural aging. This strength arises from a refined GP zone and δ' structure. Reversion at 180°C results in the dissolution of both δ' and some GP zones, leading to a lower number density of larger (~12 nm) GP1 zones. Re-aging at room temperature restores the original T4 strength, but only after an extended incubation period. The re-aged alloy is strengthened by GP zones and δ'. The structure is complicated, with the zones and δ' each occurring in at least three different morphological distributions, including new observations of the preferential nucleation of δ' on GP zones and GP zones on α'.

Acknowledgments. We thank R.K. Wyss of Alcoa for providing the 2519 plate. Some of the data included in this work were obtained under sponsorship of the National Institute For Standards and Technnology (NIST) and the Martin-Marietta Emerging Technology Program. The use of trade or brand names in the text does not imply endorsement of the products by NIST.

6. REFERENCES

[1] J.R. Pickens, F.H. Heubaum, L.S. Kramer, and K.S. Kumar, US Patent Application Serial No. 07/327,927 filed March 23, 1989, which is a continuation-in-part (CIP) of serial No. 083,333 filed August 10, 1987.

[2] J.R. Pickens, F.H. Heubaum, T.J. Langan, and L.S. Kramer, in "Aluminum-Lithium Alloys" (Proceedings of the Fifth International Aluminum-Lithium Conference), T.H. Sanders and E.A. Starke, eds., MCE Publications Ltd., Birmingham, U.K., 1989, p. 1397.

[3] A. Guinier, Ann.Physique 12, 1939, p.161.

[4] G.D. Preston, Proc.Roy.Soc.A 167, 1938, p.526.

[5] F.W. Gayle and J.B. VanderSande, Scr.Metall. 18, 1984, p.473.

[6] P.J. Gregson and H.M. Flower, J.Mat.Sci.Letters 3, 1984, p.829.

[7] F.W. Gayle and J.B. VanderSande, Acta Metall. 37, 1989, p.1033.

[8] V.A. Phillips, Acta Metall. 23, 1975, pp.751-767.

[9] R.K. Wyss and R.E. Sanders, Met.Trans.A 19A, 1988, pp.2523-2530.

[10] A.M. Drits, N.A. Vorob'yev, A.M. Zinden, O.I. Voroshilova, Russ. Metall. 4, 1981, pp. 142-145.

[11] A. Kelly and R. Nicholson, "Precipitation Hardening," Progress in Materials Science 10, pp. 149-392.

[12] M.H. Tosten, A.K. Vasudevan, and P.R. Howell, Aluminum-Lithium Alloys III (edited by C. Baker, et al., Institute of Metals, London, 1986), p.483.

[13] M.H. Tosten and P.R. Howell, Aluminum Alloys: Their Physical and Mechanical Properties (ed. by E.A.Starke and T.H.Sanders, EMAS, London, 1986), pp.727-741.

[14] V. Radmilovic and G. Thomas, J. Physique (Paris) 48, Colloque 3, 1987, p.C3-385.

[15] J.C. Huang and A.J. Ardell, Aluminum-Lithium Alloys III (edited by C. Baker, et al., Institute of Metals, London, 1986), p. 455.

[16] R. DeJesus and A.J. Ardell, in "Aluminum-Lithium Alloys" (Proceedings of the Fifth International Aluminum-Lithium Conference), T.H. Sanders and E.A. Starke, eds., MCE Publications Ltd., Birmingham, U.K., 1989, p. 1397.

II. STRUCTURE AND PROPERTIES DURING AGING OF AN Al-Cu-Li-Ag-Mg ALLOY, WELDALITE™049

Frank W. Gayle, Frank H. Heubaum, and Joseph R. Pickens

1. INTRODUCTION

An Al-Cu-Li-Ag-Mg alloy Weldalite™ 049 was recently introduced as an ultra-high strength alloy (700 MPa yield strength in artificially aged tempers) with good weldability (1). In addition, the alloy exhibits an extraordinary natural aging response (440 MPa yield strength (YS) in the unstretched condition) and a high ductility reversion condition which may be useful as a cold-forming temper (1,2). In contrast to other Al-Li alloys, these properties can essentially be obtained with or without a stretch or other coldworking operation prior to aging.

Preliminary studies have revealed that the T4 temper (no stretch, natural age) is strengthened by a combination of GP zones and δ' (Al_3Li) (2). The T6 temper (no stretch, aged at 180°C to peak strength) was reported to be strengthened primarily by the T_1 phase (Al_2CuLi) with a minor presence of a θ'-like (Al_2Cu) phase (3). On the other hand, a similar but lower solute-containing alloy was reported to contain Ω, (stoichiometry unknown), θ', and S' in the peak strength condition (4). The purpose of the present study is to further elucidate the strengthening phases in Weldalite™ 049 in the unstretched tempers, and to follow the development of the microstructure from the T4 temper through reversion (180°C for 5-45 minutes) to the T6 temper.

2. EXPERIMENTAL PROCEDURE

The alloy was examined in two product forms, sheet and extruded bar, with the compositions given in Table 1. The alloys were heat treated as follows: solutionized at 503°C for 1 hour, quenched in cold water, and allowed to naturally age at room temperature to the T4 condition. (The T4 temper was defined as >1000 hours at ambient temperature and was used as the starting condition for all artificially aged tempers.) Artificial aging was carried out by heating specimens in a circulating air furnace at 180°C. The sheet specimens were used for the T4 and reversion studies, whereas extrusions were examined in other aged conditions.

Specimens for transmission electron microscopy (TEM) analysis were twin-jet electropolished at -20°C and 12 volts in a solution of 30% HNO_3 in methanol. After polishing, the specimens were dipped in a solution of 50% HNO_3 in H_2O to remove superficial Ag which had re-deposited from the electrolyte during polishing.

TABLE 1

Alloy Compositions (wt.%)

Form	Cu	Li	Mg	Ag	Zr	Si	Fe
Sheet	6.0	1.3	0.4	0.4	0.18	0.04	0.05
Extruded bar	4.50	1.16	0.36	0.37	0.13	0.01	0.03

3. RESULTS

The aging response was monitored using Rockwell B hardness measurements. Natural aging resulted in a very high T4 hardness, R_B 80, corresponding to a tensile strength of about 585 MPa. A short artificial aging period, e.g., 5-45 minutes at 180°C, then led to a reversion with associated loss of hardness (see Figure 1). Further aging at 180°C for 16-24 hours resulted in peak hardness. Also shown in Figure 1 (dashed curve) is the *room temperature* aging response after a reversion treatment (45 minutes at 180°C. It is clear that after reversion the alloy re-ages at room temperature back to the T4 hardness level, albeit only after an extended incubation period. Typical tensile properties for various conditions are extremely high, as shown in Table 2.

TABLE 2

Longitudinal Tensile Properties
(25 mm gauge; $\dot{\varepsilon} = 3 \times 10^{-4}\ s^{-1}$)

Temper	Aging Practice	YS MPa	UTS MPa	El. %
T4	RT/1000 h	438	585	15.5
Reversion	180°C/15 min	280	480	25.5
Revert/re-age	180°C + RT/10^4h	440	610	11.0
T6	180°C/24 h	680	720	4.0

RT = room temperature

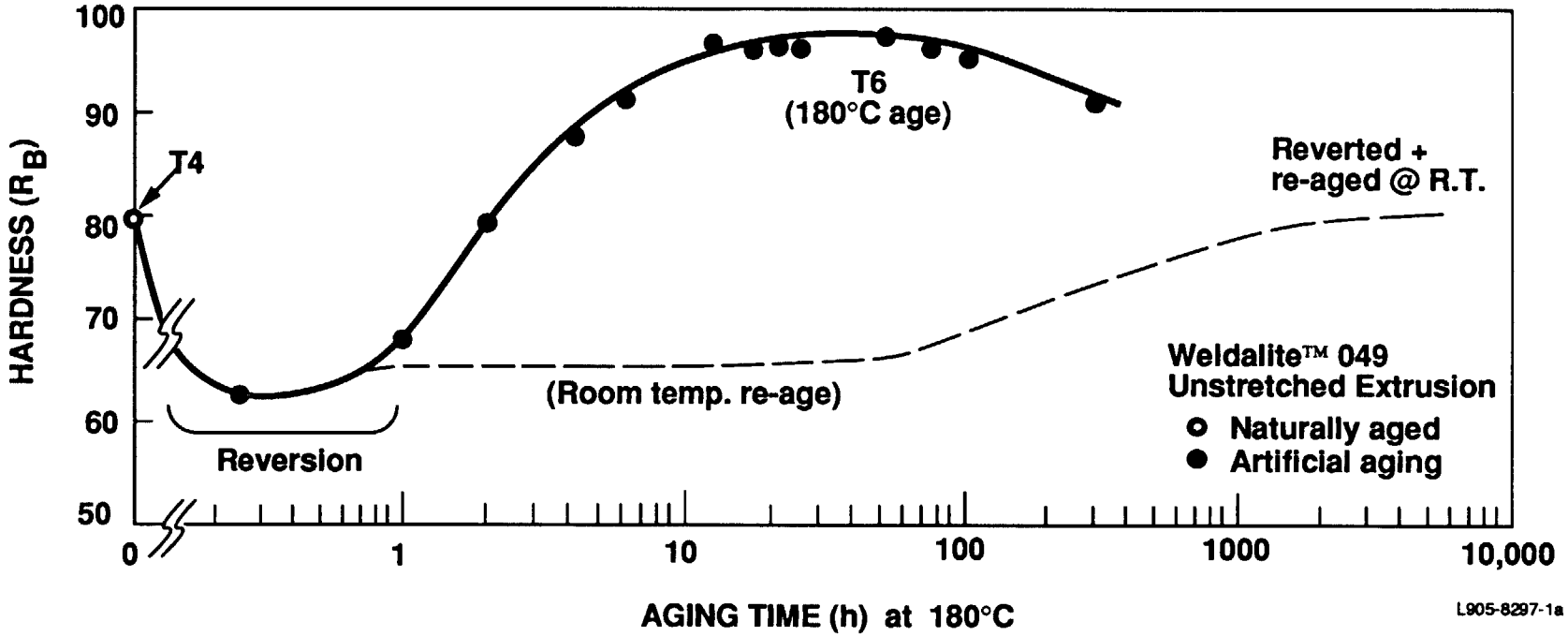

Figure 1 Aging curve at 180°C (Rockwell B hardness) from T4 to overaged condition. Also shown (dashed) is the natural aging response of the alloy following a reversion treatment of 180°C/45 minutes, showing that after an extended incubation period, re-aging at room temperature results in a return of T4 hardness.

The T4 structure exhibited a remarkably well-developed GP zone structure (Fig.2a) compared with other aluminum alloys aged at room temperature. Continuity of <100> streaks in the diffraction patterns indicates that these are classical GPI zones consisting of monolayers of Cu lying in disks on {100} matrix planes (5). δ' was also present, both as 1-2 nm spheres in a very fine uniform distribution, and as characteristic envelopes surrounding the Zr-rich α' similar to that seen in Zr-bearing higher-lithium alloys (6,7).

The reversion treatment was found to dissolve δ' and coarsen the GP zone structure. Re-aging at room temperature reprecipitated δ' and additional very fine GP zones (Fig. 3), resulting in a complex microstructure. The GP zones, all lying on {100} planes, exist in three distributions with two major populations:

1) homogeneously nucleated zones, 12-15 nm } remaining after
2) zones nucleated on α', 12-15 nm } reversion
3) homogeneously nucleated zones, 2.5-5 nm, precipitated during re-aging.

The δ' phase, although present as a small volume fraction, also assumed at least three distributions:

1) uniformly distributed, 1-2 nm spheres
2) heterogeneously nucleated envelopes on α'
3) coating the faces of larger GPI zones.

Artificial aging beyond 45 minutes brought the alloy out of the reversion well. After aging at 180°C for two hours (Figure 4), the structure contained a wealth of precipitate phases: GPI zones (minor volume fraction), θ' (Al_2Cu plates lying on {100}), T_1 (Al_2CuLi plates lying on {111}), and S' (Al_2CuMg laths on {210} extended in <001> directions). Continued aging to peak strength and beyond (16-48 hours) dissolved the GP zones leaving θ', T_1, and S' in substantial numbers, with T_1 appearing as the largest volume fraction. In the T6 condition, the precipitates remain quite thin and in a good dispersion, with T_1 typically one unit cell in thickness, and θ' and S' less than 2-3 nm in thickness.

An additional unidentified precipitate was observed (Fig. 5) for aging times from 2 to 48 hours. This precipitate lies on $\{110\}_{matrix}$

Figure 2 T4 structure, showing advanced GP zone structure (TEM BF). Continuous streaks in the SADP indicate the zones are GPI zones.

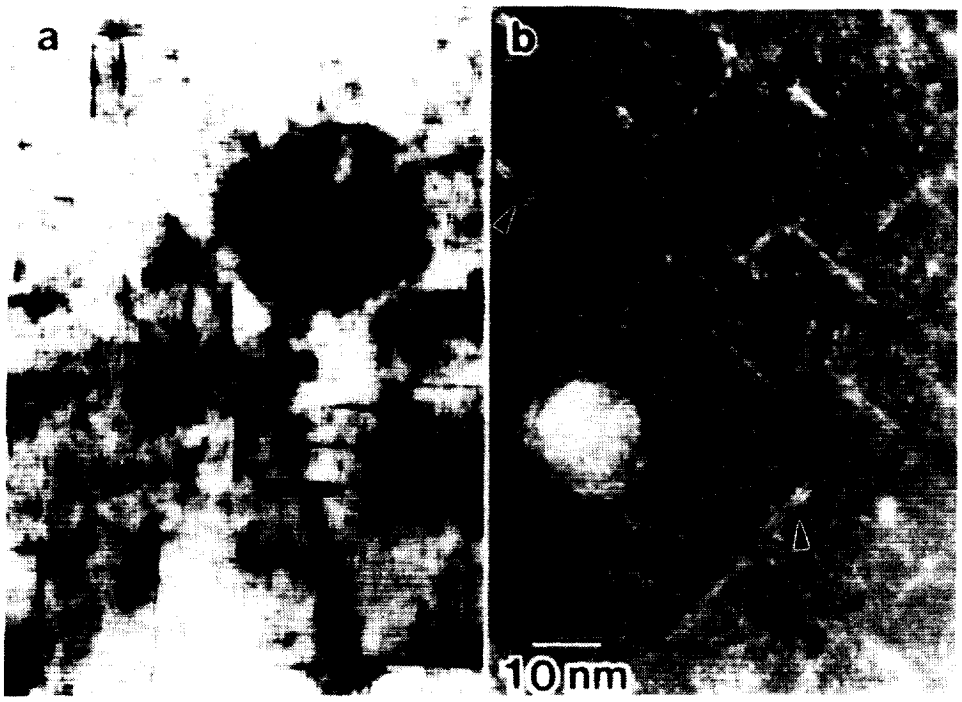

Figure 3 Microstructure after reversion (180°C/45 min) and re-aging at room temperature for 6400 hours. a) Bright field image showing very fine, duplex GP zone structure. b) Superlattice dark field image showing various distributions of δ', including the precipitation of δ' on the faces of larger GP zones (arrows). Large $L1_2$-ordered α' dispersoid is also imaged brightly.

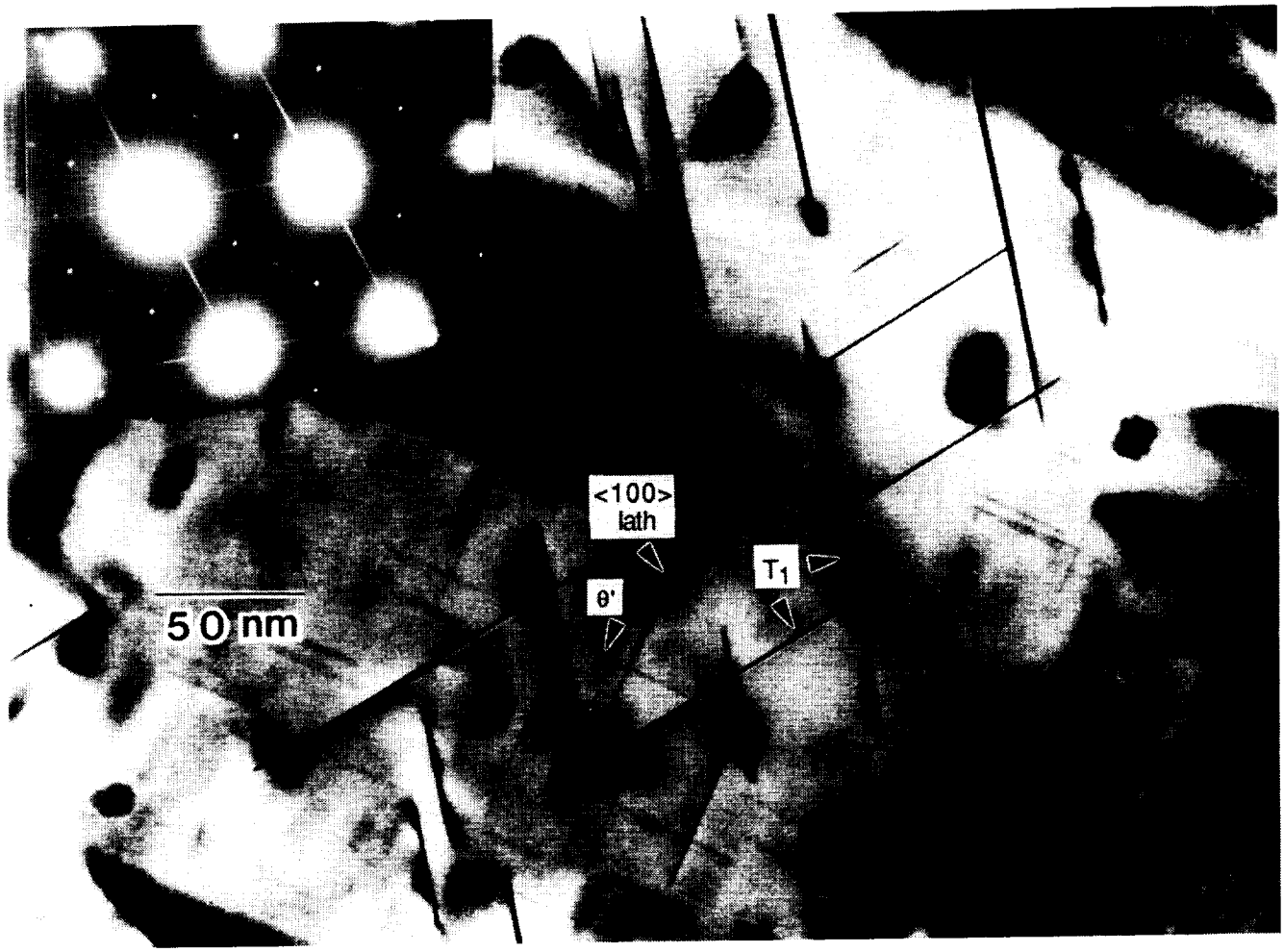

Figure 4 Aged 180°C/2 hours, showing T_1 lying on {111}, θ' lying on {100}, and laths extending in the [100] direction (Beam direction B=[011]).

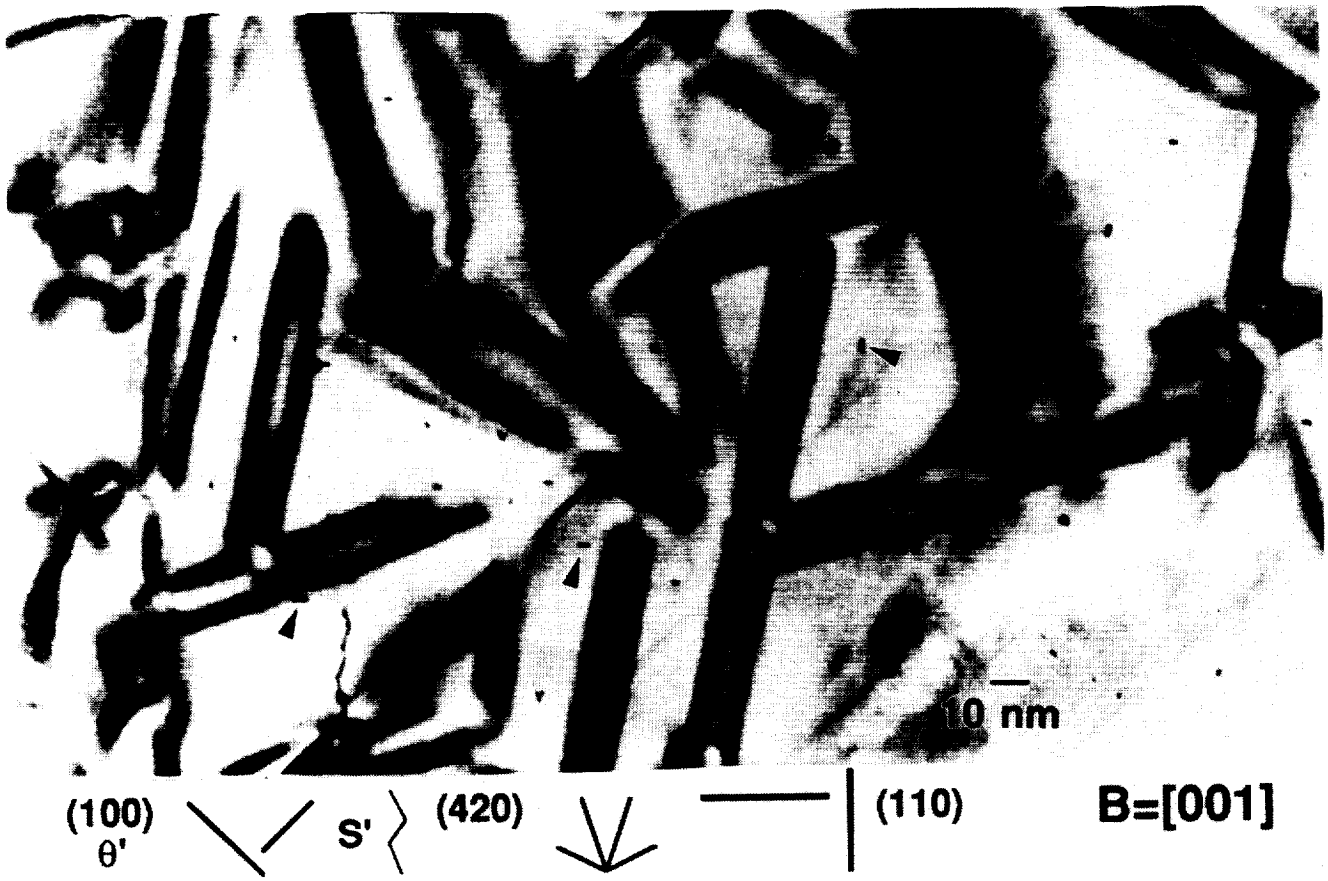

Figure 5 Aged 180°C/2 hours, showing S', lying on {210} planes, and another lath-like phase (arrows) lying on {110} planes (θ' plates on [100] planes are also visible. Wide, dark bands are T_1 plates viewed at an oblique angle.) (B=[001]).

planes, appearing as laths extending in <001> $_{matrix}$ directions. The precipitate remained very small for all aging times from 2 to 48 hours, with cross sections of 1.5 x 4.5 nm when observed end on.

A summary of the precipitate distribution as a function of aging condition is given in Figure 6. For heuristic purposes, the proposed new phase described above is designated by the Greek letter ν.

4. DISCUSSION

Weldalite™ 049 shows extraordinary T4 hardness and strength, comparable to many aerospace alloys artificially aged to peak strength. The strength is derived from a very well developed GP zone structure and the precipitation of δ'. Accelerated zone formation has been reported in Al-6Cu-0.3Mn alloys with 0.02-0.12 Mg (8) and 0.18 Mg (9) additions, and was attributed to enhanced nucleation at Mg-vacancy complexes, as previously proposed by Kelly and Nicholson (5). It is likely that Mg produces a similar effect in Weldalite™ 049. That is, the Mg atoms enhance the equilibrium vacancy concentration during solution heat treatment and help retain the vacancies through the quenching operation. These vacancies may provide a dual beneficial effect on T4 properties -- enhanced nucleation and also increased diffusivity. Whether this natural aging process is enhanced by the presence of Ag is being addressed in another study.

Room temperature precipitation of GP zones and δ' after the reversion treatment is in part made possible by the reduction in solubility of Cu and Li upon cooling from 180°C to room temperature. The long delay before a significant increase in strength upon subsequent natural aging is unexpected at first glance, considering the rapid aging response following solution heat treatment. However, the annealing out of quenched-in excess vacancies during the original aging and reversion treatments, and solute depletion associated with the coarser GP zones present after reversion likely contribute to the long incubation period.

It should be noted that all GP zones observed in this alloy are believed to be GPI zones based on the continuous nature of <100> streaks in the diffraction patterns. In the classical view (5), GPI zones are monolayers of nearly pure Cu lying in disks on {100} matrix planes. To our knowledge, this alloy system is the first one in which GPI zone nucleation on the Zr-rich α' dispersoid is reported. The unusual post-

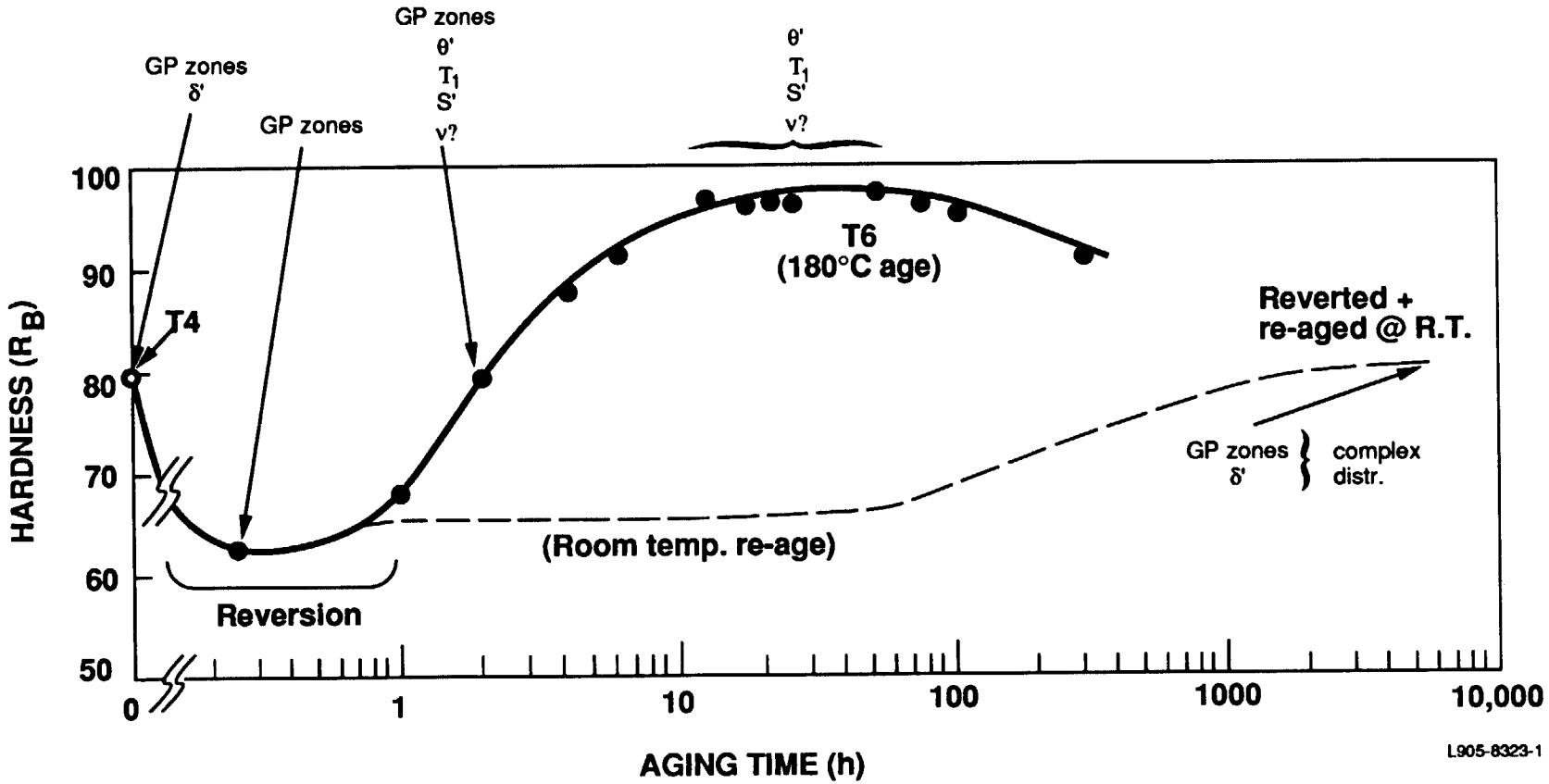

Figure 6 Summary of aging sequence: Aging curve and associated strengthening precipitates.

reversion precipitation of δ' on the faces of the larger GP zones during room temperature aging is not unique; in addition to the Weldalite™ alloy system (2), DeJesus and Ardell (11) have recently seen similar behavior in the higher Li-containing alloy 2090 (Al-2.7Cu-2.3Li-0.12Zr) after natural aging. These observations are but two new additions to the many examples (2) of heterogeneous nucleation of coherent phases in Al-Li-(Cu,Mg,Zr) systems.

The 2 hour aging treatment yields a transition state in which GP zones are still present along with the various strengthening phases that are present in the T6 temper. Longer artificial aging times produce the T6 structure, which is strengthened by a combination of several phases, including θ', S', and T_1. The T6 condition may indeed represent a metastable six-phase equilibrium between the aluminum alloy matrix, several strengthening precipitates (θ', T_1, S' and ν), and the dispersoid α'. (Six phases in stable or metastable equilibrium over a range of temperature is the maximum allowed by Gibbs' phase rule in a six component system.) T_1 is likely the dominant strengthening phase, based on apparent number density, morphology and distribution.

In Al-Cu-Mg alloys S' is reported to assume two different habits. In the first, the precipitates occur as laths lying on {210} planes, extending in <001> directions (11, 12). Corrugated precipitate sheets approximating a {110} plane may form from two or more variants lying on {210} planes with a common <100> direction. The other habit is rodlike, extending in {100} directions, with some tendency to cluster on {110} planes (13).

The proposed ν phase has characteristics similar to S'. Both phases are lath-like with the longest dimension extending in the $<100>_{matrix}$ direction. However, a clear distinction between the two phases exists, as shown in Figure 5. The laths visible in this B=[100] micrograph are all viewed end-on, with the length projected into the plane of the photomicrograph. The S' is visible both as individual laths lying on {210} planes, and as the occasional corrugated sheet which is composed of two {210} variants. This corrugated sheet approximates a {110} habit plane. Also seen are laths which lie on {110} planes. These laths are 1.5 nm in thickness by 4.5 nm in width, and appear as individual laths with a {110} habit rather than corrugated composites of S'. Therefore, these individual laths with a {110} habit are either a new phase, or else S' with a new habit and/or a new orientation relationship with the matrix. For very small precipitates, e.g., 1-5 unit

cells in the smallest dimension, interfacial energy is a predominant factor in determining the morphology. Generally, one habit will be at least slightly energetically more favorable than other possible habits and will predominate to the exclusion of the others. For similar thermodynamic reasons, it is unlikely that there is more than one orientation relationship with the matrix. Thus the observation of two habit planes ({210} and {110}) in a single microstructure wherein the precipitates are on the order of 2-3 unit cells in thickness suggests the presence of two distinct lath-like phases. Consideration has also been given to the possibility that the (110) precipitate is due to impurity effects, for example that v is high enough that it is unlikely that trace impurities are responsible. Clearly, further work must be undertaken to determine whether a new phase is indeed present.

5. CONCLUSIONS

The Al-Cu-Li-Ag-Mg alloy Weldalite™ 049 exhibits a series of unusual and technologically useful combinations of mechanical properties in different aging conditions:

1. Natural aging without prior cold work to high strength (438 MPa YS, 585 MPA UTS),

2. A reversion temper of lower yield strength and unusually high ductility (25% elongation),

3. Room temperature re-aging of the reversion temper eventually leading to original T4 hardness, and

4. Ultra-high strength T6 properties (680 MPa YS, 720 MPA UTS).

Corresponding microstructures found to be responsible for these properties are:

1. Unusually well developed GP zone structure coupled with δ' in T4 temper,

2. Dissolution of δ' and coarsening (and some dissolution) of GP zones in reversion temper,

3. Reprecipitation of fine GP zones and δ' upon reversion plus natural aging,

4. A combination of several strengthening precipitates, including S', θ', and T_1 in the T6 temper.

In addition there is evidence of a fourth, previously unidentified precipitate, present as very thin laths on {110} planes, in the T6-type conditions. The persistence of these phases (plus the Zr-rich α') in the slightly overaged condition suggests the T6 condition may represent a metastable equilibrium between six phases.

6. ACKNOWLEDGEMENTS

Some of the data included in this section were obtained under sponsorship of the Martin Marietta Emerging Technology Fund and The National Institutes for Science and Technology (NIST).

7. REFERENCES

[1] J.R. Pickens, F.H. Heubaum, T.J. Langan, and L.S. Kramer, p.1397, Aluminum-Lithium Alloys (Proceedings of the Fifth International Aluminum-Lithium Conference, T.H. Sanders and E.A.Starke, eds., MCE Publications, Ltd, Birmingham, U.K., 1989).

[2] F.W. Gayle, J.R. Pickens, and F.H. Heubaum, ibid., p. 701.

[3] T.J. Langan and J.R. Pickens, ibid., p.691.

[4] I.J. Polmear and R.J. Chester, Scr. Metall. 23, 1213 (1989).

[5] A. Kelly and R. Nicholson, Progress in Materials Science, 10, 149 (1963).

[6] F.W. Gayle and J.B. VanderSande, Scr.Metall. 18, 473 (1984).

[7] P.J. Gregson and H.M. Flower, J.Mat.Sci.Letters 3, 829 (1984).

[8] A.M.Drits, N.A. Vorob'yev, A.M. Zinden, O.I. Voroshilova, Russ. Metall. 4, 142 (1981).

[9] R.K. Wyss and R.E. Sanders, Met.Trans.A 19A, 1988,pp.2523-2530.

[10] R. DeJesus and A.J. Ardell, Aluminum-Lithium Alloys, op.cit., p.661.

[11] A. Kelly and R. Nicholson, "Precipitation Hardening," Progress in Materials Science 10,pp. 149-392.

[12] R.N. Wilson and P.G. Partridge, Acta Metall. 13, 1321 (1965).

[13] V. Radmilovic, G. Thomas, G.J. Shiflet, and E.A. Starke, Scr. Metall. 23, 1141 (1989).

[14] A.K. Gupta, P. Gaunt, and M.C. Chaturvedi, Phil.Mag.A 55, 375 (1987).

III. EFFECT OF A PRIOR STRETCH ON THE AGING RESPONSE OF AN Al-Cu-Li-Ag-Mg-Zr ALLOY

K.S. Kumar, S.A. Brown, and J.R. Pickens

1. INTRODUCTION

Recently, a family of Al-Cu-Li alloys containing minor amounts of Ag, Mg, and Zr and having desirable combinations of strength and toughness has been developed (1). These "Weldalite™" alloys exhibit a unique characteristic in that with or without a prior stretch, they obtain significant strength-ductility combinations upon natural and artificial aging. The ultra-high strength (~690 MPa yield strength) in the peak-aged tempers (T6, T8) has been primarily attributed to the extremely fine T_1 (Al_2CuLi) or T_1-type precipitates that occur in these alloys during artificial aging (2), whereas the significant natural aging response observed is attributed to strengthening from δ' (Al_3Li) and GP zones. (3) In recent work (4), the aging behavior of an Al-Cu-Li-Ag-Mg alloy without a prior stretch was followed microstructurally from the T4 to the T6 condition. Commercial extrusions, rolled plates, and sheets of Al-Cu-Li alloys are typically subjected to a stretching operation before artificial aging to straighten the extrusions and, more importantly, introduce dislocations to stimulate precipitation of strengthening phases such as T_1 by providing relatively low-energy nucleation sites (5,6).

The goals of this study are to examine the microstructure that evolves during aging of an alloy that was stretched after solution treatment and to compare the observations with those in sections I and II of this report for the unstretched alloy.

2. EXPERIMENTAL PROCEDURE

An extruded section of an aluminum alloy containing 5.3Cu-1.4Li-0.4Ag-0.4Mg-0.17Zr (wt%) and incorporating a 3% stretch was artificially aged at 160°C (433K) in a circulating air furnace. Prior to stretching, the extrusions were solutionized at 504°C (777K) for 1 h and water quenched to room temperature. The quenched and stretched material was allowed to age naturally at room temperature for >1000 hours to obtain the T3 condition.

The aging response was monitored using Rockwell B hardness measurements and select specimens along the aging curve [T3, T4 (without stretch), T4 + 15 min, T3 + 15 min, T3 + 2 h, T3 + 4 h, T3 + 20 h, and T3 + 100 h] were examined using transmission electron microscopy (TEM). Since the unstretched material in the previous

study (4) was aged at 180°C (453K), the stretched material in this study was also examined after exposure at 180°C (453K) for 15 min to allow a direct comparison with the unstretched material as well as the stretched material exposed to 160°C (433K) for the same time.

Specimens to be analyzed by TEM were sliced from the extrusions and mechanically ground to the desired thickness. These were then twin jet electropolished to perforation at 243K and 12 - 15 volts in a solution of 25% HNO_3 in methanol. After polishing, the specimens were dipped in a solution of 50% HNO_3 in H_2O to remove any Ag which may have redeposited from the electrolyte. Selected area diffraction (SAD) and centered dark field imaging (CDF) were used to follow the microstructural evolution during aging. Due to space limitations, in most cases only SAD patterns are provided, although CDF was used in each instance to confirm SAD observations.

3. RESULTS

The change in hardness with aging time at temperature is shown in Fig. 1 for both, the stretched and unstretched material. As mentioned earlier, the stretched material was aged at 160°C (433K), whereas the unstretched material was aged at 180°C (453K).* Several interesting features are present in Fig. 1 including a higher hardness for the T4 than the T3 condition and a reversion for the T3 and T4 conditions upon artificial aging for ~15 - 45 minutes, although the loss in hardness is more dramatic for the T4 condition. Subsequent artificial aging leads to equivalent peak hardness for both the stretched (T3) and unstretched (T4) material, although the T4 material ages faster than the T3 material at the temperatures investigated. In both cases, a very high peak hardness (T6 or T8) of ~95 - 97 R_B is reached. A sample of the unstretched material was also aged for 15 min at 160°C (433K) to provide a direct comparison of the reversion behavior with that of the stretched material. In this case, the hardness was found to be intermediate between that of T4 + 15 min at 180°C (453K) and T3 + 15 min at 160°C (433K).

---

* [Strictly speaking, the T3 and T4 conditions, which are naturally aged conditions, cannot be plotted in Fig. 1; however, for the purpose of providing a reference, they have been plotted on the hardness axis (T3 and T4 should actually reflect zero time at temperature)].

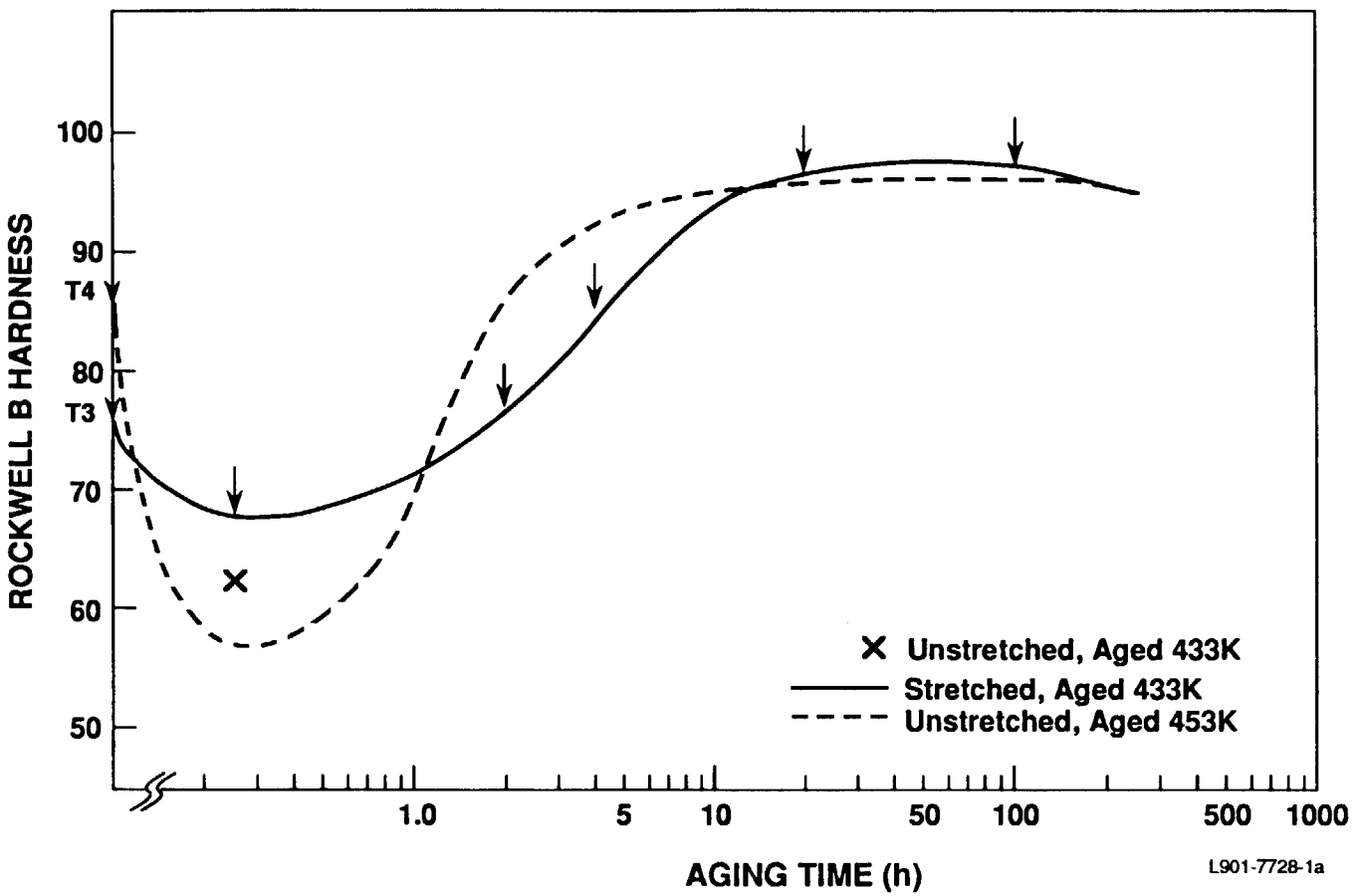

Figure1. Hardness variation with artificial aging time at 160°C (433K) for the stretched (T3) and at 180°C (453K) for the unstretched (T4) material.

The SAD patterns using a [110] zone axis for the T4 condition (Fig. 2a), and those after 15-min exposure to 160°C (433K) (Fig. 2b) or 180°C (453K) (Fig. 2c) show that a) the naturally aged microstructure consists of GP zones and θ', b) upon 15 min artificial aging at 160°C (433K), a significant amount of the δ' dissolves leaving a microstructure of some δ' and GP zones (Fig. 2b) in the aluminum solid solution, and c) 15 min artificial aging at the higher temperature of 180°C (453K) leaves a diffuse SAD pattern where <100> streaking due to the GP zones (Fig. 2c) can still be discerned.

Similarly, SAD patterns for the stretched material in the T3 condition and after aging for 15 minutes at 160°C (433K) and 180°C (453K) are compared in Figs. 3a-c. In the T3 condition (Fig. 3a), δ' (Al_3Li) spots are readily seen, although the GP zones, while present, are not as prominent as in the T4 condition (compare <100> streaking in Fig. 2a with Fig. 3a). Artificial aging at 160°C (433K) for 15 min results in the dissolution of GP zones and some δ'. In addition, θ' is possibly present as can be seen from the [100] zone axis SAD pattern in Fig. 3b. The strain and dislocation substructure introduced by the prior stretching operation make it difficult to obtain and interpret the diffraction patterns in this reverted condition. A [111] zone axis pattern of the material exposed to 180°C (453K) for 15 minutes (Fig. 3c) reveals the presence of T_1 precipitates, which suggests that this time at the higher temperature is sufficient to place the stretched material to the right of the reversion minimum on the aging curve (i.e., on the increasing hardness side). A hardness curve at this temperature for the T3 material is not shown in Fig. 1.

Microstructural evolution in the stretched material aged at 160°C (433K) for times longer than 15 min (i.e., to the right of the reversion minimum in Fig. 1) was followed on the transmission electron microscope using SAD (Figs. 4a-e). After 2 h at 160°C (433K), a [110] zone axis SAD pattern (Fig. 4a) reveals the presence of all four variants of the T_1 phase and in addition, <100> streaking typical of the θ' phase. The maximum in intensity at the mid point of the <100> streaks derives from θ' but is also coincident with a δ' superlattice reflection. In this case, the elliptical shape of this intensity maximum leads to the belief that this is a consequence of the θ' phase and not δ'.

A [100] zone axis SAD pattern (Fig. 4b) of the material exposed to 160°C (433K) for 4h reveals the presence of θ' in the form of <100>

Figure 2 SAD patterns of the unstretched material using a [110] zone axis for a) the T4, b) T4 + 15 min at 160°C (433K), and c) T4 + 15 min at 180°C (453K) conditions.

Figure 3. SAD patterns of the stretched material using a) [110] zone axis for the T3, b) [100] zone axis for the T3 + 160°C (433K), and c) [111] zone axis for the T3 + 180°C (453K) conditions.

(a)

(b)

(c)

Figure 4(a),(b),(c) SAD patterns of the stretched material using a) [110] zone axis for the T3 + 2 h, b) [100] zone axis for the T3 + 4 h, c) [112] zone axis for the T3 + 4 h.
(Figure 4 continued on next page)

ORIGINAL PAGE
BLACK AND WHITE PHOTOGRAPH

(e)

(d)

Figure 4(d),(e) SAD patterns of the stretched material using d) [110] zone axis for the T3 + 20 h, and e) [110] zone axis for the T3 + 102 h, at 160°C (433K).

streaks that intersect and give rise to a maximum in intensity that coincides with the superlattice reflection that would arise from δ'. However, the observed intensity is attributed to θ', again because of the shape of the bright spot, which appears as an intersection of two ellipses rather than a circular spot which is characteristic of the δ' phase. In addition to the θ' phase, symmetrically distributed around the <100> intersection maximum are the four spots corresponding to the T_1 variants. A [112] zone axis SAD pattern (Fig. 4c) of the 4 h specimen confirms the existence of the T_1 phase and also reveals faint streaking in the <210> directions. This family of streaks is attributed to the Al_2CuMg S' phase. Thus, after 4 h at 160°C (433K), the stretched material contains θ', T_1, and the S' phase. It must be specified that structure factor modifications due to compositional changes within the precipitate phases can account for modified diffraction spot intensities and work is currently in progress to measure the compositions of the individual phases.

Moving further up the aging curve, in the slightly underaged condition that corresponds to 20 h at 160°C (433K), an SAD pattern based on a [110] zone axis (Fig. 4d) reveals the presence of T_1 and θ'. The [112] zone axis SAD pattern confirms the presence of the S' phase.

In the overaged condition corresponding to a 102 h at 160°C (433K) (Fig. 4e), the T_1 phase is the only major strengthening phase present; the presence of <100> streaks corresponding to the θ' phase in this condition could not be reliably confirmed and, if present, is in only small amounts. Similarly, the <210> streaks due to the S' phase were not reliably confirmed.

A bright-field and a corresponding T_1 dark field micrograph in the slightly underaged condition of 20 h at 160°C (433K) are shown in Figs. 5a and 5b, respectively. Even in this near peak-aged condition, the T_1 precipitates are extremely fine and homogeneously distributed.

4. DISCUSSION

The observed higher hardness in the T4 condition compared to the T3 condition is attributed to the greater amount of GP zones in the former, although fine θ' and GP zones are present in both the T3 and T4 conditions. Likewise, the large drop in hardness upon reverting the T4 material at 180°C (453K) is associated with the dissolution of θ' and

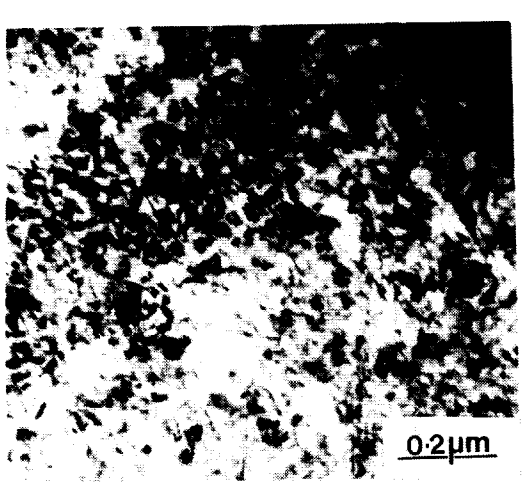

(a)

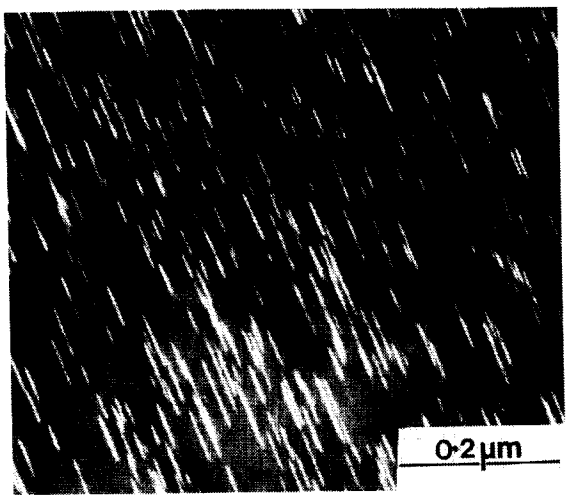

(b)

Figure 5 Typical microstructure in the near-peak-aged condition of T3 + 20 h at 160°C (433K) in a) bright field and b) T_I dark field.

some of the GP zones. The decrease in hardness for this material is not as dramatic when reversion is performed at 160°C (433K), where more GP zones are still present. A direct comparison of the reverted T4 with the reverted T3 material (433K) reveals that the hardness of the latter is higher. The exact reasons for this difference are unclear but must arise from a complicated interplay of the work-hardening residual from the stretch, δ' and what appears to be θ' precipitates.

In the underaged condition of 2 h at 160°C (433K), the stretched material contains the T_1 and θ' phases, which is in agreement with the recent work of Gayle et al. (4) on the unstretched material. However, they also found the S' phase (4) which, in this study, was observed after 4 h of aging the T3 specimens. In addition, Gayle et al. (4) provide evidence of a new phase, denoted ν, but we made no effort to locate it in this study. After 20 h at 160°C (433K), T_1, θ' and S' were present, whereas Langan and Pickens (2) observed only the T_1 phase in a similar alloy after 24 h at 160°C (433K). However, over-aging the stretched material in the present study at 160°C (433K) for 102 h causes the dissolution of both θ' and a significant amount of the S' phases leading to a microstructure which is predominantly strengthened by the T_1 phase dispersed in an a solid solution. Perhaps a significant amount of the θ' and S' dissolved after 24 h as observed earlier (2), even though they are present after 20 h at 160°C (433K) in this study.

The observed high strengths in these alloys in the naturally aged conditions (T3 and T4), are attributed to a combination of the fine δ' and GP zones. In the artificially aged conditions (T6 and T8) high strength is primarily a result of the extremely fine T_1 precipitates homogeneously distributed throughout the matrix.

Lithium, magnesium, and zirconium exhibit very high solute-vacancy binding energies in aluminum (7-9). Consequently, vacancies present at the solutionizing temperature are retained during quenching rather than migrating to sinks such as grain boundaries. For the specific case of binary Al-Li alloys, Suzuki et al. (10) suggest that excess vacancies bound to lithium atoms are confined to the δ' phase during aging. Excess vacancies may contribute to the precipitation process in Weldalite 049-type alloys by two mechanisms. First, when the δ' present during natural aging dissolves during reversion, the released vacancies may act as nucleation sites for the plate-like T_1 phase. Second, vacancies that were bound to Mg and Zr, as well as

released vacancies that are now likely bound to Li atoms, are unavailable to assist lattice diffusion, thereby retarding growth of T_1. Consequently, the vacancies are effectively utilized for enhancing nucleation and discouraging growth, which is consistent with the fine distribution of T_1 observed even in the overaged condition. The effects of such trace elemental additions on precipitation have been demonstrated previously (11, 12) in other aluminum alloys. In addition, the role of these trace elements such as Ag and Mg in influencing precipitate-matrix interfacial energies and/or the possibility of these elements segregating to the interface and acting as diffusional barriers cannot be ignored as both these factors can significantly affect precipitation kinetics.

Prior to significant δ' precipitation after quenching, the stretching operation introduces a significant number of dislocations which may act as vacancy sinks by sweeping vacancies away, thereby decreasing the vacancy concentration available for influencing the natural aging response. However, dislocations are also effective nucleation sites of the T_1 precipitates. That is, in the stretched material, heterogeneous nucleation on dislocations likely occurs in addition to the somewhat reduced nucleation frequency at vacancies in a way that approximately equals the nucleation at vacancies in the unstretched material.

5. CONCLUSIONS

The microstructural evolution during artificial aging of an Al-Cu-Li-Ag-Mg-Zr alloy has been characterized using TEM both with and without prior cold work. In the stretched and near-peak aged condition, a fine homogeneous distribution of T_1, θ' and S' phases is present in an a solid solution matrix, but on over-aging, virtually all of the θ' and most of the S' dissolve leaving behind a microstructure of essentially T_1 precipitates in an a aluminum solid solution matrix. It is suggested that trapped-in excess vacancies play a significant role in refining the microstructure by enhancing precipitate nucleation and discouraging their growth.

7. REFERENCES

[1] J.R. Pickens, F.H. Heubaum, T.J. Langan, and L.S. Kramer, in "Aluminum-Lithium Alloys" (Proceedings of the Fifth International Aluminum-Lithium Conference), T.H. Sanders and E.A. Starke, eds., MCE Publications Ltd., Birmingham, U.K., 1989, p. 1397.

[2] T.J. Langan and J.R. Pickens, ibid., p. 691.

[3] F.W. Gayle, F.H. Heubaum, and J.R. Pickens, op. cit., p. 701.

[4] F.W. Gayle, F.H. Heubaum, and J.R. Pickens, Scripta Metall., 24, 1990, p. 79.

[5] R.J. Rioja, P.E. Bretz, R.R. Sawtell, W.H. Hunt, and E.A. Ludwiczak, in "Aluminum Alloys, Their Physical and Mechanical Properties," Vol. III, Proceedings of the International Conference on Aluminum Alloys, Chameleon Press, London,U.K., 1986, p. 1781.

[6] W.A. Cassada, G.J. Shiflet, and E.A. Starke, Jr., J. de Physique, colloq. C3, Vol. 48, 1987, p. 397.

[7] M. Ahmad and T. Ericsson, Scripta Metall., 19, 1985, p. 457.

[8] S. Ozbilen and H.M. Flower, Acta Metall., 37, 1989, p. 2993.

[9] S. Ceresara, A. Giarada, and A. Sanchez, Philos. Mag., 35, 1977, p. 97.

[10] H. Suzuki, M. Kanno, and N. Hayashi, J. Jpn. Inst. Light Metals, 31, 1981, p. 122.

[11] B.C. Muddle and I.J. Polmear, Acta Metall., 37, 1989, p. 777.

[12] W.X. Feng, F.S. Lin, and E.A. Starke, Jr., Metall. Trans. A, 15, 1984, p. 1209.

N91-24408

IV. MICROSTRUCTURAL EVOLUTION DURING AGING OF AN Al-Cu-Li-Ag-Mg-Zr ALLOY

K.S. Kumar, S.A. Brown, and J.R. Pickens

I. INTRODUCTION

Alloys in the Al-Cu-Li Ag-Mg subsystems have been developed that exhibit desirable combinations of strength and ductility (1). These "Weldalite™" alloys, are unique for Al-Cu-Li alloys in that with or without a prior cold stretching operation, they obtain excellent strength-ductility combinations upon natural and artificial aging. This is significant because it enables complex, near-net shape products such as forgings and super-plastically-formed parts to be heat treated to ultra-high strengths. On the other hand, commercial extrusions, rolled plates and sheets of other Al-Cu-Li alloys are typically subjected to a cold-stretching operation before artificial aging to the highest strength tempers to introduce dislocations that provide low-energy nucleation sites for strengthening precipitates such as the T_1 phase (2,3).

The variation in yield strength (YS) with Li content in the near-peak aged condition for these Weldalite™ alloys was examined (4) and a peak in strength was observed at ~1.3 wt% Li. The associated microstructures were examined and it was proposed that the significant decrease in strength for alloys with Li content >1.3 wt% was due to the formation of δ' at the expense of the more potent strengthening phase T_1. Subsequently, research interest has centered around the "Weldalite™ 049" alloy which contains a nominal 1.3 wt. % Li. Microstructural development in Weldalite™ 049 with artificial aging has been reported, with and without a prior stretching operation (5-7). The ultra-high strength observed in this alloy in the peak-aged tempers (T6, T8) was attributed primarily to the homogeneously distributed fine T_1 phase, (4,5) although some θ' and S' were also observed (5,7). It was suggested that Ag, Mg and Zr may aid in trapping excess vacancies, thereby providing low energy nucleation sites for the precipitation of T_1, and discouraging lattice diffusion which decreases precipitate growth (5).

In this study, the microstructure in the naturally aged condition, as well as upon artificial aging for various times along the aging curve (Figure 1), has been examined for a Weldalite™ alloy containing a relatively high Li level (1.7 wt. %). The effect of a 3% stretch, prior to aging but immediately after solution treatment, on the resulting microstructure is reported. It is hoped that this study will allow the identification of processing parameters that can be modified to further improve the

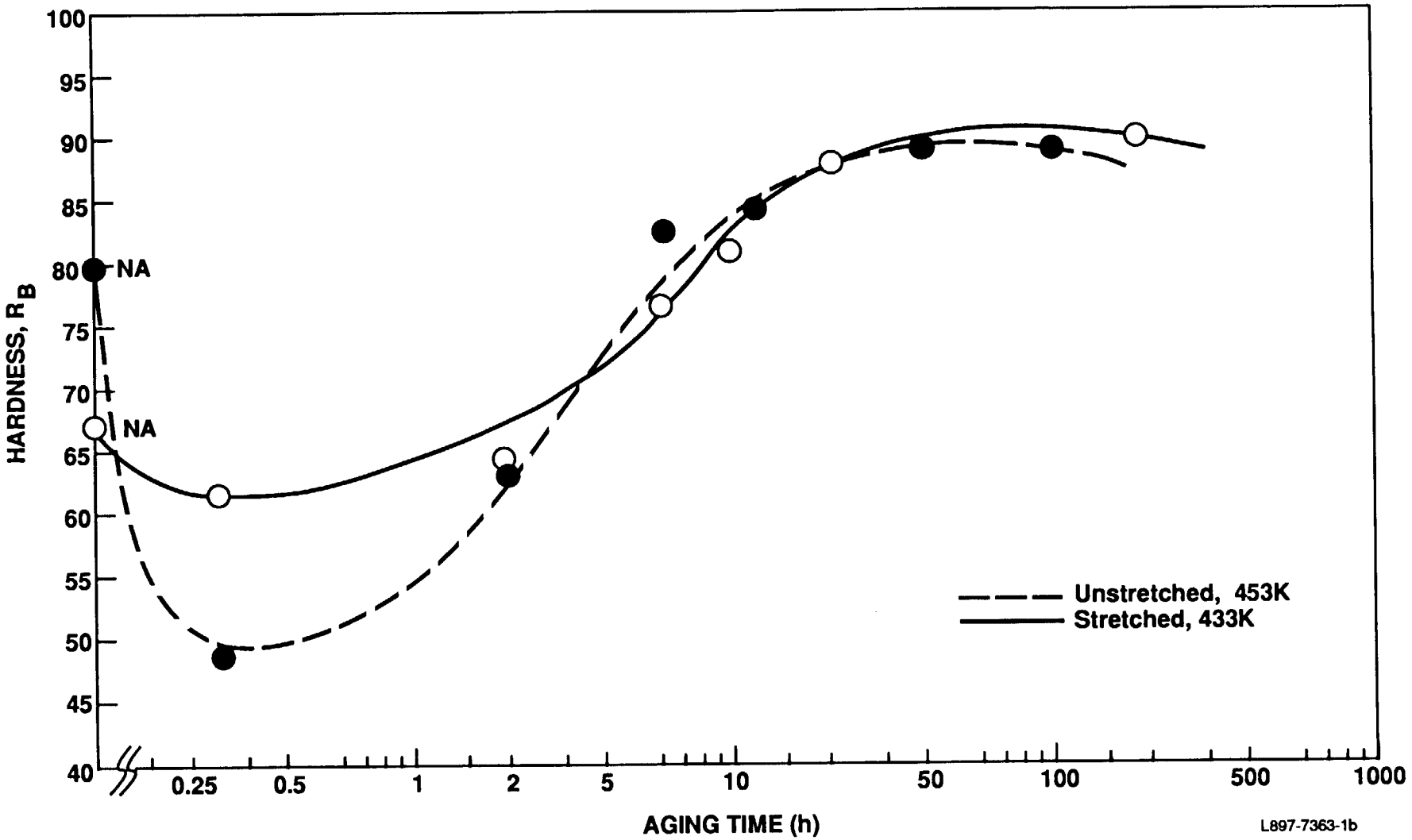

Figure 1 Isothermal aging response of the stretched and unstretched material at 433K and 453K respectively.

strength of this alloy which is more attractive than the 1.3 wt. % Li-containing alloy from a density point of view.

In such complex alloys, several metastable phases precipitate during aging. The crystallographic characteristics of these precipitates and the relationships they bear with the matrix are reviewed in the next section to provide the background for understanding the results obtained in this study.

2. PRECIPITATE CHARACTERISTICS IN THE Al-Cu-Li-Ag-Mg-Zr SYSTEM

The types of precipitates observed in such a complex system can be primarily divided into two categories. The first type are those that are stable equilibrium phases, their presence being determined by the alloy composition and the heat-treatment condition. These include binary phases such as Al_2Cu (θ), AlLi (δ), Al_3Zr (DO_{22}-type) and ternary precipitates like $T_1(Al_2CuLi)$, T_2 (Al_6CuLi_3), T_B (Al_7LiCu_4), $R(Al_5Li_3Cu)$ and S (Al_2CuMg). A large quantity of these primary phases, present from the cast and homogenized condition dissolve during the solutionizing treatment and are retained in supersaturated solid solution upon quenching, providing the driving force for precipitation of metastable phases upon subsequent aging. To maximize the alloy's capabilities in terms of its mechanical properties, it is critical to optimize the solution treatment temperature and time. Certain alloy compositions dictate the presence of excess primary phases even after optimal heat-treatment and in these cases some primary phases are carried through the entire thermal processing schedule. Whereas these primary phases, depending on the size, shape, and volume fraction can be deleterious to mechanical properties, especially toughness, they may enhance weldability (8).

While these primary phases are important, of greater significance to this paper are the metastable phases that result during aging. A list of these phases together with their morphology and habit planes is provided in Table I.

Since so many different metastable phases can be present in such alloys during aging, the corresponding SAD patterns tend to be complex. In this paper, the precipitation sequence has been characterized using SAD patterns predominantly with a [100], [110] or [112] matrix zone axis and the diffraction spots and streaks from these various

precipitates for the above orientations of the matrix are shown schematically in Figure 2.

Table I: Metastable Phases Found in the Al-Cu-Li-Ag-Mg-Zr System

Precipitate	Morphology	Habit Plane
(Al_3Zr)	Spherical	--
$\delta'(Al_3Li)$	Spherical	- -
GP Zones (Al-Cu)	Clusters	- -
$\theta'(Al_2Cu)$	Discs	{100}
$T_1(Al_2CuLi)$	Platelet	{111}
Ω(Al-Cu-Ag-Mg?)	Platelet	{111}
$S'(Al_2CuMg)$	Laths	{210}
ν	Laths	{110}

The Al_3Zr phase is metastable to the extent that it precipitates during solution-treatment with an $L1_2$ structure and a spherical morphology. The metastable $L1_2$ Al_3Zr precipitate in aluminum-lithium alloys has been variously referred to as β' or α' (9,10). The α' designation was proposed by Gayle and Vardersande (10) to indicate that Li atoms substitute for Zr atoms in this $L1_2$ precipitate in Al-Li-Zr alloys. Frequently, when Al_3Zr and δ' (Al_3Li) occur in a system simultaneously, they coprecipitate, with δ' precipitating around Al_3Zr. Dark field imaging of this "composite" precipitate causes the Al_3Li to preferentially illuminate(10,11) providing the commonly observed "donut" morphology. In addition, it was also shown (10) that in Al-Li-Zr alloys, Al_3Zr has solubility for some Li at the solution treatment temperature and could retain Li atoms in supersaturation after quenching.

The δ' precipitate has an $L1_2$ structure with a very small lattice parameter mismatch with the matrix. It has a cube-on-cube orientation relationship with the matrix with $(111)\delta' \parallel (111)Al$. The $L1_2$ structure, in addition to the fcc spots, will exhibit the superlattice reflections such as (100) and (110). This is seen clearly in Figure 2 where the zone axis is [100]. Likewise, for B=[110], the δ' spots occur at the intersection of diagonals of a rhombus described by four adjacent matrix spots. When B=[112], the δ' spots line up as vertical rows midway between the matrix rows and lying on the same

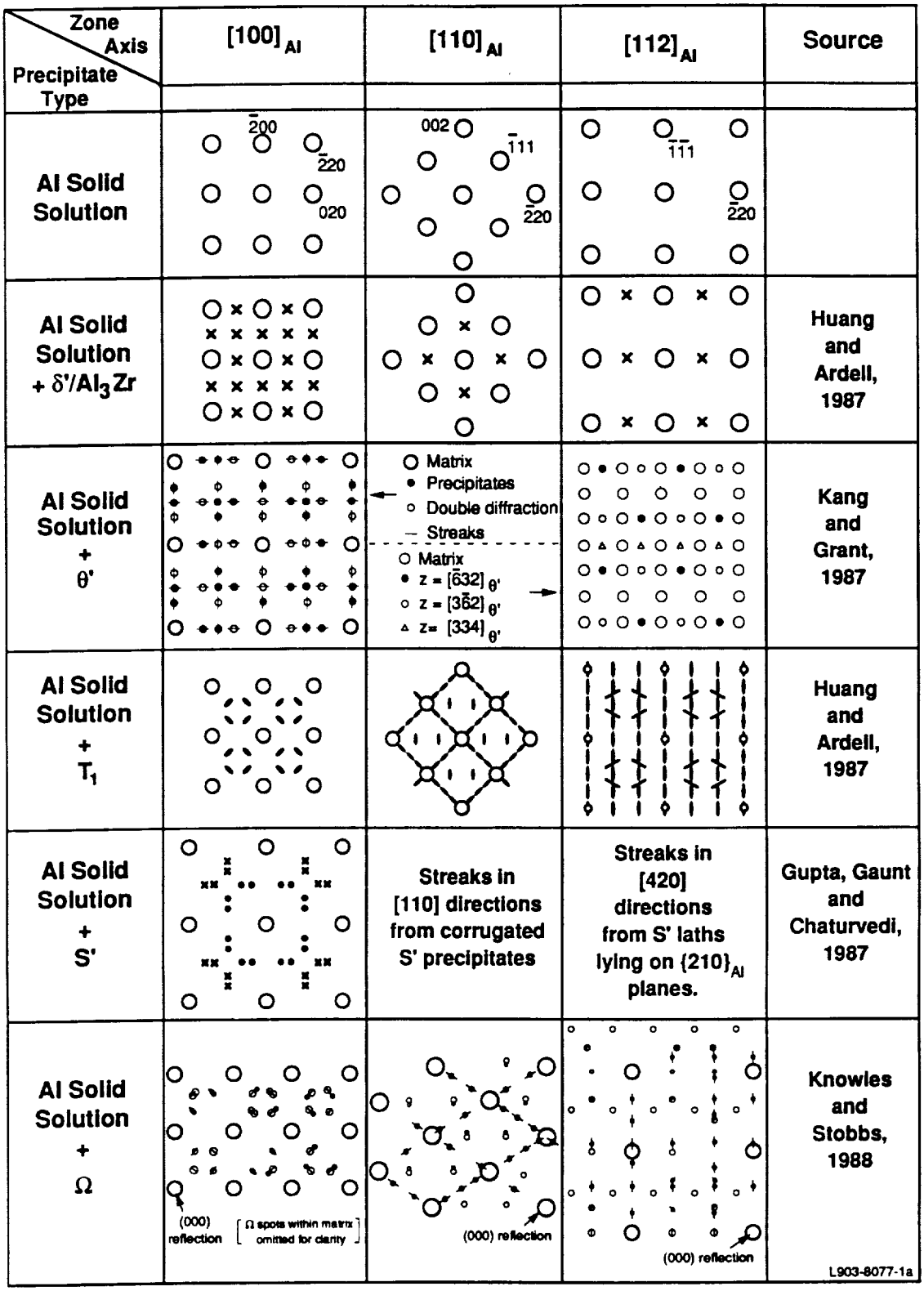

Figure 2 Schematic selected are diffraction patterns expected for the δ', θ', T_1 and S' phases in an aluminum solid solution matrix using the $[100]_{Al}$, $[110]_{Al}$ and $[112]_{Al}$ zone axes.

horizontal line as the matrix spots. It must be noted that Al_3Zr exhibits the same spot pattern as δ' and intensity effects are needed to discriminate between the two precipitates.

The θ' precipitates occur as disks lying on the {100} matrix planes. These are semi-coherent with the matrix. Since they lie on three orthogonal cube axis, for a [100] matrix zone axes, θ' manifests itself as vertical and horizontal streaks, for the two variants lying parallel to the beam direction with intensity maxima and double diffraction occurring as shown in Figure 2. The third variant lies normal to the beam direction and diffraction spots rather than streaks are generated that are coincident with the matrix and some of the δ' spots. For a [110] zone axis, θ' streaks are seen as the short diagonal of the rhombus described by four adjacent Al spots. Likewise, for a [112] matrix zone axis, the corresponding pattern due to θ' was generated by Kang and Grant (12) and is reproduced in Figure 2. Here the effect of double diffraction has not been included to retain clarity. In this case, the θ' spots lie in vertical columns midway between the columns of matrix spots and form horizontal rows of spots that alternate between matrix- and θ'-type. The GP1 zones and θ" precursors to the θ' precipitates manifests themselves as more diffuse but continuous streaks in the <001> directions, with θ" showing well defined intersection maxima at {100} matrix spots.

In Al-Cu-Li alloys, particularly 2090 and Weldalite™ 049*, the major strengthening phase is reported to be the T_1 phase. This phase has a hexagonal crystal structure with an orientation relationship of $(0001)T_1$ ∥ {111}Al and $<1010>T_1$ ∥ <110>Al (13,14). Huang and Ardell (15) have presented detailed experimental and theoretical evidence that shows that it was unnecessary to invoke the presence of the orthorhombic T_1' precursor proposed by Suzuki et al. (16) and by Rioja and Ludwiczak (17) to account for the extra diffraction spots that were observed. Subsequently, Cassada et al. (18) have independently confirmed the findings of Huang and Ardell (15).

*Lattice image work reported in the following section of this report addresses the exact nature of the "T_1-like" phase in Weldalite™ 049.

There are four variants of the T_1 phase and for an SAD pattern with a [100] matrix zone axis, these four variants produce four spots that are symmetrically distributed about the intersection of the diagonals of a square described by connecting the four adjacent matrix spots and lying on the diagonals (Figure 2). When the zone axis is matrix [110], then two variants of T_1 are inclined to the zone axis, and produce spots that lie along the long diagonal of the rhombus described by four adjacent matrix spots while the other two variants are parallel to the zone axis (the normal to the precipitate plane is normal to the zone axis) and produce streaks that form the sides of the rhombus just described. The electron diffraction pattern resulting from zone axis Z = [112] is shown in Figure 2. In this case, the four variants of T_1 produce spots and streaks. In this orientation, one variant of T_1 is normal to Z, the second is 19.5° from Z (i.e. angle included by Z and precipitate normal) and the third and fourth are 61.9° from Z. Thus, the first two variants are nearly parallel to the foil surface whereas the last two are fairly steeply inclined to it. Thus, in the diffraction pattern, spots, elongated spots and steaks are all seen making up the four variants. The two variants 61.9° away from Z produce similar elongated spots while the variant normal to Z produces the steaks.

The Ω phase (19), which is thought to be related to the equilibrium θ phase (Al_2Cu) and responsible for the unusually high strengths in non-lithium containing Al-Cu-Ag-Mg alloys, has an orthorhombic crystal structure (20-22) although, previously, Kerry & Scott (23) incorrectly ascribed a hexagonal structure to it based on SAD patterns. It was believed that the addition of trace amounts of Ag and Mg were together responsible for the formation of the Ω phase either directly or indirectly (22). Recently, however, a silver-free Al-Cu-Mg alloy was shown to contain small amounts of the Ω phase although adding trace amounts of Ag to it enhanced the amount of this phase (24). Two recent studies have attempted to identify the composition of the Ω phase (22,25) although there is no agreement in results.

A comparison of the SAD patterns for T_1 and Ω using [100], [110] and [112] matrix zone axis reveals only subtle differences that are difficult to discern when these precipitates are very thin due to streaking. In Al-Cu-Li-Ag-Mg alloys, as is the case in the present study, it becomes difficult to distinguish between the two if both indeed co-exist. It is conceivable that these two phases exhibit a mutual solid solution behavior and are indistinguishable from each

other. However, the high resolution work described in the next section indicates that Ω is not present in Weldalite™ 049 under the conditions investigated.

The orthorhombic S' phase(26) occurs in Al-Cu-Mg alloys and is the precursor to the equilibrium S phase (Al_2CuMg). When the Cu:Mg ratio is 2.2:1 then a pseudo-binary Al-Al_2CuMg system results (27,28). The S' phase nucleates on dislocation loops and helices formed during quenching (27) and grows as laths on {210} matrix planes along <100> matrix directions with the orientation relationship given by

$$[100]_{S'} \parallel [100]_{Al},\ [010]_{S'} \parallel [021]_{Al},\ [001]_{S'} \parallel [012]_{Al}$$

This precipitate matrix-orientation relationship gives rise to 12 possible orientation of S' laths in the Al matrix, four variants corresponding to each <100> matrix direction. Since these laths lie on {210} planes having a common <100> zone axis, they can form corrugated sheets of precipitate (27), lying on a (110) matrix plane (see Figure 11 of reference 27). According to another study (29), S' precipitated as rods with a diameter of ~90 Å rather than laths, and the observed difference in morphology was speculated to result from differences in the Cu:Mg ratio in the alloy. The small diameter was consistent with the streaking observed for the $(020)_{S'}$ and $(002)_{S'}$ reflection in the $[120]_{Al}$ and $[210]_{Al}$ directions. Long term aging did not cause these rods to coalesce to form laths; rather, there was some tendency for the rods to group together parallel to (110) and (110) and occasionally parallel to (100) and (010) matrix planes. A schematic diffraction pattern for the S' phase with a [001] matrix zone axis is shown in Figure 2. In addition, the S' phase can produce streaking in the $<210>_{Al}$ directions for $[100]_{Al}$ and $[112]_{Al}$ zone axis and in the $<110>_{Al}$ direction for a $[110]_{Al}$ zone axis. The observation of streaking in the $<110>_{Al}$ directions is rationalized on the basis of corrugated precipitate sheets lying on {110} matrix planes.

The role of the v phase (7) in affecting mechanical behavior remains to be established and whether it is indeed a new phase or a hitherto unreported variant of another phase such as S' remains to be confirmed.

3. EXPERIMENTAL PROCEDURE

An extrusion of an aluminum alloy, 9.5mm x 102mm in cross section, and of composition, 5.4Cu-1.64Li-0.4Ag-0.4Mg-0.16Zr (wt%), was solutionized at 493°C(766K) for 1h and water quenched to ambient temperature. A section of the extrusion was stretched 3% within 1h after quenching. The stretched and unstretched materials were allowed to naturally age at room temperature for >1000h to obtain the T3 and T4 conditions, respectively.

The artificial aging response was monitored using Rockwell B hardness measurements. The stretched material was aged at 160°C(433K) whereas the unstretched material was aged at 180°C(453K). Specimens were selected along the aging curves for microstructural examination in the transmission electron microscope (TEM).

Specimens for microstructural examination were sliced from the extrusions and mechanically ground to the desired thickness. These were then twin jet electropolished to perforation at -30°C(243K) and 12-15 volts in a solution of 25% HNO_3 in methanol. After polishing, the specimens were dipped in a solution of 50% HNO_3 in H_2O to remove any Ag which may have redeposited from the electrolyte. Bright field (BF), selected area diffraction (SAD) and centered dark field (CDF) imaging were used to follow the microstructural evolution during aging.

4. RESULTS AND DISCUSSION

4.1 Hardness Versus Aging Time

The unstretched material exhibits a stronger natural aging response compared to the stretched material, (R_B 80 vs R_B 68 after >1000h), Figure 1. Artificial aging was performed at 160°C(433K) for the stretched material and at 180°C(453K) for the unstretched condition. The open and full circles along the aging curves indicate the locations from where specimens were taken for microstructural analysis. In both instances, a reversion is observed with an appreciable decrease in hardness. This reversion is typically observed after approximately 15 minutes at temperature with the depth of the "reversion trough" being considerably greater for the unstretched material. Further aging causes an increase in hardness with a peak being observed, for both the stretched and unstretched material after

40-50h of artificial aging at the respective temperatures. For longer times at each aging temperature (~200h), the hardness decrease is minimal, Figure 1.

The observed reversion trough is of technological relevance because at the bottom of the reversion trough, the material is in a lower-strength, high-ductility condition, i.e. 24% typical elongation (1) -- one that provides the potential for near-net shape cold forming after solution heat treatment and quenching thereby eliminating the distortion that would accompany a subsequent quench. Gayle, et al. (6) have shown that in Weldalite™ 049, (i.e., a similar alloy but with 1.3 wt%Li), room temperature re-aging of the unstretched material following a reversion treatment returned the strength to the original T4 level after an extended incubation period. The incubation time can be about 5 days before hardness increases again and this allows sufficient time for a part to be formed.

4.2 Microstructure of the Naturally-Aged Material

The microstructure of the naturally aged unstretched material (T4) was examined using TEM and an SAD pattern corresponding to the $[100]_{Al}$ zone axis (Figure 3a) reveals streaking associated with GP zone formation and superlattice reflections characteristic of δ'. The GP zones lie on $\{100\}_{Al}$ planes, are fine and appear fairly well developed compared to other Cu-containing aluminum alloys. The δ' precipitates are also extremely fine and evenly distributed throughout the matrix, except for the situation where they precipitate around the previously existing Al_3Zr to form the "composite" precipitates. These observations are consistent with earlier reports on the natural aging response of the 1.3 wt.% Li content alloy, Weldalite™ 049.

In the stretched, naturally aged material, (T3), streaking due to well developed GP zones observed for the T4 condition is not seen and only δ' reflections are evident, Figure 3b. Apparently the stretching operation discourages GP zone formation. The volume fraction and size of the δ' precipitation relative to the unstretched material is approximately the same as observed from dark field studies. A similar response was also observed in the alloy containing 1.3 wt.% Li (5).

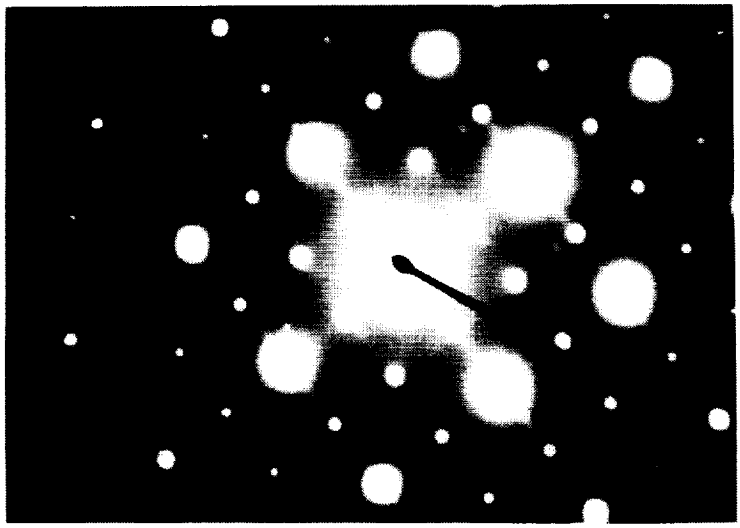

(a)

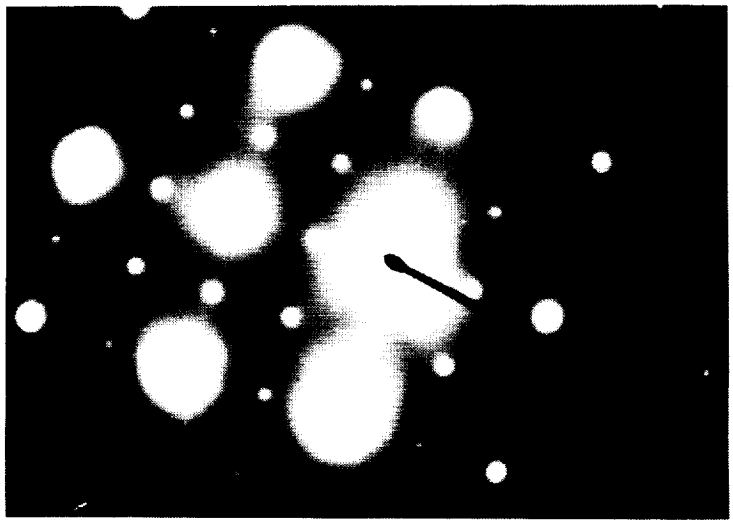

(b)

Figure 3 SAD patterns obtained using $[100]_{Al}$ zone axis for the naturally aged material (a) previously unstretched and (b) with 3% prior stretch.

4.3 Microstructure of the Artificially Aged Unstretched Material

Although the hardness-versus-aging time profile for the unstretched material was generated at 180°C(453K), specimens were heat treated at 160°C(433K) also for 15 minutes to provide a direct comparison of the reversion behavior with the stretched material. A diffraction pattern with a $[112]_{Al}$ zone axis of a specimen heat treated for 15 minutes at 160°C(433K) reveals the presence of δ' (Figure 4a). A similar heat-treatment at 180°C(453K) however, causes all the δ' to dissolve as evidenced by the absence of superlattice reflections in the SAD pattern in Figure 4b, taken using a $[100]_{Al}$ zone axis. In both instances, the GP zones were not longer seen. These observations are different from those reported by Gayle et al. (6,7) on the lower Li-containing Weldalite™ alloy. When the thin foil specimen used to obtain Figure 4b was examined two weeks later, room temperature aging had caused the δ' to reprecipitate as can be seen from the superlattice spots in Figure 4c. This natural aging response of the reverted material is consistent with earlier observations and may have technological significance as discussed earlier.

Aging the unstretched material at 180°C(453K) for longer times causes the hardness to increase and after 2h, the hardness is approximately equal to that in the naturally aged condition (Figure 1). A thin foil specimen oriented with a $[110]_{Al}$ zone axis (Figure 5a) reveals the presence of faint spots characteristic of the T_1 variants, δ', superlattice spots and streaking in the $[100]_{Al}$ direction, indicating the presence of the θ' phase. It is interesting to note that the T_1 with its four variants should exhibit streaking in the [111] directions in addition to the two spot variants but these streaks are not obvious in this heat-treated condition. A dark field image of the δ' precipitates using the corresponding superlattice reflection in Figure 5a is shown in Figure 5b. The δ' precipitates are seen either as halos around the Al_3Zr precipitates or forming independently. At this stage, these δ' precipitates are ~100Å in size. The Al_3Zr precipitates tend to be larger (~250-300Å). As the [100] streak corresponding to θ' (Figure 5a) passes through the δ' superlattice spot, dark field imaging of δ' will include information characteristic of θ'. A bright field-dark field pair in figures 5c and 5d show the precipitation of fine, thin T_1 platelets, primarily on the sub-boundaries. These platelets are approximately 600 Å in length. Clearly T_1 precipitation commences on the sub

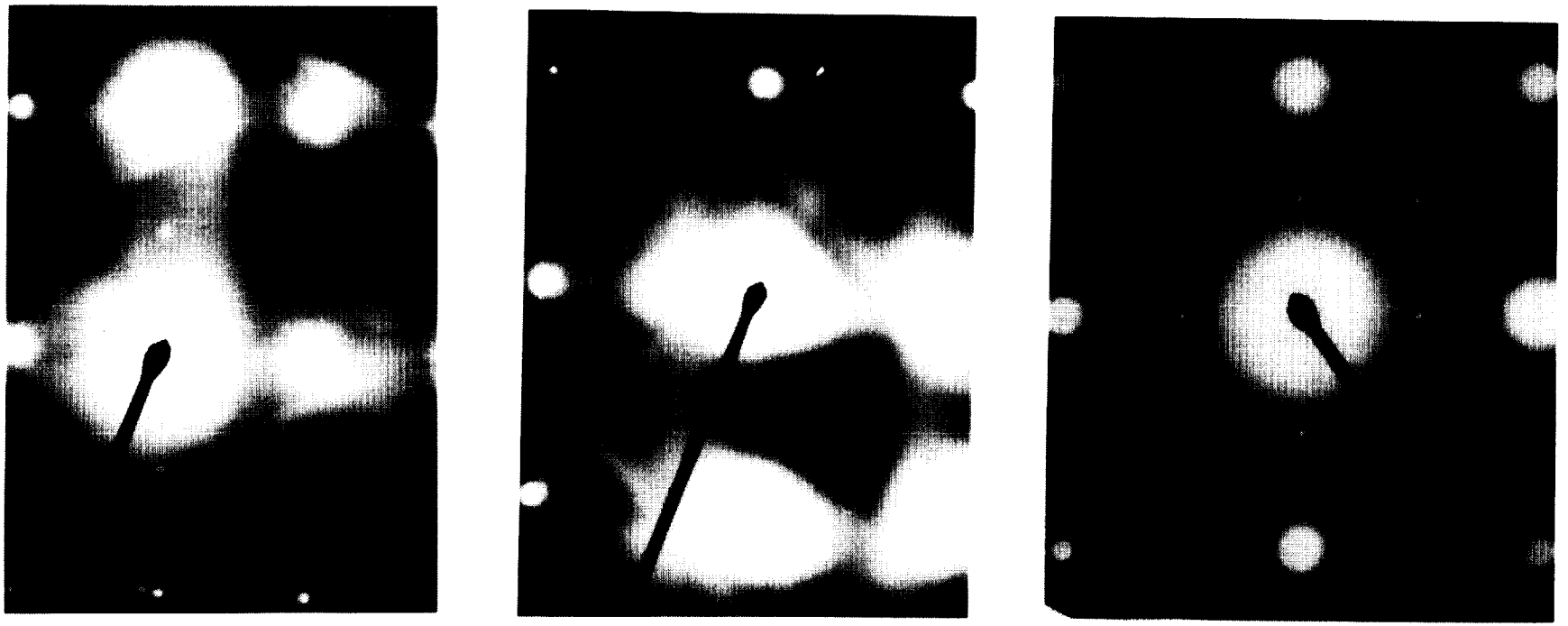

(a) (b) (c)

Figure 4 Diffraction patterns from unstretched material: (a) $[112]_{Al}$ zone axis of a specimen heat-treated for 15 minutes at 433K, (b) $[100]_{Al}$ zone axis of a specimen heat-treated for 15 minutes at 453K and (c) $[100]_{Al}$ zone axis of a specimen aged as in (b) and then subsequently naturally aged for two weeks at room temperature.

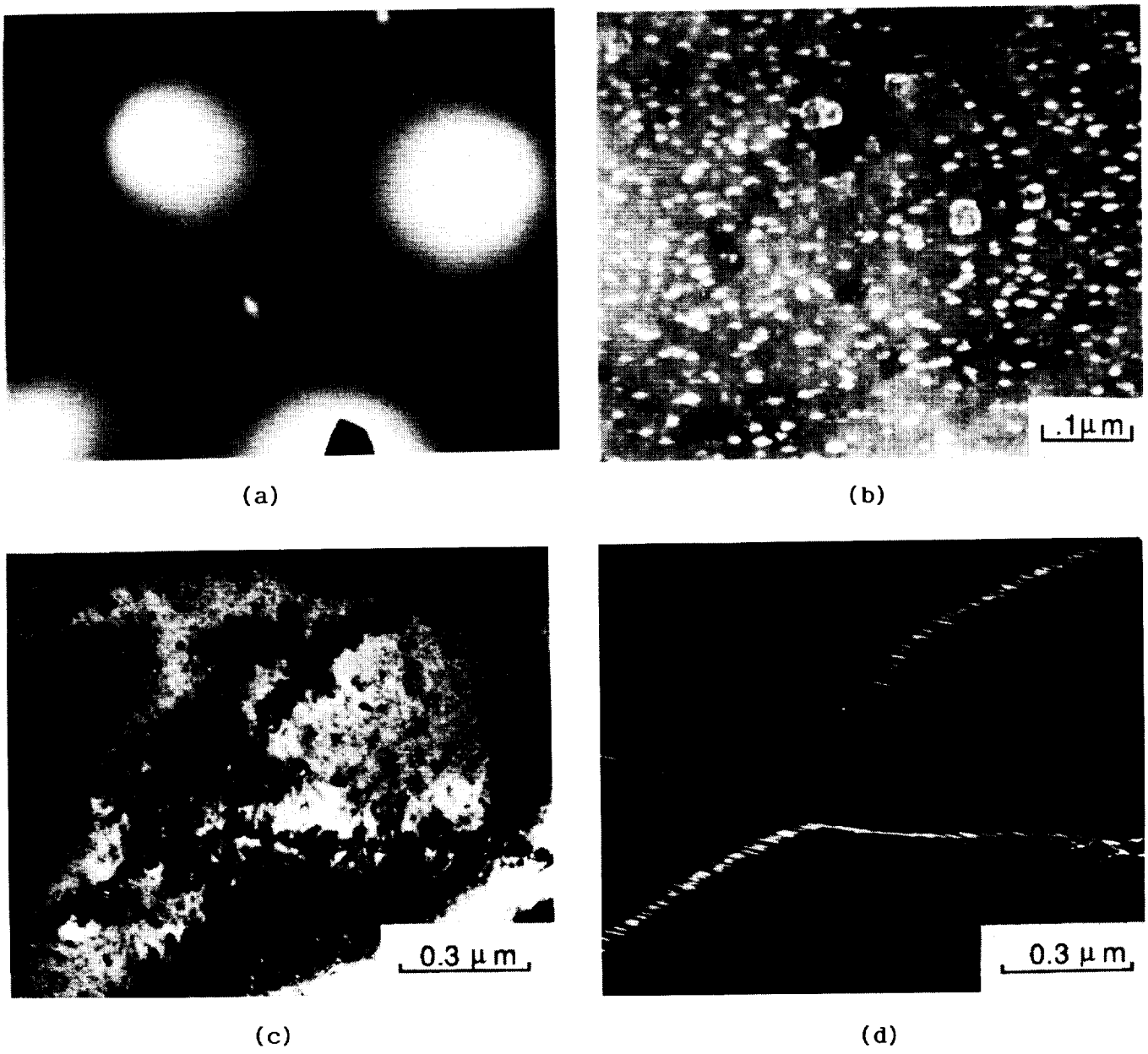

Figure 5 An unstretched specimen heat treated for 2h at 453K: (a) $[110]_{Al}$ zone axis SAD pattern, (b) δ' dark field micrograph, (c) general bright field showing sub-boundaries and (d) T_1 dark field showing preferential precipitation of T_1 at sub-boundaries seen in (c).

boundaries during these early stages of aging, with the loosely knit walls of dislocations serving as preferential nucleation sites.

Aging the unstretched material for even longer times (for 6h at 180°C causes further precipitation of T_1 as can be seen in the bright field image in figure 6a. At least three of the four T_1 variants are readily seen with fringe contrast from the extremely thin T_1 platelets being observed for two variants. The third variant is seen with an edge-on orientation. These precipitates appear to be distributed in the matrix, in contrast to those observed at the earlier aging time of 2h at 180°C(453K) where the T_1 precipitates were observed primarily at the sub-boundaries (Figure 5d). A diffraction pattern obtained using the $[110]_{Al}$ zone axis reveals the presence of a wealth of precipitates. The four variants of the T_1 phase manifest themselves as two sets of streaks and two sets of spots. The streaks correspond to the edge-on orientation and describe a rhombus in Figure 6b. The two sets of spots lie on the long diagonal of this rhombus at one third and two thirds of this diagonal (see Figure 6b and compare with Figure 2). In addition, faint streaking is also observed along this long diagonal which corresponds to the $[110]_{Al}$ orientation and suggests the presence of precipitates on the $(110)_{Al}$ planes. This likely occurs from the S' precipitates that have $\{210\}_{Al}$ habit planes and form a corrugated sheet that lie on the (110) matrix planes. Streaking is also observed in the $[100]_{Al}$ orientation corresponding to the short diagonal of the rhombus and indicative of the presence of θ' precipitates with $[100]_{Al}$ habit planes. A bright spot is also observed at the intersection of the long and short diagonals of the rhombus. This can simply be an intersection maximum or, alternately, it can correspond to a δ' superlattice reflection. In this case dark-field imaging was used to confirm the presence of δ' precipitates. Dark field imaging of one of the four T_1 variants using one of the two spots in Figure 6b shows the fine T_1 platelets in Figure 6c. The edge-on variant at the sub-boundaries and in the matrix is shown in figure 6d and at this stage of aging T_1 has precipitated within the matrix causing a sub-boundary precipitate free zone.

After 12h at 180°C(453K), a still substantially underaged condition based on hardness variation with aging time (Figure 1), the microstructure consists of T_1, θ', S', and δ'. The presence of these phases can be verified in Figure 7a which shows a diffraction pattern obtained using a $[110]_{Al}$ and $[100]_{Al}$ orientations (long and short

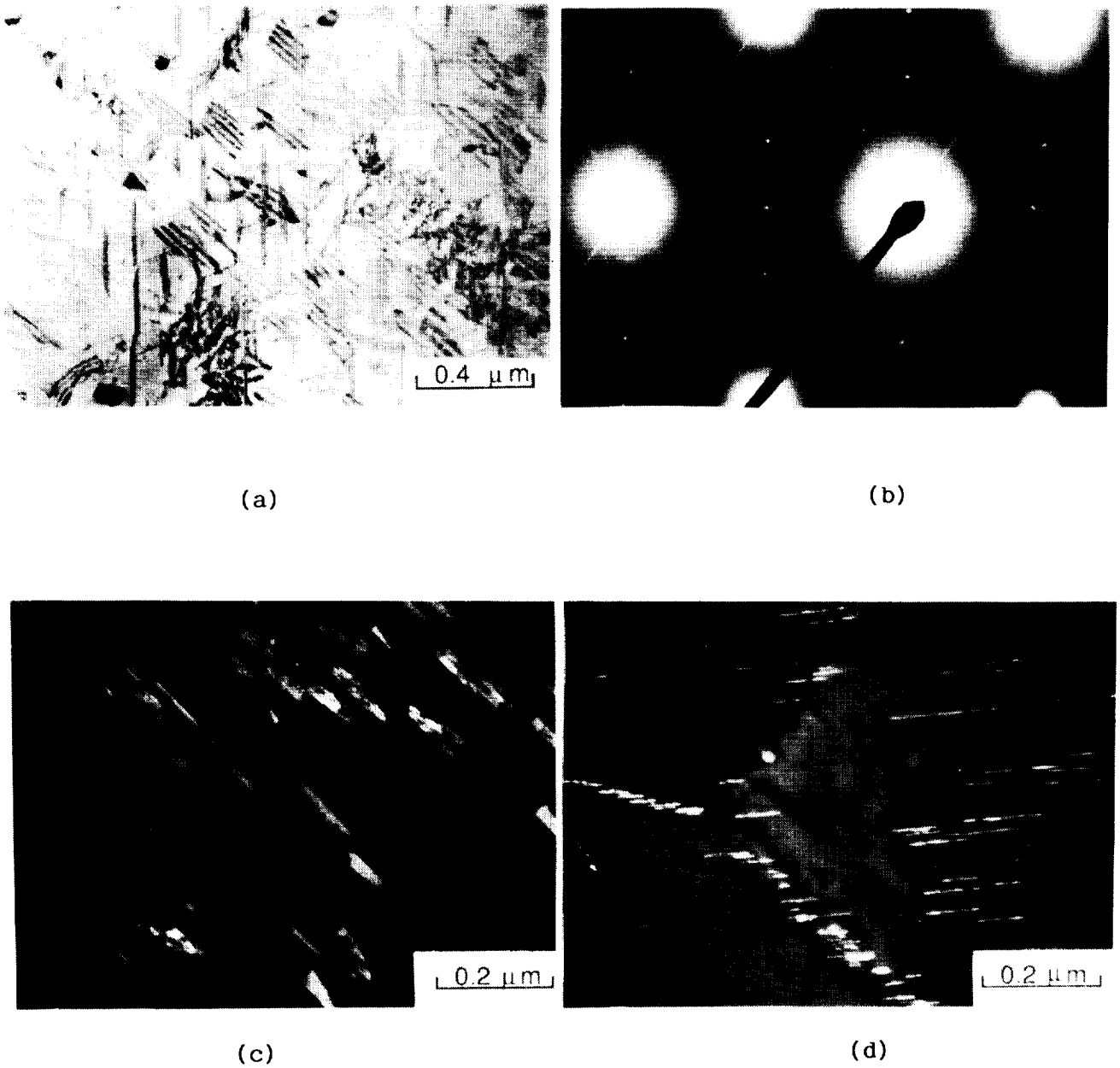

Figure 6 Microstructure of the unstretched material aged for 6h at 453K showing (a) variants of T_1 using bright field, (b) SAD pattern with $[110]_{Al}$ zone axis confirming T_1, δ', θ' and S', (c) dark field of one of the T_1 variants and (d) dark field of T_1 precipitation in the interior of subgrains and at sub-boundaries.

diagonals respectively of the rhombus described using four adjacent matrix spots) confirms the presence of S' and θ' while the bright spot at the intersection of the two streaks verifies the existence of δ'. A bright field image (Figure 7b) located adjacent to a sub boundary reveals the presence of T_1, in the matrix, at the sub-boundaries and in the regions which previously appeared to be precipitate free zones (Figure 6d). Thus, it appears that in the unstretched material, T_1 precipitation commences at the sub-boundaries, then occurs within the subgrains, creating a subgrain precipitate free-zone which fills out fairly homogeneously with further aging. This whole sequence occurs within the first 12h of artificial aging, which still lies well within the underaged regime (R_B = 83), since near-peak aging requires ~34h at 180°C (R_B = 88).

A bright field reference, the associated SAD pattern taken with a $[110]_{Al}$ zone axis and dark field images of δ', θ', one variant of T_1 and S' are shown in Figures 8a-f. The SAD pattern in Figure 8b reveals the four T_1 variants, δ', streaking in the [110] orientation associated with S' and streaking in the [100] direction associated with θ'. The SAD pattern was intentionally oriented so as to maximize θ' and S' streak intensities. A dark field image of the δ' precipitates reveals some unusual features, Figure 8c. These δ' precipitates are ellipsoidal in shape rather than spherical and appear to have a thin line of extinction running along the major axis of the ellipse (see inset in Figure 8b). If this figure is superimposed on Figure 8c, which is a dark field image of θ', it is found that the θ' precipitates fit quite well along the major axis of several of the δ' precipitates in Figure 8b suggesting δ' precipitation on θ'. The S' precipitates (Figure 8f) appear to be fairly uniformly distributed in this unstretched material which is unusual considering a recent study (30) on Al-Li-Cu-Mg alloys that shows that the stretching operation prior to aging is essential to obtain a uniform distribution of the S' phase.

A region adjacent to sub-boundaries after 12h aging at 180°C(453K) (Figure 9a) reaveals that the sub-boundaries contain the T_1 phase as does the matrix. In addition to the two-edge-on variants of T_1 in Figure 9a, two additional edge-on variants are visible almost parallel and perpendicular to the sides of the figure, and are thought to correspond to S'. A dark field image of δ' in Figure 9b reveals δ' precipitation around Al_3Zr. The region corresponding to the far right

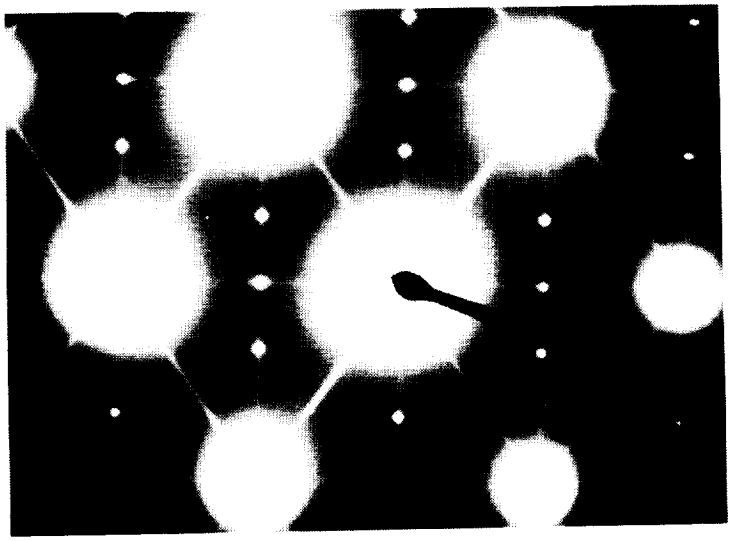

(a)

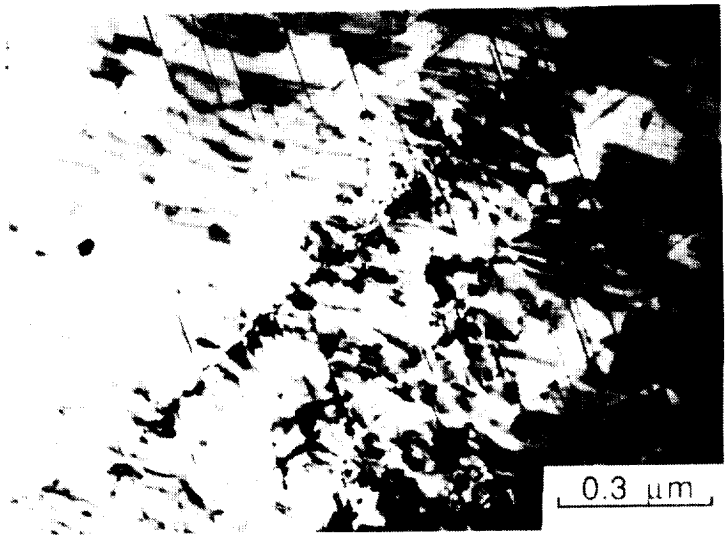

(b)

Figure 7 An unstretched specimen aged for 12h at 453K reveals (a) the presence of T_1, δ', θ' and S' in a $[110]_{Al}$ zone axis SAD pattern and (b) a homogeneous distribution of T_1 at sub-boundaries, interior of sub-grains and in the regions adjacent to the sub-boundaries.

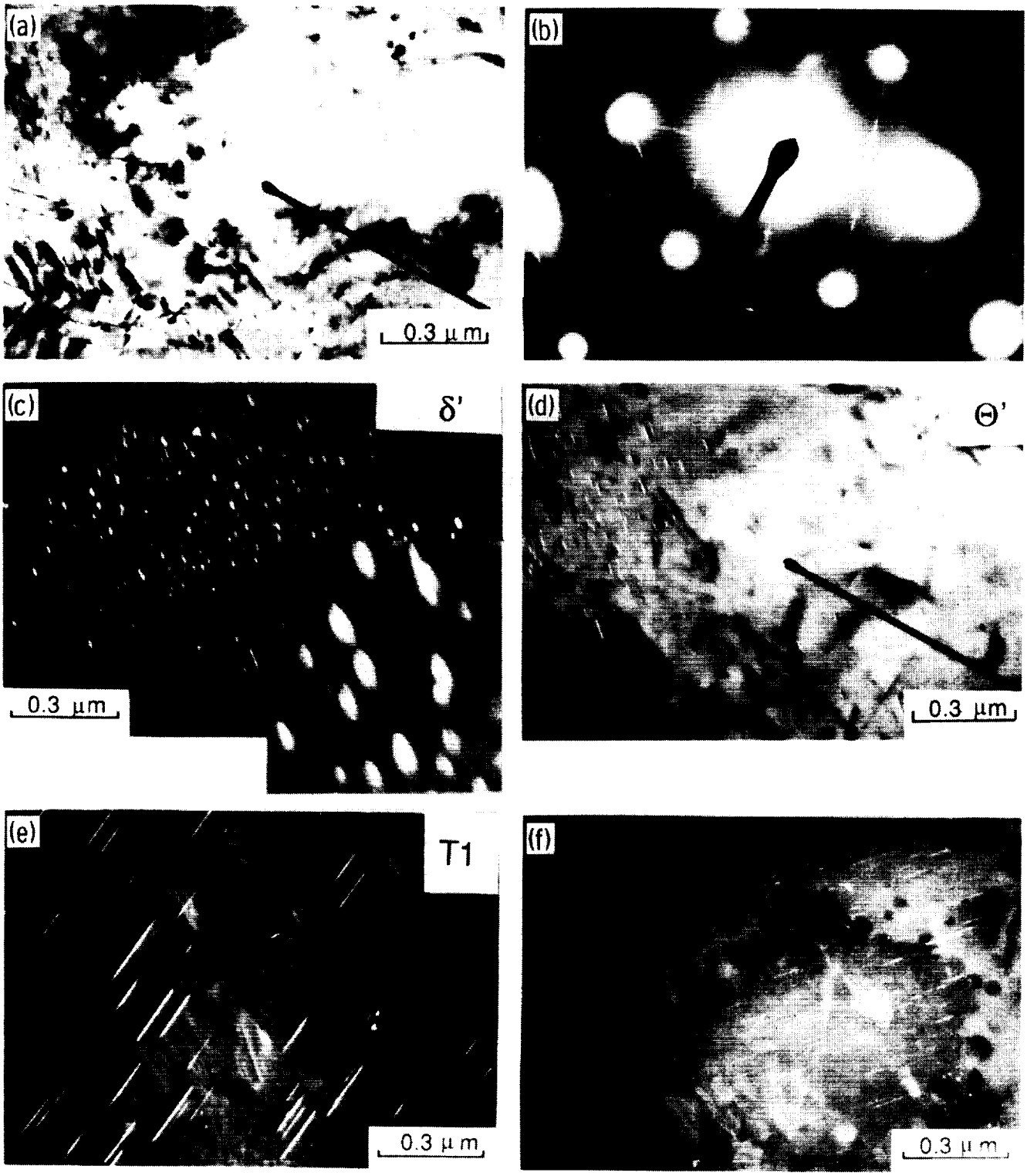

Figure 8 Microstructure of an unstretched specimen aged 12h at 453K using (a) reference bright field image, (b) associated SAD pattern, (c) δ' dark field, (d) θ' dark field, (e) T_1 dark field and (f) S' dark field.

ORIGINAL PAGE
BLACK AND WHITE PHOTOGRAPH

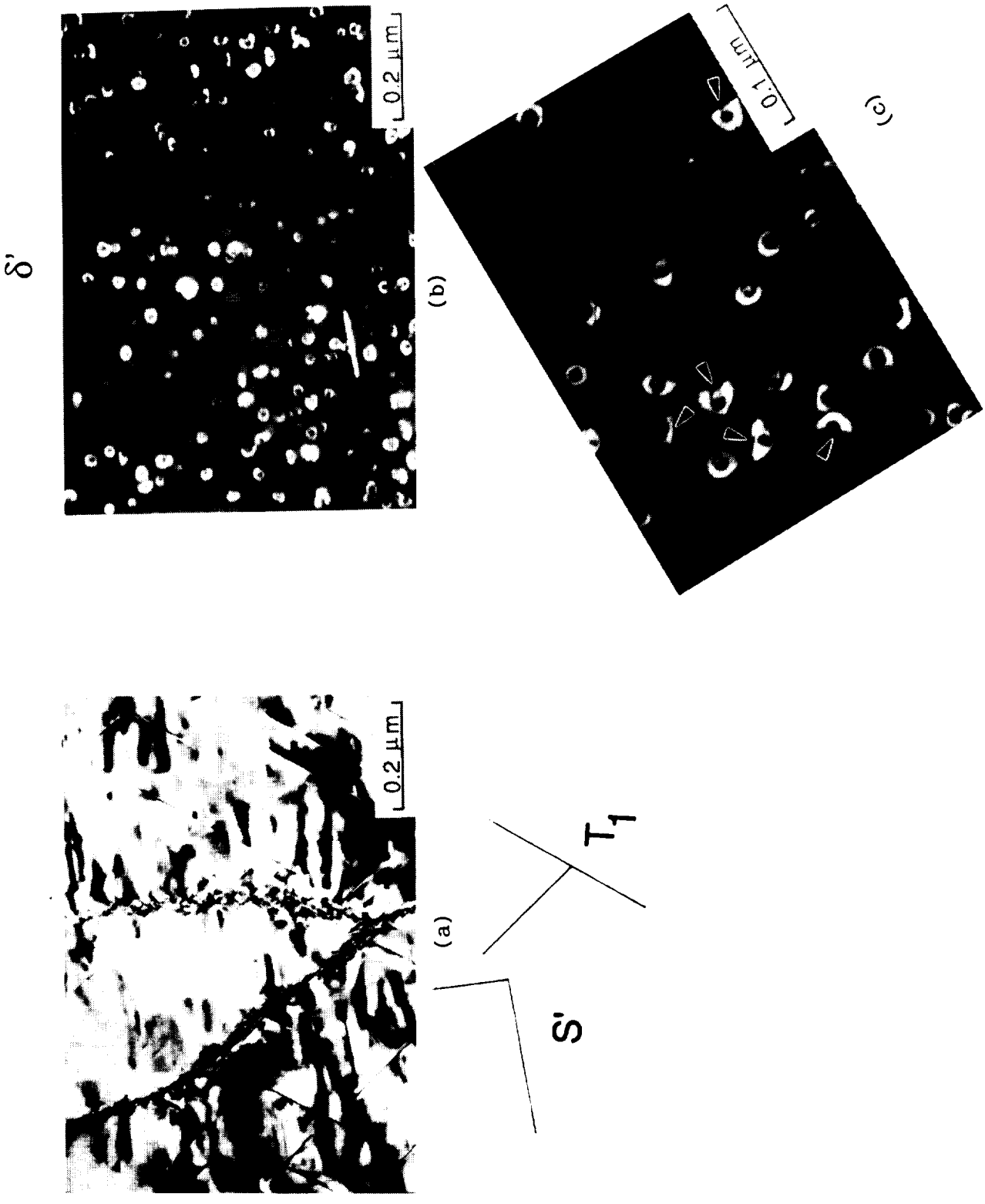

section of Figure 9b is shown at a higher magnification in Figure 9c, after accounting for the rotation involved due to changes in magnification in the TEM. From the two dark field micrographs, Figures 9b and 9c, it is seen that the δ' precipitates do not form a complete "halo" around Al_3Zr; rather in several instances they end abruptly forming a cross section contained by a chord of a circle on that side. Several such instances are indicated in Figure 9c. A comparison of the orientation of the "chords" in Figure 9c with Figure 9a reveals them to be frequently coincident with the orientation of the S' precipitates although occasionally they also are parallel to T_1 edge-on variants. This may suggest the heterogeneous precipitation of T_1 and S' at the $Al_3Zr/Al_3Li/\alpha$-matrix interfaces. It is possible that the precipitation of Al_3Li causes a local enrichment of Cu and Mg, allowing the formation of S' and to a lesser extent T_1 at these interfaces.

Overaging the unstretched material for 48h at 180°C(453K) results in a significant decrease in intensity of the δ' superlattice spots (Figure 10a) located at the center of each rhombus described by joining four adjacent matrix spots in an SAD pattern generated using a [110]m zone axis. An enlargement of a portion of the SAD pattern is also shown in Figure 10a to emphasize this observation. All four variants of T_1 are present and, in addition, streaking due to θ' and S' are still visible. The [420] streaks in Figure 10b arising from S' with {210} habit planes are also clearly seen. Further, the [100] streaks due to θ' in Figure 10a and the θ' streaks and spots in the SAD pattern in Figure 10c generated using a $[100]_{Al}$ zone axis, are weaker relative to the T_1 streaks and spots, suggesting some dissolution of θ'.

Further over-aging for 100h at 180°C(453K) causes only a negligible decrease in hardness (Figure 1) and the associated microstructure is shown in Figure 11a as a bright field image. Both, a grain boundary and a sub boundary can be seen and a small grain boundary precipitate free zone is present whereas this is not the case for the sub boundary. Additionally, coarse (~0.1μm) grain boundary precipitates are seen and based on their size, it is not clear whether they were present prior to aging or occurred during aging. An enlarged portion of an SAD pattern, obtained using a $[110]_m$ zone axis is shown in Figure 11b. This Figure shows the region bound by four adjacent matrix spots and it is seen that the T_1 phase predominates with a faint δ' spot being present in the center of the rhombus. Streaking in the [420] orientation in Figure 11c, obtained using a $[112]_{Al}$ zone axis

Figure 10 Selected Area Diffraction patterns obtained from an unstretched specimen-aged for 48h at 453K using (a) $[110]_{Al}$ zone axis, zone axis, (b) $[112]_{Al}$ zone axis and (c) $[100]_{Al}$ zone axis.

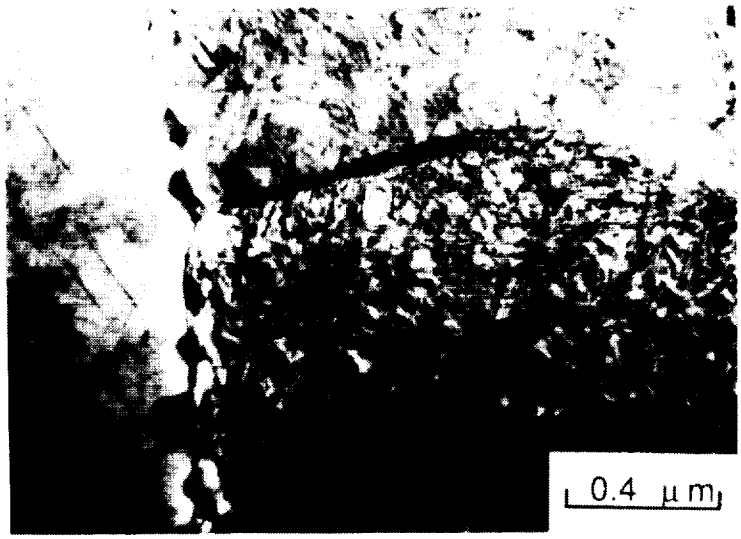

(a)

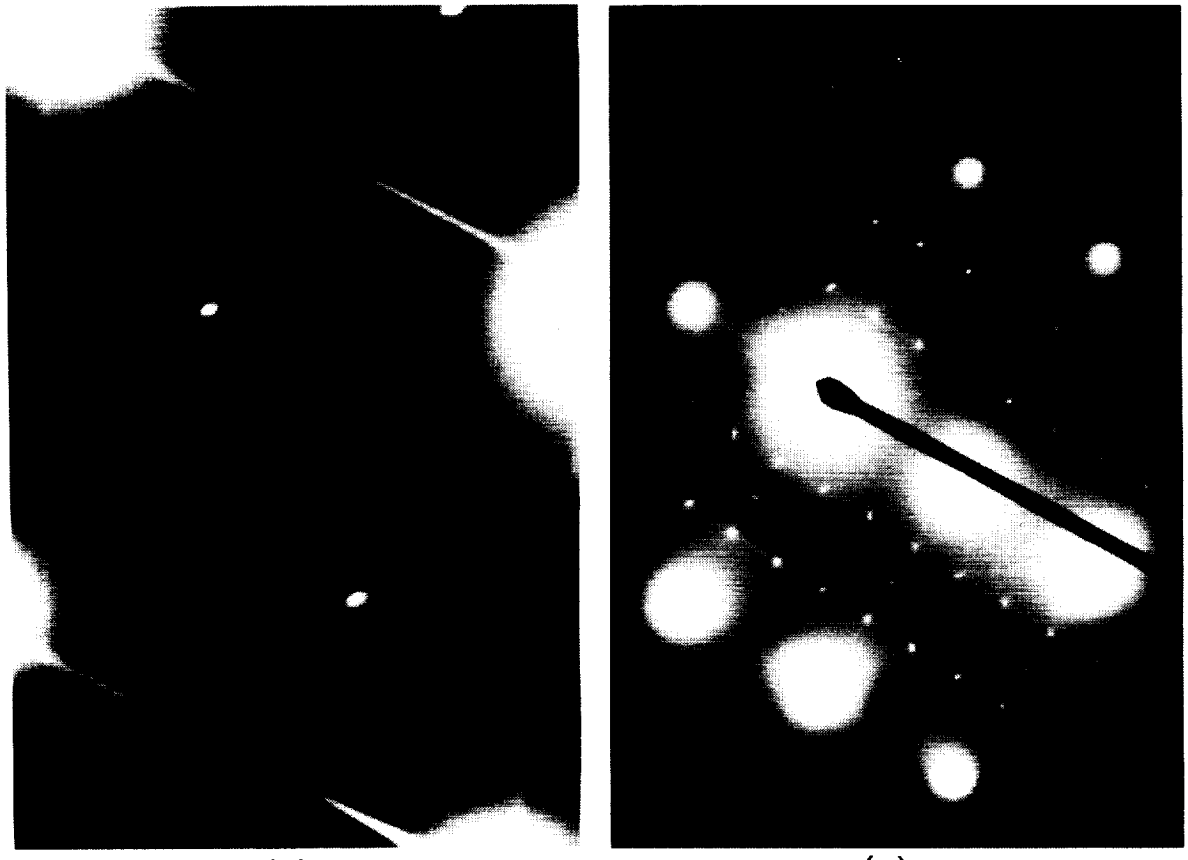

(b) (c)

Figure 11 Overaged microstructure (100h at 453K) of an unstretched specimen revealing (a) sub-boundary and grain boundary precipitation in bright field (b) the absence of θ' streak and faint δ' spot in an SAD pattern with $[110]_{Al}$ zone axis and (c) presence of [420] S' streaks in an SAD pattern obtained using $[112]_m$ zone axis.

confirms the existence of the S' phase. If θ' is present it is only in very small amounts, as any streaking in the [100] orientation is extremely weak in intensity.

In summary, for the unstretched material, naturally aged strength results from fine δ', GP zones, and probably solid solution strengthening. Upon artificial aging at 180°C(453K), the GP zones dissolve as do some of the δ' precipitates causing a reversion associated with a decrease in hardness. Additional exposure to the artificial aging temperature results in the precipitation of T_1, initially at sub-boundaries, then in the interior of the subgrains. In addition, S', θ' and more δ' precipitate. Extensive over-aging appears to cause δ' and θ' to redissolve leaving predominantly T_1, and some S' precipitates, in the matrix.

4.4 Microstructure of the Artificially-Aged Stretched Material

It was shown in Figure 3b that natural aging of the stretched material results in strengthening predominantly from δ'; the formation of GP zones appears to be inhibited by the prior stretch.

Upon artificially aging the naturally aged material at 160°C(433K) for ~15 minutes, a decrease in hardness is observed (Figure 1) due to a reversion phenomenon. The decrease in hardness however, is not as large as was observed for the unstretched material; further, the hardness of the reverted material is higher than that of the unstretched material, similarly heat treated for 15 minutes, although at the higher temperature of 180°C(453K). A diffraction pattern of the stretched and reverted material, using a $[110]_{Al}$ zone axis, Figure 12a reveals the complete dissolution of the δ' precipitates as evidenced by the absence of the superlattice reflections indicative of δ'. Natural aging of the reverted material for a period of two weeks, causes the reprecipitation of δ', Figure 12b, likely restoring most, if not all of the hardness of the naturally aged material, prior to the reversion treatment.

While a 15 minutes exposure to 160°C(433K) causes essentially the complete dissolution of δ', leading to the observed reversion behavior, longer exposures to this temperature leads to the precipitation of some θ' and reprecipitation of δ', as is observed after

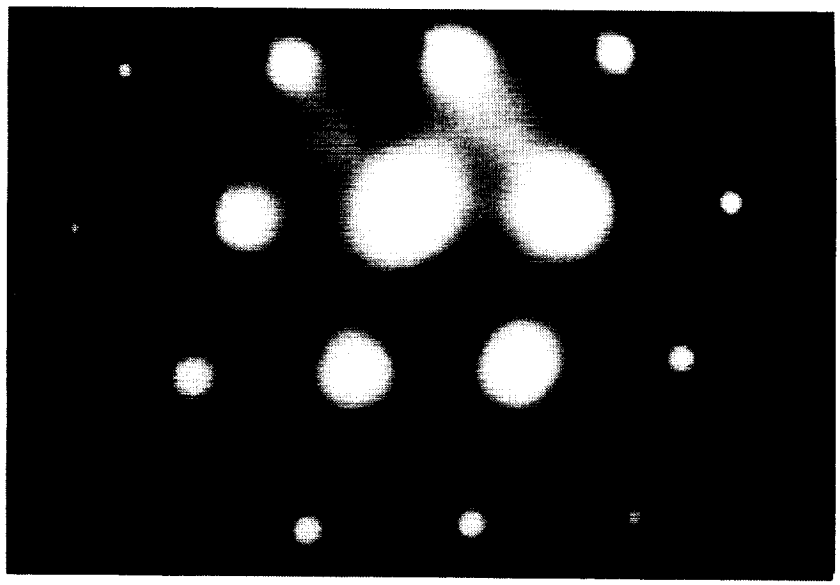

(a)

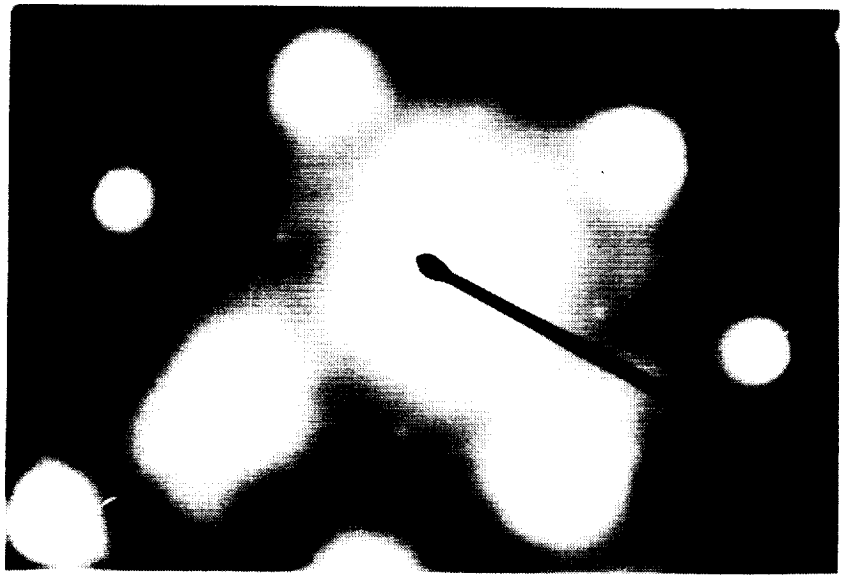

(b)

Figure 12 Diffraction patterns form the stretched material: (a) $[110]_{Al}$ zone axis of a specimen heat-treated for 15 minutes at 433K and (b) $[100]_{Al}$ zone axis of specimens in (a), subsequently naturally aged for two weeks at room temperature.

2h at 160°C(433K) (Figure 13a). After 6h at 160°C(433K), the δ' diffraction spots are much stronger (Figure 13b), and in addition, streaking is observed in the $[100]_{Al}$ directions, which is indicative of θ'. The four variants of the T_1 phase manifest themselves as 4 spots, positioned symmetrically around the δ' spots in Figure 13b, obtained using a $[100]_{Al}$ zone axis. At this stage, the intensity of the T_1 spots is weak relative to the δ' spots. A $[112]_{Al}$ zone axis SAD pattern in Figure 13c reveals the presence of streaks in the <420> directions indicative of the presence of the S' phase. The hardness of the stretched material after 6h at 160°C(433K) is R_B 78, which is similar to the hardness of the naturally-aged unstretched material, although the phases responsible for providing these similar levels of strength in two cases are different; in the naturally aged material, it was a combination of GP zones and δ', in this artificially aged condition it is a mixture of δ', θ', S' and T_1. The intensity of the T_1 spots increases significantly with a longer aging time of 10h at 160°C(433K) as can be seen by comparing Figure 13d with Figure 13c, although the θ' streaks in the $[100]_{Al}$ directions continue to remain weak. In the peak-aged condition of 34h at 160°C(433K), T_1, δ' and θ' were observed using a $[100]_{Al}$ zone axis to obtain the SAD pattern in Figure 14a. The intensities of the θ' spots and [100] streaks were weak and this behavior was also observed using a $[100]_{Al}$ zone axis. Thus the θ', spots and streaks remain weak for the stretched material in all the specimens examined after aging for various times at (433K).

Over-aging, i.e. 240h at 160°C(433K) causes additionally a decrease in the intensity of δ' spots, leaving behind only T_1 spots and streaks, as seen in the SAD pattern in Figure 14b obtained using a $[100]_{Al}$ zone axis. The presence of S' was confirmed using a $[112]_{Al}$ zone axis SAD pattern. Thus in the overaged condition, θ' could not be detected and intensity from δ' spots had decreased significantly compared to the peak-aged condition leaving behind some δ', predominantly T_1, and additionally, the S' phase.

In summary, stretching prior to aging appears to discourage GP zone formation in the naturally aged material, thereby causing the natural aging response to be less dramatic relative to the unstretched material. Upon artificial aging at 160°C(433K), reversion occurs, associated with the dissolution of δ'. Longer aging times at temperature results in the precipitation of T_1, S', and θ' and the

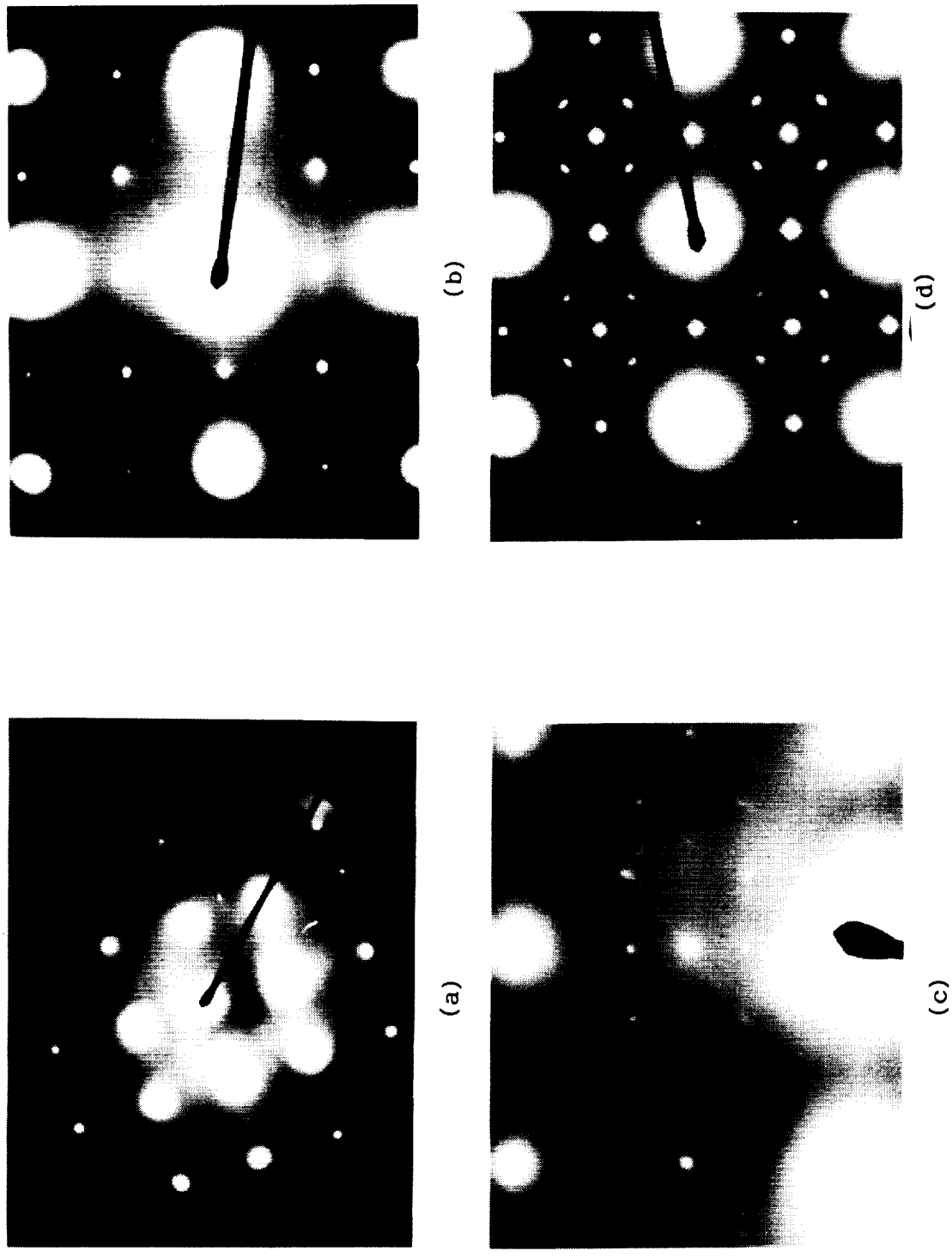

Figure 13 Selected are diffraction patterns from specimens aged for various time at 433K: (a) $[100]_{Al}$ zone axis from a specimen aged for 2h, (b) $[100]_{Al}$ zone axis and (c) $[112]_{Al}$ zone axis from a specimen aged for 6h and (d) $[100]_{Al}$ zone axis for a specimen aged for 10h.

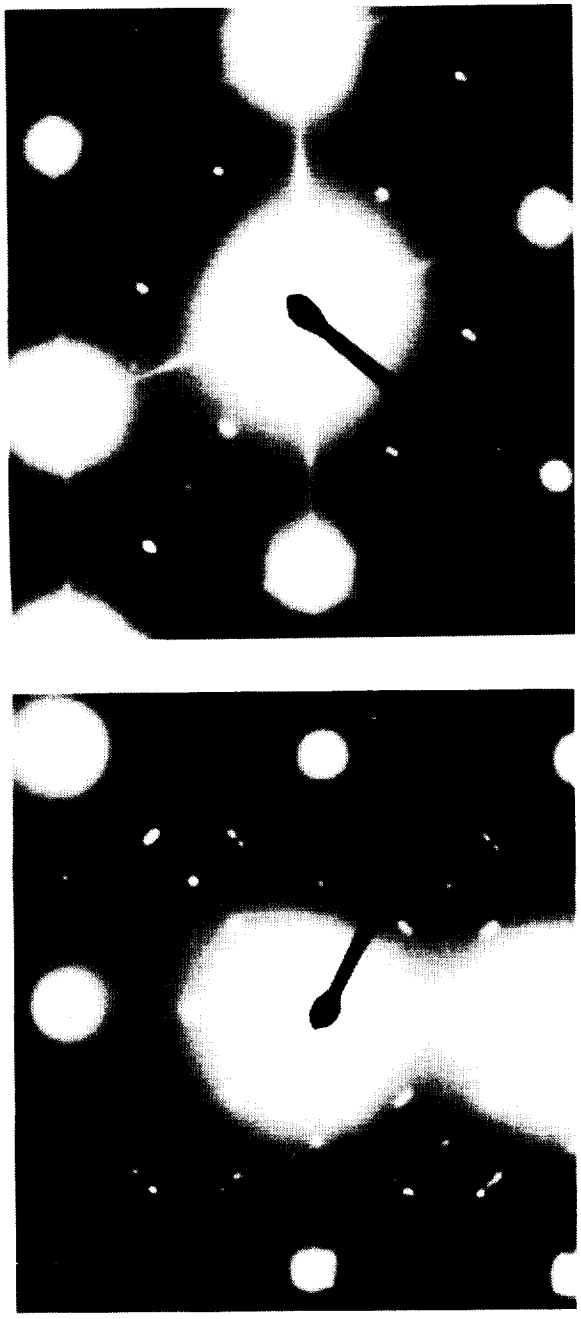

Figure 14 Stretched specimens aged for (a) 34h at (433K), [100]Al zone axis and (b) 240h at 433K, [110]Al zone axis.

reprecipitation of δ'. The intensity of spots and streaks related to θ' remain weak up to the peak-aged condition signifying that the prior stretch discourages θ' formation. This is unusual in high Cu-containing Al alloys and possibly arises from competitive nucleation and growth between T_1 and θ'; in this instance it appears that T_1 is the favored phase. In the overaged condition θ' was not detected and the intensity of δ' spots is low suggesting redissolution of δ', possibly related to the dissolution of θ'. Finally, the phases found at the various stages of aging after stretching are compared with those found without stretch in Table 15.

Table 15. Summary of Phases Present and Diffraction Information in Higher Li-Containing Weldalite™ Alloy

(Al-5.35Cu-1.64Li-0.40Ag-0.44Mg-0.16Zr, wt%)

Aging Time	Unstretched 180°C (aging temperature)	Stretched 3% 160°C (aging temperature)
0 (i.e. T4, T3)	δ', GP Zones	δ' + weak GP Zones
+ 1/4 h	weak δ'	weak δ'
+ 2 h	δ', θ', T_1, <110> streaks	δ', T_1?
+ 6 h	δ', θ', T_1, <110> streaks	δ', T_1, weak θ', weak <110>, S'
+ 10 h	-	δ', T_1, θ', <110>, S'
+ 12 h	δ', T_1, θ', <110> streaks, S'	-
+ 34 h	-	δ', T_1, θ', S'
+ 48 h	weak δ', T_1, θ', <110> streaks, S'	-
+ 100 h	weak δ', T_1, weak θ', <110> streaks, S'	-
+ 240 h	-	δ', T_1, S' [θ', not seen]

5. REFERENCES

[1] J.R. Pickens, F.H. Heubaum, T.J. Langan and L.S. Kramer in "Aluminum-Lithium Alloys" (Proceedings of the Fifth International Aluminum-Lithium Conference), eds: T.H. Sanders and E.A. Starke, MCE Publication Ltd., Birmingham, U.K., 1989, p. 1397.

[2] R.J. Rioja, P.E. Bretz, R.R. Sawtell, W.H. Hunt and E.A. Ludwiczak, in "Aluminum Alloys, Their Physical and Mechanical Properties," Vol. III, Proceedings of the International Conference on Aluminum Alloys, Chameleon Press, London, U.K., 1986, p. 1781.

[3] W.A. Cassada, G.J. Shiflet and E.A. Starke, Jr., J. de Physique, Colloq. C3, Vol. 48, 1987, p. 397.

[4] T.J. Langan and J.R. Pickens in "Aluminum-Lithium Alloys" (Proceedings of the Fifth International Aluminum-Lithium Conference), eds: T.H. Sanders and E.A. Starke, MCE Publication Ltd., Birmingham, U.K., 1989, p. 691.

[5] K.S. Kumar, S.A. Brown and J.R. Pickens, Scripta Metall. et Mater., 24, 1990, p. 1245.

[6] F.W. Gayle, F.H. Heubaum and J.R. Pickens in "Aluminum-Lithium Alloys" (Proceedings of the Fifth International Aluminum-Lithium Conference), eds: T.H. Sanders and E.A. Starke, MCE Publications Ltd., Birmingham, U.K., 1989, p. 701.

[7] F.W. Gayle, F.H. Heubaum and J.R. Pickens, Scripta Metall., 24, 1990, p. 79.

[8] J.R. Pickens, F.H. Heubaum, T.J. Langan, and L.S. Kramer, in "Aluminum-Lithium Alloys" (Proceedings of the Fifth International Aluminum-Lithium Conference), T.H. Sanders and E.A. Starke, eds., MCE Publications Ltd., Birmingham, U.K., 1989, p. 1397.

[9] P.L. Makin and B. Ralph, J. Mater. Sci., 19, 1984, p. 3835.

[10] F.W. Gayle and B. VanderSande, Acta Metall., 37, 1989, p. 1033.

[11] P.L. Makin, D.J. Lloyd and W.M. Stobbs, Philos. Mag. Letters, Philos. Mag. A, Vol. 51, #5, 1985, p. L41.

[12] S.Kang and N.J. Grant, Metall. Trans., 18A, 1987, p. 2037.

[13] H.K. Hardy and J.M. Silcock, J. Inst. of Met., 84, 1955-56, p. 423.

[14] B. Noble and G.E. Thompson, Met. Sc., 6, 1972, p. 167.

[15] J.C. Huang and A.J. Ardell, Matl. Sc. and Tech., 3, 1987, p. 176.

[16] H. Suzuki, M. Kanno and N. Hayashi, J. Jap. Inst. Light Met., 32, 1982, p. 88.

[17] R.J. Rioja and E.A. Ludwiczak in "Aluminum Alloys, Their Physical and Mechanical Properties," Vol. III, Proceedings of the International Conference on Aluminum Alloys, Chameleon Press, London, U.K., 1986, p. 471.

[18] W.A. Cassada, G.J. Shiflet and E.A. Starke, Scripta Metall., 21, 1987, p. 387.

[19] R.J. Chester and I.J. Polmear in "The Metallurgy of Light Alloys," Inst. Metall., Ser. 3, London, Vol. 20, 1983, p. 75.

[20] J.H. Auld and J.T. Vietz in "The Mechanism of Phase Transformations in Crystalline Solids," Proceedings of the International Symposium of the Institute of Metals, London, 1969, p. 77.

[21] K.M. Knowles and W.M. Stobbs, Acta Cryst., B44, 1988, p. 207.

[22] B.C. Muddle and I.J. Polmear, Acta Metall., 37, 1989, p. 777.

[23] S. Kerry and V.D. Scott, Met. Sc., 18, 1984, p. 289.

[24] A. Garg, Y.C. Chang and J.M. Howe, Scripta Metall. et Mat., 24, 1990, p. 677.

[25] B.A. Shollock, C.R.M. Grovenor and K.M. Knowles, Scripta Metall. et Mat., 24, 1990, p. 1239.

[26] D. Khireddine, R. Rahouadj and M. Clavel, Scripta Metall., 22, 1988, p. 167.

[27] R.N. Wilson and P.G. Partridge, Acta Metall., 13, 1965, p. 1321.

[28] H. Watanabe and E. Sato, J. of Japan Inst. Light Metals, 31, 1981, p. 64.

[29] A.K. Gupta, P. Gaunt and M.C. Chaturvedi, Philos Mag. A., 55, 1987, p. 375.

[30] X. Xiaoxin and J.W. Martin, J. de Physique, Calloque C3, Vol. 48, 1987, p. 433.

N91-24409

V. HIGH-RESOLUTION ELECTRON MICROSCOPY STUDY OF A HIGH Cu VARIANT OF WELDALITE™ 049 AND A HIGH STRENGTH Al-Cu-Ag-Mg-Zr ALLOY

R.A. Herring, F.W. Gayle, and J.R. Pickens

I. INTRODUCTION

Weldalite™ 049 is an Al-Cu-Li-Ag-Mg alloy that is strengthened in artificially-aged tempers primarily by very thin plate-like precipitates lying on {111} matrix planes [1,2]. This precipitate might be expected to be the T_1 phase, Al_2CuLi, which has been observed in Al-Cu-Li alloys. However, in several ways this precipitate is similar to the Ω phase which also appears as {111} plates and is found in Al-Cu-Ag-Mg alloys. [3-5] The present study was undertaken to identify the {111} precipitate or precipitates in Weldalite™ 049 in the T8 (stretched and artificially aged) temper, and to determine whether T_1, Ω, or some other phase is primarily responsible for the high strength (i.e. 700 MPa tensile strength) in this Al-Cu-Li-Ag-Mg alloy.

2. BACKGROUND METALLURGY

Polmear [4] developed a nominal Al-6.3Cu-0.5Ag-0.5Mg-0.5Mn-0.2Zr alloy that had exceptionally high ambient and warm temperature properties for an ingot metallurgy 2xxx (i.e. Al-Cu) alloy. He noted that the Ag+Mg addition stimulated precipitation of the Ω phase, whose presence was apparently responsible for the significant strength increase (~25%) over that for conventional high strength Al-Cu alloys such as 2219 and 2618.

Langan and Pickens [2] performed transmission electron microscopy investigations of Weldalite™ 049 and a model Al-6Cu-0.4Ag-0.4Mg-0.14Zr alloy similar to that innovated by Polmear. Langan and Pickens identified the platelike phase in Weldalite™ 049 as T_1, but a cursory investigation of the Al-Cu-Ag-Mg alloy underscored the similarities between T_1 and Ω. Moreover, because of the similarity in the diffraction patterns for T_1 and Ω, they [2] could not rule out the existence of Ω in Weldalite™ 049 and, consequently, referred to the platelike precipitates as T_1-type.

Additions of Ag have little or no effect on the strengthening or precipitation behavior of binary Al-Cu alloys but a marked increase in strength occurs if a small addition of Mg is also added [3, 4, 13]. The combined presence of Ag and Mg in Al-Cu alloys significantly enhances the formation of the Ω phase [3, 13]. The mechanism by which these minor alloying additions jointly stimulate precipitation remains unclear although it is suggested that Ag and Mg may reduce the stacking fault energy in Al, which is quite high, resulting in enhanced fault

formation on matrix {111} planes which provide nucleation sites for the Ω phase [14]. It has also been speculated that Ag and Mg form fine-scale particles on the {111} planes which serve to both nucleate Ω and determine its morphology [15], although no evidence was presented to support this theory. More recently, Muddle and Polmear [16] found that Ag partitions to the Ω phase in an Al-Cu-Ag-Mg alloy and concentrates at the precipitate/matrix interface in the overaged condition, perhaps to help accommodate the misfit strain that is present normal to the habit plane in the matrix. In that study [16], Mg was not detected and the role of Mg in Ω phase formation is unknown. A recent study by Garg, et al. [18] has also shown that Ag is not required for Ω phase formation in Al-Cu-Mg alloys.

3. ATOMIC STRUCTURE OF Ω AND T_1 PHASE

The structure of the Ω phase in the Al-Cu-Mg alloy subsystem was proposed by Auld [6] and verified by Knowles and Stobbs [7] to be monoclinic with a = b = 0.496 nm, c = 0.848 nm and γ =120 degrees (Figure 1). This structure is equivalent to and more appropriately described as orthorhombic with a = 0.496, b = 0.859, and c = 0.848 nm and space group Fmmm [7,16]. Auld showed that this structure is best regarded as a slight distortion of the tetragonal θ (Al_2Cu) precipitate found in over-aged Al-Cu alloys [6].

In the Al-Cu-Li alloy subsystem, controversy exists as to the structure of the T_1 phase -- nominally Al_2CuLi. Hardy and Silcock [8] determined that the T_1 structure belonged to one of the hexagonal space groups P622, P6mm, $P\bar{6}m2$, or P6/mmm with a = 0.4965 and c = 0.9345 nm, based on a cast, stoichiometric Al_2CuLi alloy. Vecchio and Williams [9] further determined, using convergent beam electron diffraction, that a cast Al_2CuLi phase had P6/mmm symmetry. Huang and Ardell [10] proposed the space-group symmetry P6/mmm (Figure 2a) from calculated X-ray intensities which compared with "fair agreement" with the Debye-Scherrer X-ray intensity measurements reported by Hardy and Silcock [8]. Huang and Ardell [10] suggested the positional stacking of planes to be ABAB..., where the A planes are close-packed with ordered arrangements of Li and Al in 2:1 and 1:2 ratios for alternate A planes, and the B planes having a disordered arrangement of Cu and Al atoms which are not close packed. Cassada et al. [11] performed a high-resolution electron microscopy study of T_1.

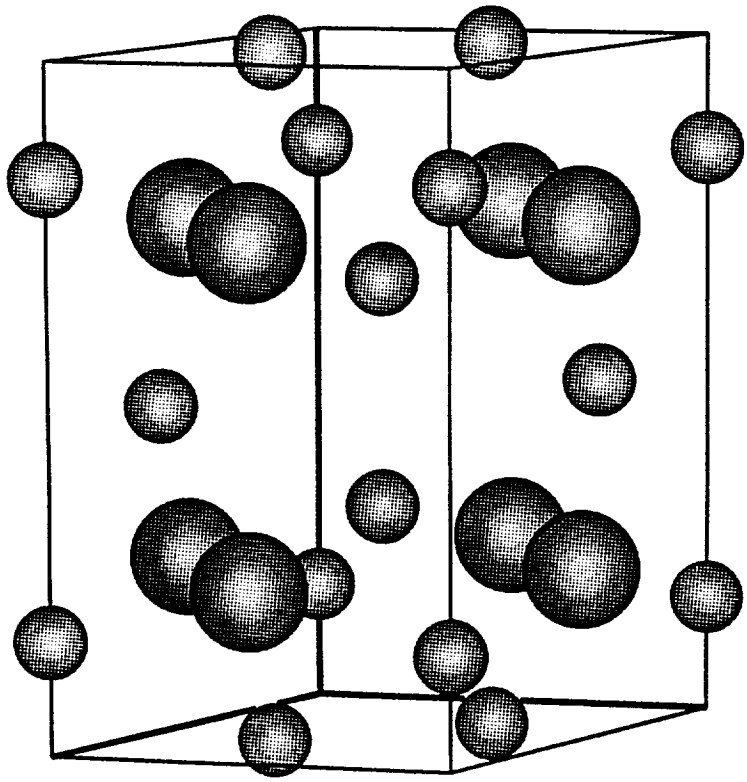

Figure 1. Monoclinic structure of the Ω phase showing the corrugated planes in the Z direction where the small balls are Al at Z = 0, 1/6, 1/3, 1/2, 2/3, 5/6, and 1, and the large balls are Cu at Z = 1/4 and 3/4.

They proposed a modification of Huang and Ardell's structure which consists of four close packed layers. (Fig. 2b).

A model for T_1 was recently proposed by Howe, Lee and Vasudevan [12] based on high-resolution electron microscopy image calculation. They reported a space group of P6mm. Their favored structure consists of four close-packed basal planes within the unit cell, as shown in Figure 2c, having a stacking sequence of ABAC... Alternate A planes consist of pure Al or pure Li atoms. The B and C planes consist of 50% Al plus 50% Cu which are randomly mixed. Evidence was also given that the B and C planes may vary from the 50/50 Al/Cu mixture.

Thus, several models for T_1 have been proposed and none is completely satisfactory with respect to matching experimental X-ray intensities or HREM images. The various T_1 structures are listed by space group and atomic positions in Table 1 along with the structure of Ω as given by Knowles and Stobbs [7]. In the course of the present work it was found that Howe et al.'s structure was not P6mm (this is most easily seen by a lack of the required 2-fold rotation axes for this space group). Indeed, the structure is not hexagonal but is a closely related trigonal space group $P\bar{3}m1$. Lattice parameters of the trigonal lattice are a = 0.286 and c = 0.935 nm, giving coherent matching with $[111]_{Al}$ planes. Though this trigonal structure does not agree with the space groups given by Hardy and Silcock [8], it is possible that the latter, being from a stoichiometric Al_2CuLi cast structure, is not the same as the T_1 that precipitates within the aluminum matrix.

3.1 Experimental Procedure

Two alloys were fabricated: a relatively high Cu variant of Weldalite™ 049, and a nominal Al-6Cu-0.4Ag-0.4Mg-0.1Zr alloy. These alloys are the same materials used by Langan and Pickens [2] and will be referred to as Weldalite™ 049 and alloy 2 respectively, with measured compositions given in Table 2. Each alloy was cast into a 16.5-cm diameter permanent mold and was homogenized by the practices developed by Pickens et al [1]. Each alloy was extruded at a ratio of 21:1 into 10.2 x 0.95-cm bar at a nominal preheat temperature of 370°C. The Weldalite™ 049 extrusion was solutionized at 504°C and Alloy 2 was solutionized at 530°C, each for 1 h. Each extrusion was

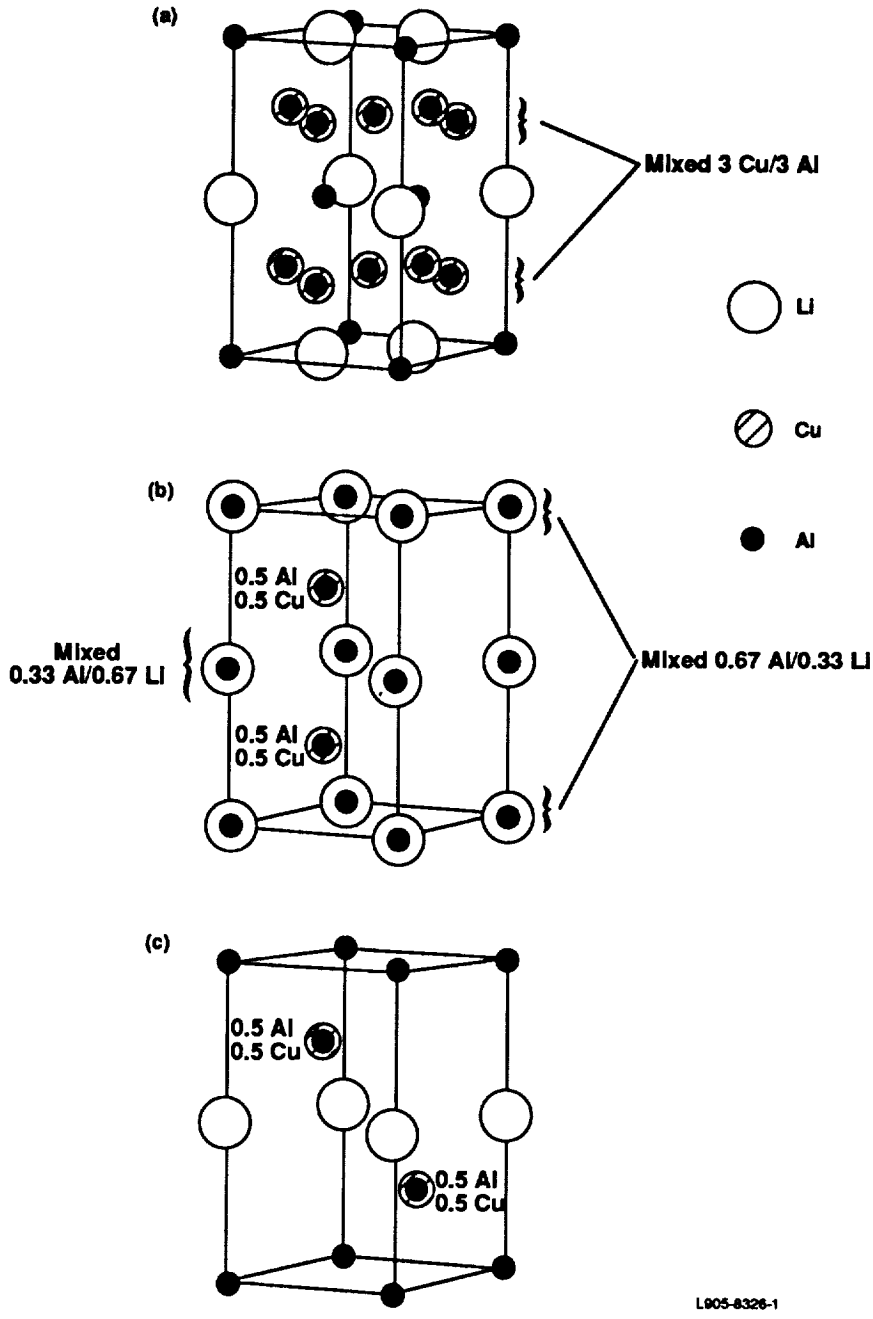

Figure 2. Various models proposed for the T_1 structure showing (a) Huang and Ardell's [10] having space group P6/mmm, (b) Cassada et al's [11] sites at z = 0 are occupied by an average of 0.67 Al and 0.33 Li, whereas at z = 1/2 the occupancy is 0.33 Al and 0.67 Li (c) Howe et al's [12] having space group $P\bar{3}m1$. The structure in (a) has 12 atoms/unit cell and (b) and (c) have 4 atoms/unit cell.

Table 1.

Space groups and atom positions of Ω and T_1 structures reported in the literature.

Phase	Ref.	Structure	Group	Multiplicity/ Wyckoff Letter	Positions x	y	z	Occupancy
Ω	Knowles & Stobbs [7]	Orthorhombic a=0.496 b=0.859 c=0.848	Fmmm (#69)	8h 8i 8f	0 0 1/4	1/3 0 1/4	0 1/6 1/4	8Al 8Al 8Cu
T_1	Howe et al. [12]*	Trigonal a=0.286 c=0.935	$P\bar{3}m1$ (#164)	1a 2d 1b	0 1/3 0	0 2/3 0	0 1/4 1/2	1Al 1Al/1Cu 1Li
T_1	Cassada et al. [11]	Hexagonal a=0.286 c=0.935	$P\bar{6}m2$ (#187)	1a 1b 2i	0 0 2/3	0 0 1/3	0 1/2 1/4	0.67Al/0.33Li 0.33Al/0.67Li 1Al/1Cu
T_1	Huang & Ardell [10]	Hexagonal a=0.496 c=0.935	P6/mmm (#191)	1a 1b 2c 2d 6i	0 0 1/3 1/3 1/2	0 0 2/3 2/3 0	0 1/2 0 1/2 1/4	1Al 1Li 2Li 2Al 3Al/3Cu

*This is the Howe et al. [12] structure rewritten as trigonal.

water quenched to about 20°C, stretched 3%, and artificially aged at 160°C for 24 h to the near-peak strength, T8 temper.

Table 2

Alloy Compositions (wt%)

Alloy	Cu	Li	Ag	Mg	Zr
Weldalite™ 049	5.83	1.25	0.38	0.42	0.13
Alloy 2	6.16	-----	0.41	0.42	0.16

4. RESULTS

High-resolution images of the Ω phase in alloy 2 and the {111} strengthening phase (i.e., "T_1-like") in Weldalite™ 049 were obtained in the [112] and [110] matrix orientations. The low symmetry of the Ω phase leads to the presence of three variants of Ω lying on each {111} matrix plane. Alloy 2 at the [110] matrix orientation, which is equivalent to the [010] and [310] orthorhombic variants of the Ω phase, shows {111} precipitates with thin Cu-rich (dark) and thick Al-rich (light) layers (Figure 3a) for a multi-unit-cell-thick precipitate. Lattice images of the Ω phase show the two variants that exist at the [112] matrix orientation (equivalent to the [100] and [110] orthorhombic orientations of the phase) which produce a square array of dark and light spots in one image (Figure 3b) and a wavy pattern in another (Figure 3c).

For the {111} precipitates in Weldalite™ 049, the lattice image (Figure 4) at the [110] matrix orientation gives an image similar to the T_1 lattice images reported by others in Ag- and Mg- free alloys [11, 12]. The [112] matrix orientation produced only one distinct type of lattice image of the precipitates with examples being given in Figure 5. These images always have three rows of bright spots per unit cell. Two adjacent rows of spots form a rectangular pattern and the third row of spots, of decreased intensity, are positioned at a (sometimes variable) distance between the rectangular pattern, i.e., they are slightly offset to one side. This pattern of spots is different from previously reported T_1 lattice images at the [112] matrix orientation which also have three rows of bright spots but which do not form a rectangular array for adjacent rows of spots [11, 17]. The

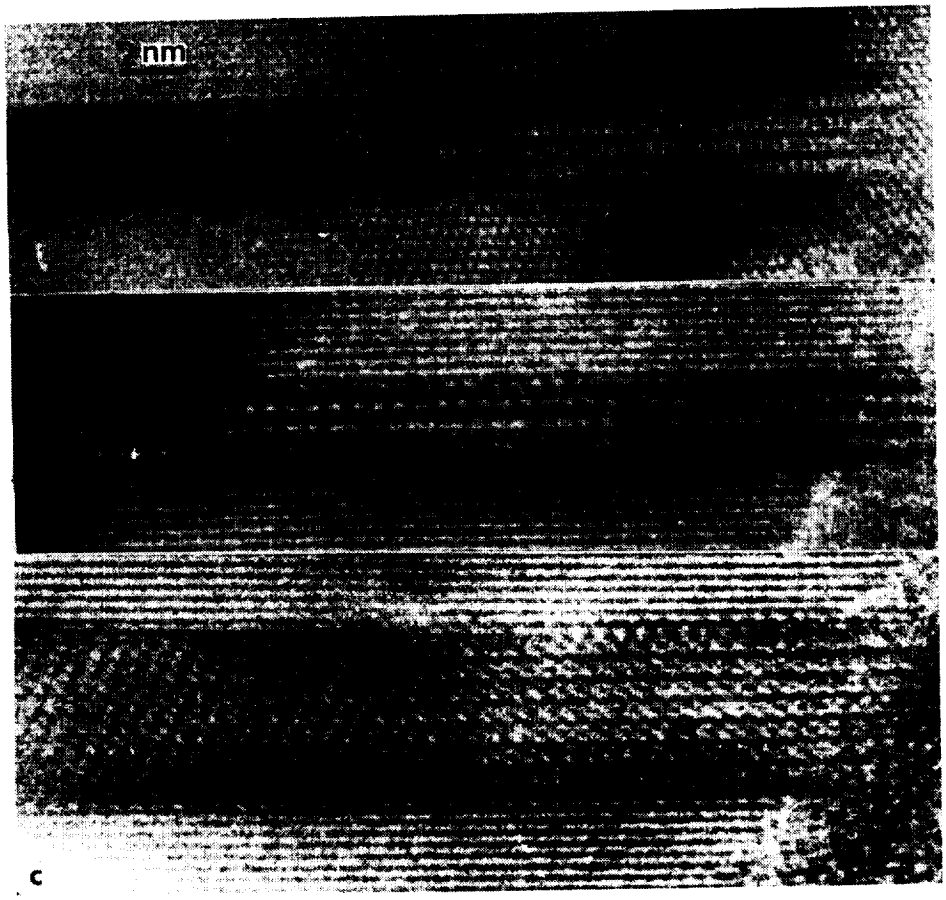

Figure 3. Lattice images of the Ω phase in Li-free alloy-2 showing a) then, Cu-rich and thick Al-rich layers at the [110] matrix orientation, b) and c) square array of black and white spots, and wavey light and dark pattern at the [112] matrix orientation (see text).

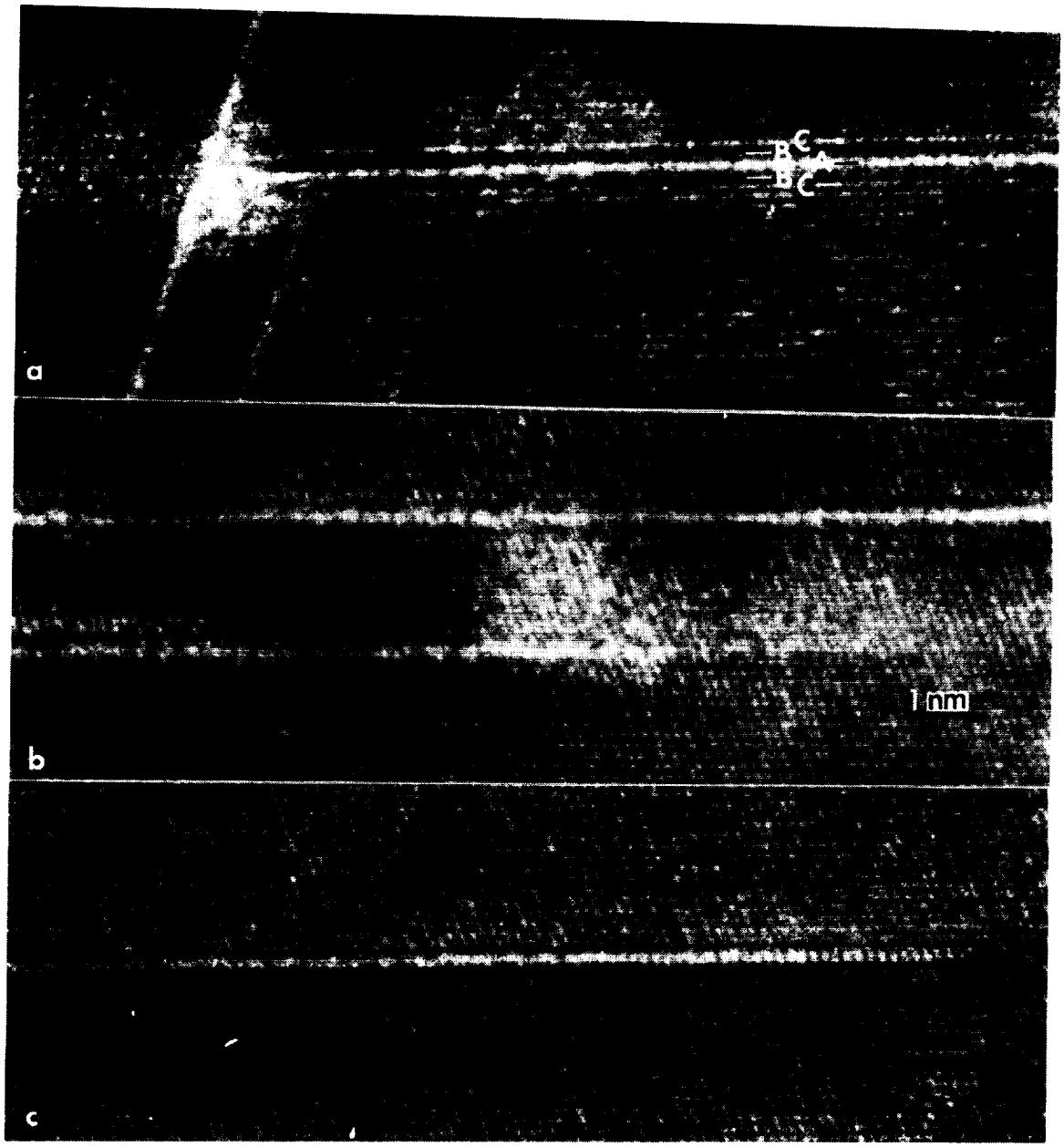

Figure 4 Lattice images of the primary strengthening phase in Weldalite™ 049 at the [110] matrix orientation showing the "classic" T_1 structure in (a) where the layers A, B, and C have been designated as being Li rich, Cu rich and Al rich, respectively (see text).

ORIGINAL PAGE
BLACK AND WHITE PHOTOGRAPH

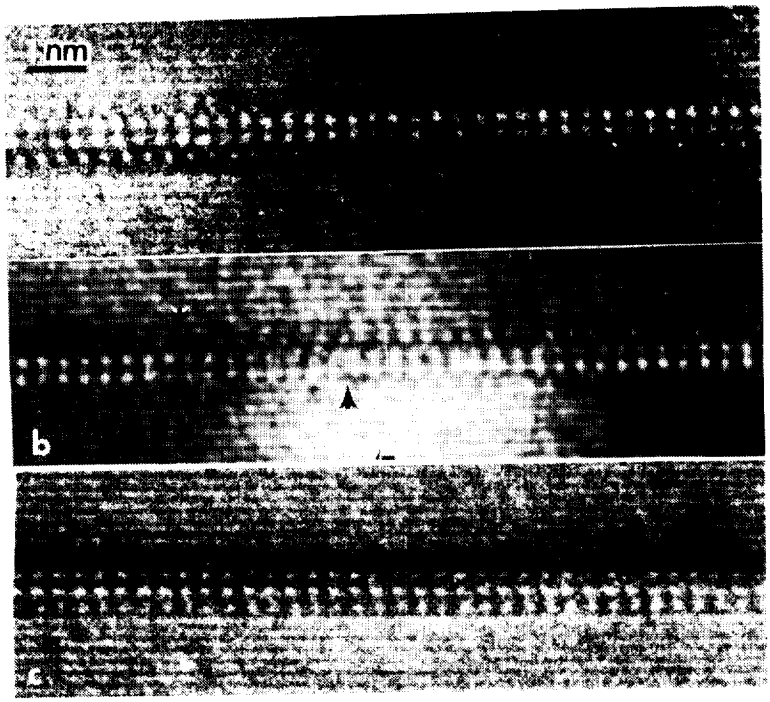

Figure 5 Lattice images of Weldalite™ 049 showing the 'non-classic' structure at the [112] matrix orientation (see text) where in (b) faulting appears to be occurring in between the arrows and in (c) the rectangular array of white spots changes from the top two rows to bottom two rows when scanning from left to right.

distance between the spots along the precipitate length were measured for both Weldalite™ 049 and the T_1 images of references 11 and 17, using the {111} matrix planes for a reference length in each case, and the white spots in Weldalite™ 049 were found to have the same separation as those in previously reported T_1 images. The platelike precipitates in Weldalite™ 049 thus have a different structure from that of the Ω precipitates in alloy 2. Furthermore, the structure is similar to that of T_1 reported in other Al-Cu-Li alloys, although the pattern viewed along the [112] matrix orientation is different.

5. DISCUSSION

The lattice images of the Ω phase in alloy 2 fit well with those produced by Knowles and Stobbs in an Al-Cu-Ag-Mg alloy [7]. Figure 3a has the thick-light layers and thin-dark layers equivalent to the [310] orthorhombic orientation image of Knowles and Stobbs. The square array of Figure 3b is equivalent to the $[100]_O$ and the wavy array of Figure 3c is equivalent to the $[110]_O$ orientation.

The presence of only one type of lattice image at the [110] and [112] orientations for alloy Weldalite™ 049, which is different from that seen in alloy 2, indicates that the Ω phase is not present in Weldalite™ 049 in the condition investigated. The primary strengthening phase in Weldalite™ 049 has the previously reported T_1 image at the [110] matrix orientation. However, at the [112] matrix orientation, they have a consistently different lattice image from the T_1 images reported by Cassada et al. [11] and Blackburn and Starke [17] in the same matrix orientation. It is significant that every {111} precipitate in Weldalite™ 049 T8 investigated (dozens) shows this distinct structure.

6. CONCLUSIONS

High-resolution micrographs of the primary strengthening phase in the T8 temper in each of the two alloys listed in Table 1 have been obtained. By comparing these experimental images to those images published by Knowles and Stobbs [7] it was found that the Ω phase exists in alloy 2, i.e., the Al-6Cu-0.4Mg-0.4Ag -0.1Zr alloy. By comparing the lattice images of the Ω phase to those of Weldalite™ 049, it was found that the Ω phase is not present in the Weldalite™

049 alloy under the conditions investigated. In this alloy, the lattice images have the "classic" T_1 lattice image at the [110] but not at the [112] matrix orientations. Thus, the primary strengthening phase in Weldalite™ 049 in the T8 temper examined appears to be T_1 or a closely related variation. This structure may be a faulted (with respect to that seen in Ag-free Al-Cu-Li alloys) version of the T_1 phase.

7. ACKNOWLEDGEMENTS

Part of Dr. Gayle's time spent in preparing this section was supported by the National Institute of Standards and Technology. The authors are grateful to T.J. Langan for providing the experimental materials in the appropriate tempers and to S. Mannan for his technical assistance.

8. REFERENCES

[1] J.R. Pickens, F.H Heubaum, T.J. Langan, and L.S. Kramer, "Aluminum-Lithium Alloys" (Proceedings of the Fifth International Aluminum-Lithium Conference, T.H. Sanders and E.A. Starke, eds., MCE Publications, Ltd., Birmingham, U.K., 1989), p. 1397.

[2] T.J. Langan and J.R. Pickens, ibid., p. 691.

[3] J.T. Vietz and I.J. Polmear, J. Inst. Metals, Vol. 94 (1966) p. 410.

[4] I.J. Polmear, Aluminum Alloys - Physical and Mechanical Properties, Vol. 1 of Conference Proceedings at International Conference held at Univ. of Virginia, Charlottesville, VA, 15-20 June 1986, Chameleon Press Ltd. Publ., pp. 661-674.

[5] R.J. Chester and I.J. Polmear, Micron, 10, 1980, pp. 311-312.

[6] J.H. Auld, Acta Cryst. A28 (1972) S98; Materials Science and Technology 2, (1986), p. 784.

[7] K.M. Knowles and W.M. Stobbs, Acta Cryst. B44, (1988) p. 207.

[8] H.K. Hardy and J.M. Silcock, J. Inst. Met. 84 (1955-56) p. 423.

[9] K.S. Vecchio and D.B. Williams, Metall. Trans. A 19 (1988) p. 2885.

[10] J.C. Huang and A.J. Ardell, Mat. Sci. and Technol., 3, (1987) p. 176.

[11] W.A. Cassada, G.J. Shiflet, and E.A. Starke, Jr., J. de Physique 48, supp. C3(9) (1988) p. C397.

[12] J.M. Howe, J. Lee and A.K. Vasudevan, Metall. Trans. A 19A (1988) p. 2911.

[13] I.J. Polmear, Trans. Metall. Soc. A.I.M.E. 230 (1964) p. 1331.

[14] S. Kerry and V.D. Scott, Metal Sci., Vol. 18 (1984) p. 289.

[15] J.A. Taylor, B.A. Parker and I.J. Polmear, Metal Sci., Vol. 12 (1978) p. 478.

[16] B.C. Muddle and I.J. Polmear, Acta Metall., Vol. 37, No. 3 (1989) p. 777.

[17] L.B. Blackburn, E.A. Starke, Jr. in Aluminum-Lithium alloys, ed. T.H. Sanders, Jr. and E.A. Starke, Jr., Vol II (1989) p. 751.

[18] A. Garg, Y.C. Change and J.M. Howe, Scripta Metall. Mater. 24, (1990) p. 677.

NASA National Aeronautics and Space Administration

Report Documentation Page

1. Report No.	2. Government Accession No.	3. Recipient's Catalog No.
NASA CR-4368		

4. Title and Subtitle	5. Report Date
Evaluation of the Microstructure of Al-Cu-Li-Ag-Mg Weldalite™ Alloys	May 1991
	6. Performing Organization Code

7. Author(s)	8. Performing Organization Report No.
J.R. Pickens, K.S. Kumar, S.A. Brown, and F.W. Gayle	MML TR 90-69c
	10. Work Unit No. 505-63-50-02

9. Performing Organization Name and Address	11. Contract or Grant No.
Martin Marietta Laboratories 1450 S. Rolling Road Baltimore, MD 21227	NAS1-18531
	13. Type of Report and Period Covered: Contractor Report

12. Sponsoring Agency Name and Address	14. Sponsoring Agency Code
National Aeronautics and Space Administration Langley Research Center Hampton, VA 23665-5225	

15. Supplementary Notes

NASA Langley Technical Monitor: William D. Brewer
Final Report, Part IV

16. Abstract

Weldalite™ 049 is an Al-Cu-Li-Ag-Mg alloy designed to have ultrahigh strength and to serve in Aerospace Applications. The alloy displays significantly higher strength than competitive alloys in both naturally aged and artificially aged tempers. The strengthening phases in such tempers have been identified to, in part, explain the mechanical properties attained. In general, the alloy is strengthened by δ' (Al_3Li) and GP zones in the naturally aged tempers. In artificially aged tempers in slightly underaged conditions, strengthening is provided by several phases including GP zones, Θ' (Al_2Cu), S' (Al_2CuMg), T_1 (Al_2CuLi) and possibly a new phase. In the peak strength artificially aged tempers, T_1 is the predominant strengthening phase.

17. Key Words (Suggested by Author(s))	18. Distribution Statement
Aluminum alloys, aluminum lithium alloys, strengthening phases	Unclassified-Unlimited Subject Category 26

19. Security Classif. (of this report)	20. Security Classif. (of this page)	21. No. of pages	22. Price
Unclassified	Unclassified	107	A06

NASA FORM 1626 OCT 86

For sale by the National Technical Information Service, Springfield, Virginia 22161-2171

NASA-Langley, 1991

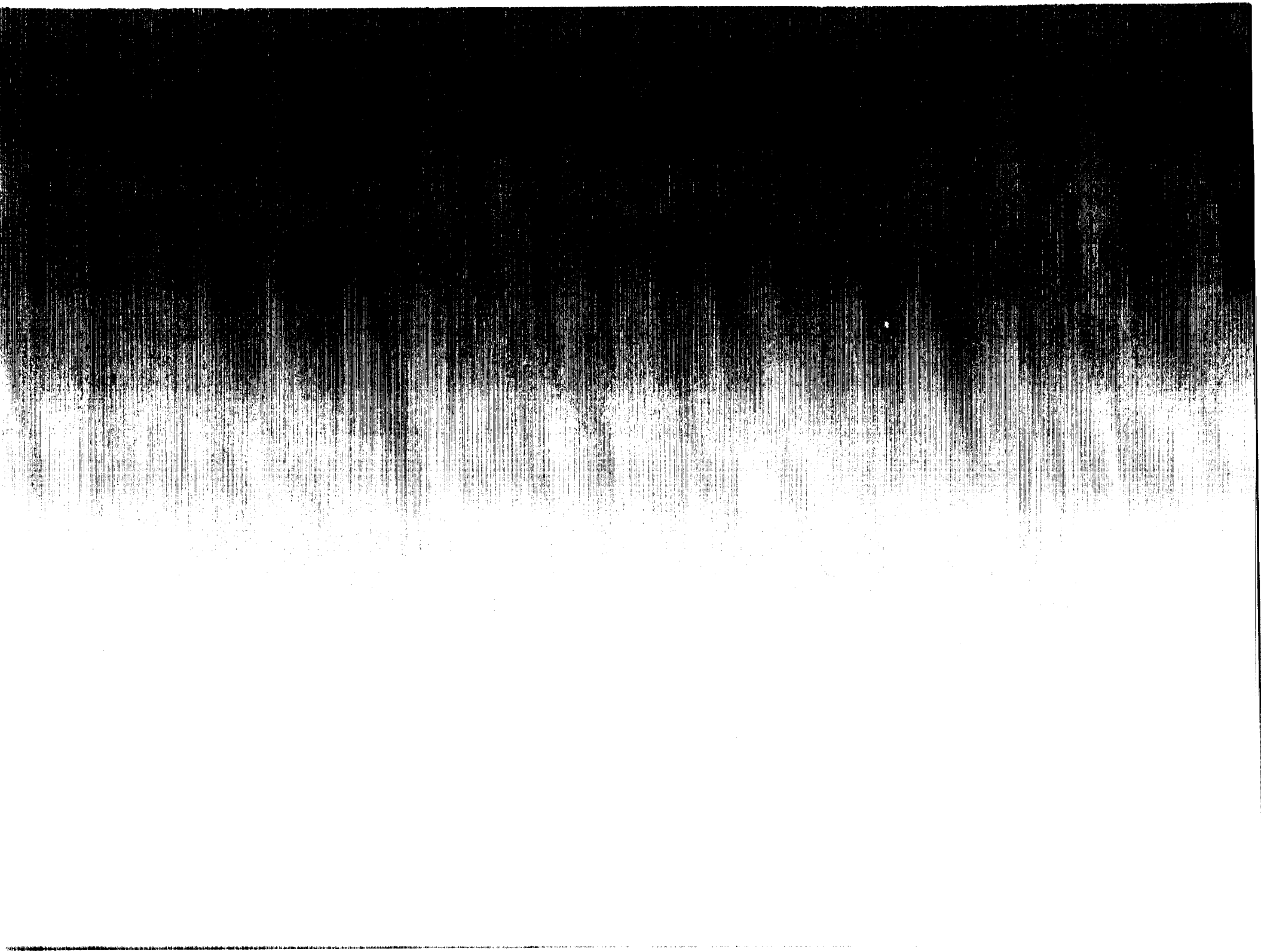

National Aeronautics and Space Administration

Washington, D.C.